

*Volume 19, Number 5*

*November, 1965*

# **SOVIET ATOMIC ENERGY**

**АТОМНАЯ ЭНЕРГИЯ  
(АТОМНАЯ ЭНЕРГИЯ)**

**TRANSLATED FROM RUSSIAN**



**CONSULTANTS BUREAU**

## THE LEBEDEV PHYSICS SERIES

Series Editor: Academician D. V. Skobel'tsyn

Each of these important new volumes from the proceedings ("Trudy") of the famed Lebedev Physics Institute of the Academy of Sciences of the USSR is devoted to a specific area of advanced physics research. Published irregularly in the USSR — 4 to 6 volumes per year — these proceedings, in cover-to-cover translation, include from 2 to 20 papers.

The P. N. Lebedev Physics Institute, one of the largest and best equipped in the Soviet Union, employs a research staff of 300-400 scientists and some 1500 technical assistants. The 1958 Nobel laureates Frank, Tamm, and Cherenkov and the 1964 laureates Bašov and Prokhorov are among its most outstanding scientists. Consultants Bureau's Special Research Report translations in this series begin with Volume 25. Two earlier proceedings of the Institute, *Soviet Maser Research* (Volume 21) and *Soviet Researches on Luminescence* (Volume 23), have also been translated and published by Consultants Bureau.

### "Trudy" Volume 25: OPTICAL METHODS OF INVESTIGATING SOLID BODIES

194 pages 1965 \$22.50

### "Trudy" Volume 26: COSMIC RAYS

254 pages 1965 \$27.50

### "Trudy" Volume 27: RESEARCH IN MOLECULAR SPECTROSCOPY

206 pages 1965 \$22.50

### "Trudy" Volume 28: RADIO TELESCOPES

Approx. 200 pages Fall 1966 \$22.50

### "Trudy" Volume 29: QUANTUM FIELD THEORY AND HYDRODYNAMICS

Approx. 260 pages Summer 1966 \$27.50

### "Trudy" Volume 30: PHYSICAL OPTICS

Approx. 300 pages Summer 1966 \$27.50

### "Trudy" Volume 31: QUANTUM RADIOPHYSICS

In preparation

### "Trudy" Volume 32: PLASMA PHYSICS

In preparation

### "Trudy" Volume 33: RESEARCH ON THE ATOMIC NUCLEUS USING CHARGED PARTICLES AND NEUTRONS

Approx. 215 pages Summer 1966 \$22.50

### "Trudy" Volume 34: PHOTOMESONIC AND PHOTONUCLEAR PROCESSES

In preparation

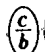
The following "Trudies" of the Lebedev Physics Institute  
have also been translated  
and published by Consultants Bureau:

### "Trudy" Volume 21: SOVIET MASER RESEARCH

186 pages 1964 \$27.50

### "Trudy" Volume 23: SOVIET RESEARCHES ON LUMINESCENCE

152 pages 1964 \$27.00

 **CONSULTANTS BUREAU** 227 West 17th Street, New York, New York 10011

# YOU ARE INVITED...

## to select free sample copies from the following list of major scientific journals

Forty-eight Russian and Chinese journals published by Consultants Bureau in complete, authoritative cover-to-cover English translation are listed. Several of them may be of interest and importance to you or your library.

### 48 MAJOR JOURNALS IN...

#### CHEMICAL ENGINEERING

1. Chemical and Petroleum Engineering.....(CPE)
2. Chemistry and Technology of Fuels and Oils.....(CTF)
3. (NEW) Theoretical Foundations of Chemical Engineering .....(TCE)

#### CHEMISTRY

4. (NEW) Acta Chimica Sinica (from Chinese) .....(ACS)
5. Bulletin of the Academy of Sciences of the USSR: Division of Chemical Science .....(BAS)
6. Colloid Journal of the USSR .....(COL)
7. Doklady Chemical Technology .....(DCT)

8. Doklady Chemistry .....(DCH)
9. Doklady Physical Chemistry .....(DPC)
10. (NEW) High Energy Chemistry .....(HEC)
11. Journal of Analytical Chemistry .....(JAN)
12. Journal of Applied Chemistry .....(JAC)
13. Journal of General Chemistry .....(JGC)
14. Journal of Organic Chemistry .....(JOC)
15. Journal of Structural Chemistry .....(JSC)
16. Kinetics and Catalysis .....(KAC)
17. Soviet Electrochemistry .....(ELE)
18. Soviet Radiochemistry .....(RAD)

continued

IF BOTH REPLY CARDS HAVE ALREADY BEEN USED PLEASE SEND US YOUR REQUEST ON YOUR LETTERHEAD

### CONSULTANTS BUREAU

a division of Plenum Publishing Corporation 227 West 17th St., N. Y., N. Y. 10011

Please send me a free sample copy of each journal I have circled from the list below:

ACS	AUT	BIO	CPE	DBI	DCH	DPC	GAC	IOM	JAN	JSC	MAT	MIN	PES	PRO	SME
AEP	BAS	COL	CTF	DBO	DCT	ELE	HEC	JAC	JGC	KAC	MET	MOL	PLP	RAD	SMI
AMS	BBM	COS	DBC	DBP	DEF	FAA	HTP	JAE	JOC	LMR	MIC	MST	PMT	REF	TCE

NAME \_\_\_\_\_

TITLE \_\_\_\_\_

AFFILIATION \_\_\_\_\_

ADDRESS \_\_\_\_\_

CITY \_\_\_\_\_ STATE \_\_\_\_\_ ZIP \_\_\_\_\_

### CONSULTANTS BUREAU

a division of Plenum Publishing Corporation 227 West 17th St., N. Y., N. Y. 10011

Please send me a free sample copy of each journal I have circled from the list below:

ACS	AUT	BIO	CPE	DBI	DCH	DPC	GAC	IOM	JAN	JSC	MAT	MIN	PES	PRO	SME
AEP	BAS	COL	CTF	DBO	DCT	ELE	HEC	JAC	JGC	KAC	MET	MOL	PLP	RAD	SMI
AMS	BBM	COS	DBC	DBP	DEF	FAA	HTP	JAE	JOC	LMR	MIC	MST	PMT	REF	TCE

NAME \_\_\_\_\_

TITLE \_\_\_\_\_

AFFILIATION \_\_\_\_\_

ADDRESS \_\_\_\_\_

**CIVIL ENGINEERING**

19. Soil Mechanics and Foundation Engineering .....(SME)

**GEOLOGY**

20. (NEW) Lithology and Mineral Resources .....(LMR)

21. Soviet Mining Science .....(MIN)

**LIFE SCIENCES**

22. Biochemistry .....(BIO)

23. Bulletin of Experimental Biology and Medicine .....(BBM)

24. Doklady Biochemistry .....(DBC)

25. Doklady Biological Sciences .....(DBI)

26. Doklady Biophysics .....(DBP)

27. Doklady Botanical Sciences .....(DBO)

28. Microbiology .....(MIC)

29. (NEW) Molecular Biology .....(MOL)

30. Soviet Plant Physiology .....(PLP)

**MATERIALS SCIENCE**

31. Glass and Ceramics .....(GAC)

32. Inorganic Materials .....(IOM)

**MATHEMATICS**

33. (NEW) Functional Analysis and Its Applications .....(FAA)

34. (NEW) Mathematical Notes .....(MAT)

35. (NEW) Siberian Mathematical Journal of the Academy  
of Sciences of the USSR, Novosibirsk .....(SMJ)

**METALLURGY AND CORROSION**

36. Metallurgist .....(MET)

37. Metal Science and Heat Treatment .....(MST)

38. Protection of Metals .....(PRO)

39. Refractories .....(REF)

40. Soviet Powder Metallurgy and Metal Ceramics .....(PMT)

**PHYSICS AND ENGINEERING**

41. (NEW) Acta Mechanica Sinica (from Chinese) .....(AMS)

42. Applied Electrical Phenomena .....(AEP)

43. (NEW) Autometry .....(AUT)

44. Cosmic Research .....(COS)

45. Defectoscopy: The Soviet Journal of  
Nondestructive Testing .....(DEF)

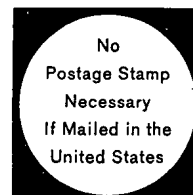
46. High Temperature .....(HTP)

47. (NEW) Physics and Engineering of Semiconductors (PES)

48. Soviet Atomic Energy .....(JAE)



**BUSINESS REPLY MAIL**  
FIRST CLASS PERMIT NO. 14728, NEW YORK, N. Y.



**PLENUM PUBLISHING CORPORATION**

Divisions: CONSULTANTS BUREAU • PLENUM PRESS • PLENUM PRESS DATA DIVISION • DA CAPO PRESS

227 West 17th Street  
New York, N. Y. 10011



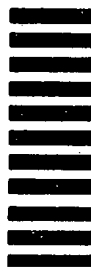
**BUSINESS REPLY MAIL**  
FIRST CLASS PERMIT NO. 14728, NEW YORK, N. Y.



**PLENUM PUBLISHING CORPORATION**

Divisions: CONSULTANTS BUREAU • PLENUM PRESS • PLENUM PRESS DATA DIVISION • DA CAPO PRESS

227 West 17th Street  
New York, N. Y. 10011



ATOMNAYA ÉNERGIYA

EDITORIAL BOARD

A. I. Alikhanov	M. G. Meshcheryakov
A. A. Bochvar	M. D. Millionshchikov ( <i>Editor-in-Chief</i> )
N. A. Dollezhal'	P. N. Palei
V. S. Fursov	V. B. Shevchenko
I. N. Golovin	D. L. Simonenko
V. F. Kalinin	V. I. Smirnov
N. A. Kolokol'tsov ( <i>Assistant Editor</i> )	A. P. Vinogradov
A. K. Krasin	N. A. Vlasov ( <i>Assistant Editor</i> )
A. I. Leipunskii	
V. V. Matveev	

# SOVIET ATOMIC ENERGY

A translation of **ATOMNAYA ÉNERGIYA**,  
a publication of the Academy of Sciences of the USSR

© 1966 CONSULTANTS BUREAU, A DIVISION OF PLENUM PUBLISHING CORPORATION, 227 West 17th Street, New York, N. Y. 10011

Volume 19, Number 5

November, 1965

## CONTENTS

	PAGE	RUSS. PAGE
Plasma Stability in a Mirror Machine with Stabilizing Rods—B. A. Trubnikov . . . . .	1369	415
Magnetic Mirror Trap with a Field Increasing in All Directions—A. I. Morozov and L. S. Solov'ev . . . . .	1376	420
Self-Consistent Distribution of Particles and Limiting Current in a Linear Accelerator —B. I. Bondarev and A. D. Vlasov . . . . .	1381	423
Use of Time Integration to Calculate the Differential Scattering Cross Sections of Slow Neutrons—V. F. Turchin . . . . .	1387	428
The Hydration of Cations in Heavy Water—V. M. Vdovenko, Yu. V. Gurikov, and E. K. Légin . . . . .	1393	433
The Binary System UF <sub>4</sub> —UCl <sub>4</sub> —L. A. Khripin, Yu. V. Gagarinskii, G. M. Zadneprovskii, and L. A. Luk'yanova . . . . .	1398	437
NOTES ON ARTICLES RECEIVED		
Construction of a Sectored 300 keV Cyclotron with External Injection—V. A. Gladyshev, L. N. Katsaurov, A. N. Kuznetsov, E. M. Moroz, and L. P. Nechaeva . . . . .	1403	442
Magnetic Field of a 300-keV Sector Cyclotron with External Injection—V. A. Gladyshev, L. N. Katsaurov, A. N. Kuznetsov, E. M. Moroz, and L. P. Nechaeva . . . . .	1404	443
Improvement of the Sensitivity of Alpha-Scintillation Chambers—L. V. Gorbushina and V. G. Tyminskii . . . . .	1406	443
Certain Methods for Reducing the Fluxes of Penetrating Secondary $\gamma$ -Radiation —D. L. Broder, A. P. Kondrashov, and A. V. Kudryavtseva . . . . .	1408	444
LETTERS TO THE EDITOR		
Measurement of the Pressure Distribution behind the Front of a Strong Shock Wave —V. I. Fedulov and V. D. Borman . . . . .	1409	446
Use of Surface-Barrier Silicon Detectors for Measuring Fast-Particle Spectra —G. F. Bogdanov and B. P. Maksimenko . . . . .	1414	449
Dependence of the Energy Loss Averaged with Respect to the Electron Spectrum on the End-Point Energy of the $\beta$ -Spectrum, the Atomic Number of the $\beta$ -Radiator, and the Transition Type—V. F. Baranov . . . . .	1416	450
Coefficients of Secondary $\gamma$ -Radiation for Aluminum, Copper, and Tungsten —S. P. Belov, V. P. Demin, Yu. A. Kazanskii, A. P. Lobakov, and V. I. Popov . . . . .	1419	452

Annual Subscription: \$95

Single Issue: \$30

Single Article: \$15

All rights reserved. No article contained herein may be reproduced for any purpose whatsoever without permission of the publisher. Permission may be obtained from Consultants Bureau, A Division of Plenum Publishing Corporation, 227 West 17th Street, New York, N. Y. 10011, U.S.A.

## CONTENTS (continued)

	PAGE	RUSS. PAGE
Viscosity Coefficient of Hydrogen (H <sub>2</sub> , D <sub>2</sub> ), Neon (Ne <sup>20</sup> , Ne <sup>22</sup> ) and Helium (He <sup>3</sup> ) Isotopes in the Temperature Range -195 to +25° C—N. E. Menabde . . . . .	1421	453
Determination of the Spectral Characteristics of Isotopic Neutron Sources by Paired Scintillation Crystals of the LiI(Eu) Type—P. L. Gruzin, A. Z. Kichev, V. M. Minaev, V. T. Samosadnyi, and Su Ch'ang-sung . . . . .	1423	454
Cross Sections for the Inelastic Interaction of Neutrons with Nuclei of Li <sup>7</sup> , C <sup>12</sup> , N <sup>14</sup> , Al <sup>27</sup> , Fe <sup>56</sup> , Cu, Pb, U <sup>235</sup> , U <sup>238</sup> , and Pu <sup>239</sup> —Yu. G. Degtyarev . . . . .	1426	456
Cross Sections for the Radiative Capture of Fast Neutrons in Rhenium and Tantalum —V. N. Kononov and Yu. Ya. Staviskii . . . . .	1428	457
Producing Stable Isotopes of Krypton and Xenon by Irradiating Aluminum Halides in a Reactor—A. N. Murin, L. K. Levskii, and A. E. Zakharova . . . . .	1430	458
Measurement of Gd <sup>156</sup> Absorption Cross Section—E. I. Grishanin, G. M. Kukavadze, V. I. Lependin, L. Ya. Mamelova, I. G. Morozov, V. V. Orlov, and D. T. Pilipets . . . . .	1432	459
Changes in Fast-Neutron Spectra After Penetrating Aluminum, Paraffin, and Water —G. G. Doroshenko, V. A. Fedorov, and E. S. Leonov . . . . .	1434	460
An Estimate of the Accuracy of the Variational Method—E. N. Erykalov . . . . .	1437	462
Comparison of Calculated and Experimental Parameters of Homogeneous Uranium-Water Critical Assemblies—A. S. Dochenov, N. Ya. Lyashchenko . . . . .	1439	463
Tangential Channels and Thermal Column Reconstruction at the VVR-M Reactor —G. Ya. Vasil'ev, E. A. Konovalov, V. G. Pankov, and D. A. Yashin . . . . .	1441	465
The Effect of Core Configuration on Neutron Spectrum from a Horizontal Channel of the VVR-M Reactor—V. P. Vertebnyi, M. F. Vlasov, and A. L. Kirilyuk . . . . .	1445	467
New Data on Atmospheric Radioactivity and Fallout Intensity in the Black Sea Basin —V. P. Kotel'nikov, V. N. Markelov, and B. A. Nelepo . . . . .	1447	469
The Relative Levels of Stratospheric Fission Fragment Fallout—P. I. Chalov and M. A. Tsevelev . . . . .	1450	470
Atmospheric Radioactivity above the Atlantic Ocean During May-July, 1964 —L. I. Gedeonov, V. N. Dmitriev, B. A. Nelepo, A. V. Stepanov, and G. V. Yakovleva . . . . .	1452	472
Features of the Equilibrium Shift in the Uranium-Radium Series in Uranium Deposits with Hard Bitumens—G. N. Kotel'nikov . . . . .	1455	474
SCIENCE AND ENGINEERING NEWS		
[Scientific Meeting of the Nuclear Physics Division of the Academy of Sciences of the USSR . . . . .		476]
[The Detroit Fast Reactor Conference—O. D. Kazachkovskii . . . . .		477]
CHRONICLES, COMMUNICATIONS		
[Reprocessing and Disposal of Radioactive Wastes in the USA—B. S. Kolychev . . . . .		481]
[Radiation Chemistry and Nuclear Chemistry at Canada's Research Centers —V. Gromov . . . . .		484]
A Glove Box Train—G. I. Lukishov, K. D. Rodionov, and N. I. Noskov . . . . .	1457	486
New German Whole Body Counter—Yu. V. Sivintsev . . . . .	1460	488
Erratum . . . . .	1462	

## CONTENTS (continued)

RUSS.  
PAGE PAGE

### NOTE

The Table of Contents lists all material that appears in Atomnaya Énergiya. Items originally published in English or generally available in the West are not included in the translation and are shown in brackets. Whenever possible, the English-language source containing the omitted items is given.

The Russian press date (podpisano k pečati) of this issue was 11/10/1965. Publication therefore did not occur prior to this date, but must be assumed to have taken place reasonably soon thereafter.

## PLASMA STABILITY IN A MIRROR MACHINE WITH STABILIZING RODS

(UDC 533.9)

B. A. Trubnikov

Translated from *Atomnaya Énergiya*, Vol. 19, No. 5,  
pp. 415-420, November, 1965  
Original article submitted March 10, 1965

The well-known criterion for plasma stability  $\delta \int dl/B < 0$  is generalized to the case of an anisotropic plasma ( $p_{\parallel} \neq p_{\perp}$ ) in an axially nonsymmetric field. Stability conditions are found for a mirror machine with stabilizing rods. The theoretical results are in satisfactory agreement with experimental data obtained on the PR-5 device.

A stability criterion was obtained in [1] for a plasma with an anisotropic pressure and an axially symmetric field:

$$\int \frac{p_{\parallel} + p_{\perp}}{rRB^2} dl > 0, \quad (1)$$

where  $r$  is the distance of a line of force from the axis;  $R$  is the radius of curvature ( $R > 0$  for a concave line and  $R < 0$  for a convex line);  $B$  is the magnetic field intensity;  $p_{\parallel}$  and  $p_{\perp}$  are the components of the plasma pressure parallel and perpendicular to the field; the integral is taken along the line of force. This criterion can be generalized to the case of axially nonsymmetric fields. For this purpose we write it in the form

$$\int \frac{\delta B}{B^2} (p_{\parallel} + p_{\perp}) dl > 0, \quad (2)$$

where  $\delta B$  is the increment in field to the next (outer) line of force. If all plasma ions have the same  $v^2$  ( $v$  is the velocity) and the same value of  $J_{\perp} = v_{\perp}^2/B$ , the adiabatic invariant ( $J_{\perp}$  is conserved during a displacement), criterion (2) is equivalent to

$$\int \frac{\delta B}{B} \left( v_{\parallel}^2 + \frac{v_{\perp}^2}{2} \right) \frac{dl}{v_{\parallel}} > 0, \quad (3)$$

which can be obtained from the conservation of the adiabatic invariant  $J_{\parallel} = \int v_{\parallel} dl = \text{const}$  and the fact that the increment in the energy of a particle when it undergoes a convective transition from one line of force to the next (outer) must be positive.

We shall apply criteria (2) and (3) to the study of plasma stability in a mirror machine with stabilizing rods. When there are  $2n$  rods with a current  $J$  in each (the current flows in opposite directions in adjacent rods), the scalar potential of the field  $B = \nabla \psi$  near the axis has the form:

$$\psi = \int B_0(z) dz - \frac{1}{4} B'_0(z) r^2 + 4 \frac{J}{c} \left( \frac{r}{a} \right)^n \cos n\varphi, \quad (4)$$

where  $B_0(z)$  is the field on the axis itself, and  $a$  is the radius of the circle within which the rods are situated. Further



$$\left. \begin{aligned} B_r &= -\frac{1}{2} B_0' r + \frac{4nJ}{ca^n} r^{n-1} \cos n\varphi; \\ B_\varphi &= -\frac{4nJ}{ca^n} r^{n-1} \sin n\varphi; \\ B_z &= B_0 - \frac{1}{4} B_0'' r^2. \end{aligned} \right\} \quad (5)$$

Taking  $B_r$  and  $B_\varphi$  as quantities of the first order of smallness and  $\delta B_z = -\frac{1}{4} B_0'' r^2$  as a second-order quantity, we find for the modulus of the field:

$$\begin{aligned} B &= B_0 + \frac{1}{2B_0} \left[ \left( -\frac{1}{2} B_0 B_0'' + \frac{1}{4} B_0'^2 \right) r^2 \right. \\ &\quad \left. - B_0' \frac{4nJ}{ca^n} r^n \cos n\varphi + \left( \frac{4nJ}{ca^n} \right)^2 r^{2n-2} \right]. \end{aligned} \quad (6)$$

In order to determine the quantity  $\delta B = \mathbf{s} \nabla B$  appearing in criteria (2) and (3) ( $\mathbf{s}$  is the vector with coordinates  $\delta r, r\delta\varphi, \delta z$ ), we must know the vector  $\nabla B$ :

$$\left. \begin{aligned} \nabla_r B &= \frac{1}{2B_0} \left[ \left( -B_0 B_0'' + \frac{1}{2} B_0'^2 \right) r^2 \right. \\ &\quad \left. - B_0' \frac{4nJ}{ca^n} n r^{n-1} \cos n\varphi \right. \\ &\quad \left. + \left( \frac{4nJ}{ca^n} \right)^2 (2n-2) r^{2n-3} \right]; \\ \nabla_\varphi B &= \frac{1}{2B_0} B_0' \frac{4nJ}{ca^n} n r^{n-1} \sin n\varphi. \end{aligned} \right\} \quad (7)$$

Second-order corrections can be neglected in the term  $\nabla_z B = B_0'$ . On integrating the equations of the lines of force, we find

$$\left. \begin{aligned} r &= \frac{r_0}{\sqrt{\beta}} \left( \frac{\sin n\varphi_0}{\sin n\varphi} \right)^{1/n}; \\ \int_{\varphi_0}^{\varphi} \frac{d\psi}{\sin^{2/n} n\psi} &= -\alpha (\sin n\varphi_0)^{1-\frac{2}{n}} \int_0^{\frac{z/l}{\beta^{n/2}}} \frac{dt}{\beta^{n/2}}, \end{aligned} \right\} \quad (8)$$

where  $\beta(z) = \frac{B_0(z)}{B_0(0)}$ ;  $\alpha = \frac{4nJl r_0^{n-2}}{ca^n B_0(0)}$ ;  $l$  is the typical length over which the axial field  $B_0(z)$  varies. In the

simplest case the field on the axis of a mirror machine can be approximated by the parabola  $B_0(z) = B_0^0 (1 + z^2/l^2)$ . Then  $\beta = 1 + t^2$ , where  $t = z/l$ . Expressions (8) are correct to within terms of the second order of smallness in the parameter  $\epsilon = r_0/l \ll 1$ . Although  $r_0$  appears in  $\alpha$ , we shall nevertheless consider  $\alpha$  and  $\epsilon$  as different parameters (it is shown below that the plasma is stable when  $\alpha \approx 1$ ).

We shall now work out the quantity  $\delta B$  appearing in (2) and (3). We may assume from symmetry considerations that the plasma surface in the plane  $z = 0$  is bounded by the circle  $r_0 = \text{const}$ . Then  $\delta B = \mathbf{s} \nabla B$  is the increment in field in going from the line  $(r_0, \varphi_0)$  to the line  $(r_0 + \delta r_0, \varphi_0)$  and  $\mathbf{s} \perp \mathbf{B}$ . Formulas (8) determine the line  $r = r(r_0, z)$ ,  $\varphi = \varphi(r_0, z)$ . Consequently, we may write

$$\delta r = \frac{\partial r}{\partial r_0} \delta r_0 + \frac{\partial r}{\partial z} \delta z; \quad \delta \varphi = \frac{\partial \varphi}{\partial r_0} \delta r_0 + \frac{\partial \varphi}{\partial z} \delta z. \quad (9)$$

Writing  $\rho = r/r_0$ , we find from (8)

$$\left. \begin{aligned} \frac{\partial r}{\partial r_0} &= \rho \left( 1 - r_0 \frac{\partial \varphi}{\partial r_0} \text{ctg} n\varphi_0 \right); \\ r_0 \frac{\partial \varphi}{\partial r_0} &= -r_0 \frac{\partial \alpha}{\partial r_0} \frac{\sin n\varphi_0}{\beta \rho^2} \int_0^{z/l} \frac{dt}{\beta^{n/2}(t)}, \end{aligned} \right\} \quad (10)$$

where

$$r_0 \frac{\partial \alpha}{\partial r_0} = (n-2) \alpha.$$

On solving the equation  $\mathbf{sB} = 0$ , where  $\mathbf{B}$  is determined by formulas (5), we obtain

$$\delta z = -\frac{\delta r_0}{B_0} \left( B_r \frac{\partial r}{\partial r_0} + B_\varphi Q r_0 \frac{\partial \varphi}{\partial r_0} \right) \quad (11)$$

Thus,  $\delta z \sim B_\perp / B_0$ , and is consequently a quantity of the first order of smallness. Dropping the second terms in (9) (for example,  $\partial r / \partial z \sim B_r / B_z \sim B_\perp / B_0$ ), we finally obtain

$$\left. \begin{aligned} s_r &= \frac{\partial r}{\partial r_0} \delta r_0; & s_\varphi &= Q r_0 \frac{\partial \varphi}{\partial r_0} \delta r_0; \\ s_z &= -\frac{\delta r_0}{B_0} \left( B_r \frac{\partial r}{\partial r_0} + B_\varphi Q r_0 \frac{\partial \varphi}{\partial r_0} \right). \end{aligned} \right\} \quad (12)$$

Utilizing formulas (7) and writing  $t = z/l$ , we find finally

$$\delta B = \mathbf{s} \nabla B = \delta r_0 \frac{r_0 B_0(0)}{l^2} \cdot \frac{A_\alpha^n(t)}{\beta(t)}, \quad (13)$$

where

$$\begin{aligned} A_\alpha^n(t) &= \left( r_0 \frac{\partial \varphi}{\partial r_0} \right) \left( \frac{n}{2} + 1 \right) \alpha \dot{\beta} Q^n \sin n\varphi \\ &+ \left( 1 - r_0 \frac{\partial \varphi}{\partial r_0} \cotan n\varphi \right) \left[ Q^2 \left( \frac{3}{4} \dot{\beta}^2 - \frac{1}{2} \beta \ddot{\beta} \right) \right. \\ &\left. - \left( \frac{n}{2} + 1 \right) \alpha \dot{\beta} Q^n \cos n\varphi + (n-1) \alpha^2 Q^{2n-2} \right]; \end{aligned} \quad (14)$$

the dot denotes differentiation with respect to  $t = z/l$ . When the unimportant constant factor in  $\delta B$  is dropped, criterion (3) can be written in the form:

$$\int_{-x}^{+x} A_\alpha^n(t) \frac{2\beta(x) - \beta(t)}{\beta^2(t)} \cdot \frac{dt}{\sqrt{\beta(x) - \beta(t)}} > 0, \quad (15)$$

where  $x = z_{\text{ref}}/l$  is the point at which particles are reflected;  $\beta(x) = v^2/J_\perp B_0(0)$ . Criterion (2) takes the form:

$$\int_{-x}^{+x} A_\alpha^n(t) (p_\parallel + p_\perp) \frac{dt}{\beta^3(t)} > 0, \quad (16)$$

where  $x = z_{\text{max}}/l$  is the plasma boundary. Here we have utilized the fact that terms of order  $\varepsilon^2$  can be dropped in the remaining factors under the integral signs, thus allowing integration to be carried out directly along the axis.

The above criteria contain only the parameter  $\alpha$ . We must now determine the critical value of  $\alpha$ , above which the plasma becomes stable.

In the particular case of  $n = 2$ ,  $r_0$  does not appear in  $\alpha$  and so the plasma will be stable for  $\alpha > \alpha_{\text{crit}}$  at all values of the radius (near the axis). If, however,  $n \geq 3$ , the critical value of  $\alpha_{\text{crit}}$  will determine a radius

$$r_0^{\text{crit}} = \left[ \frac{c a^n B_0(0)}{4n J l} \alpha_{\text{crit}} \right]^{\frac{1}{n-2}}, \quad (17)$$

beyond which (for  $r > r_0^{\text{crit}}$ ) the plasma becomes stable.

Let us examine the case  $n = 2$  more closely. For the field on the axis we shall apply the parabolic approximation  $\beta = 1 + t^2$ . We then have from (8)

$$\operatorname{tg} \varphi = \operatorname{tg} \varphi_0 e^{-2\alpha \operatorname{arctan} t} \varrho = \frac{\sin \varphi_0}{\sqrt{\beta} \sin \varphi} e^{-\alpha \operatorname{arctan} t} \quad (18)$$

After some simple manipulation we find

$$\begin{aligned} A_{\alpha}^{(2)}(t) &= \frac{1}{\beta} [(\alpha^2 - 1 + 2t^2) \operatorname{ch} T_{\alpha} - 4at \operatorname{sh} T_{\alpha}] \\ &+ \frac{1}{\beta} [(\alpha^2 - 1 + 2t^2) \operatorname{sh} T_{\alpha} - 4at \operatorname{ch} T_{\alpha}] \cos 2\varphi_0, \end{aligned} \quad (19)$$

where  $T_{\alpha} = 2\alpha \operatorname{arctan} t$ . The second term, being an odd function of  $t$ , drops out the criteria (15) and (16), and consequently they will not contain the angle  $\varphi_0$ . If we write

$$\Lambda_{\alpha}(t) = (\alpha^2 - 1 + 2t^2) \operatorname{ch} T_{\alpha} - 4at \operatorname{sh} T_{\alpha},$$

then criterion (15) takes the form

$$I_{\alpha}(x) = \int_0^x \Lambda_{\alpha}(t) \frac{1 + 2x^2 - t^2}{(1 + t^2)^3} \cdot \frac{dt}{\sqrt{x^2 - t^2}} > 0. \quad (20)$$

For  $\alpha = 0$  (no current in rods)  $\Lambda_0(t) = 2t^2 - 1$ , and it can be seen on working out the integral  $I_0(x) = -\pi/8 [\sqrt{\beta} + (3/\beta)\sqrt{\beta}]$ , that stability cannot be attained at any value of  $x$  (we recall that this pertains to the parabolic approximation for the field on the axis). Stability results only if  $\alpha > 1$ ; this is clear from the expression:

$$I_{\alpha}(x)|_{x \rightarrow 0} = \frac{\pi}{2} (\alpha^2 - 1) > 0 \quad \text{for } \alpha > 1. \quad (21)$$

As  $\alpha$  is increased small values of  $x$  first begin to be stabilized, and then larger values. The function  $x_{\text{crit}} = f(\alpha)$ , found by integration from the condition  $I_{\alpha}(x_{\text{crit}}) = 0$ , is shown in Fig. 1 (curve 1) for a system consisting of four rods ( $n = 2$ ). It is clear that  $x = 1$  (and so also  $x < 1$ ) is stabilized for  $\alpha = 8Jl / ca^n B_0^0 \approx 3$ .

Criterion (20) refers to the case when the plasma contains ions with identical values of  $\nu^2$  and  $J_{\perp}$ . The above results remain qualitatively the same, however, even if the plasma contains particles with different values of  $\nu^2$ . We consider the case of a  $J_{\perp}$  "cutoff" Maxwell distribution:

$$f(\nu) = \begin{cases} 0 & \text{for } \frac{J_{\perp}}{\nu^2} < \frac{1}{B(z_{\text{max}})}, \\ \text{const exp} \left( -\frac{M\nu^2}{2T} \right) & \text{for } \frac{J_{\perp}}{\nu^2} > \frac{1}{B(z_{\text{max}})}. \end{cases} \quad (22)$$

Here  $M$  is the ion mass,  $T$  the ion temperature, and  $z_{\text{max}}$  the plasma boundary. For this case we readily find ( $x = z_{\text{max}}/l$ ):

$$\begin{aligned} p_{\parallel} + p_{\perp} &= M \int \left( \nu_{\parallel}^2 + \frac{\nu_{\perp}^2}{2} \right) f d\nu \\ &= \text{const} [4\beta(x) - \beta(t)] \sqrt{\beta(x) - \beta(t)}, \end{aligned} \quad (23)$$

and in particular we find for the parabolic approximation

$$p_{\parallel} + p_{\perp} \sim (3 + 4x^2 - t^2) \sqrt{x^2 - t^2}. \quad (24)$$

If we insert this expression in formula (16), we obtain the following condition in place of criterion (20):

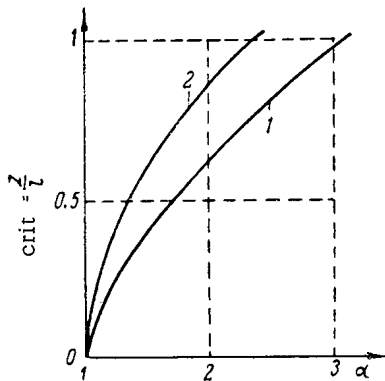


Fig. 1. Length of stable region  $z$  as a function of the parameter  $\alpha = 8Jl / ca^2B_0^0$  for a system with four rods ( $n = 2$ ): 1) for given  $v_{\perp}^2$  and  $J_{\perp} = v_{\perp}^2 / B$  (identical particles); 2) for "cutoff" Maxwell distribution.

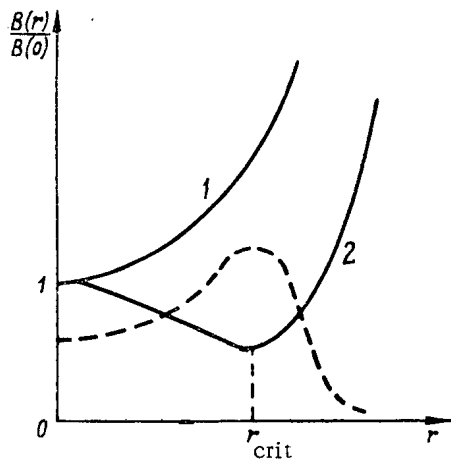


Fig. 2. Relative value of modulus of magnetic field  $|B|$  in the plane  $z = 0$ ; 1) four rods; 2) six rods; dotted line shows stable pressure distribution  $p(r)$  in the system with six rods.

$$\tilde{T}_{\alpha}(x) = \int_0^x \Lambda_{\alpha}(t) \frac{3+4x^2-t^2}{(1+t^2)^4} \sqrt{x^2-t^2} dt > 0. \quad (25)$$

For  $\alpha = 0$

$$\tilde{T}_0(x) = -\frac{3\pi}{16} \cdot \frac{\beta-1}{\beta\sqrt{\beta}} (9\beta-3-2\beta^2). \quad (26)$$

This expression is negative for  $0 < x < 1$ , as is  $I_0(x)$  [see (20)]. In real devices the mirror ratio rarely exceed 2, and so there is not much point in considering  $x > 1$ ; also, the parabolic approximation for the field on the axis breaks down in this case. In particular, we shall not discuss the "stability" appearing in formula (26) when  $9\beta - 3 - 2\beta^2 < 0$ , which corresponds to  $\beta > 4.14$  or  $x > 1.77$ . Stability appears only when  $\alpha > 1$ , which follows from the expression [for comparison see (21)]:

$$\tilde{T}_{\alpha}(x)_{x \rightarrow 0} = (\alpha^2 - 1) x^2 \frac{\pi}{4} > 0 \quad \text{for } \alpha > 1. \quad (27)$$

As  $\alpha$  is further increased, more remove values of  $x$  will be stabilized. Figure 1 (curve 2) shows the relationship  $x_{\text{crit}} = f(\alpha)$ , found from condition (25) by numerical integration. In particular,  $x = 1$  ( $z_{\text{max}} = l$ ) is stabilized at  $\alpha \approx 2.4$ .

We now consider the case  $n \geq 3$ . In this case Eqs. (8) for the lines of force cannot be integrated in a closed form. Only the "moment" at which the stability appears for limitingly small  $x$  can be fairly easily determined. Putting  $t = 0$  in formula (14) for  $A_{\alpha}^{(n)}(t)$  (with  $\rho = 1$ ,  $\varphi = \varphi_0$ ), we find that for  $\beta = 1 + t^2$  the quantity  $A_{\alpha}^{(n)}(0) = (n-1)\alpha^2 - 1$ . From expressions (15) and (16) we find that for  $x \rightarrow 0$  the plasma becomes stable when:

$$\alpha > \alpha_{\text{crit}} = \frac{1}{\sqrt{n-1}}, \quad (28)$$

i.e., [see (17)] for

$$r_0^{\text{crit}}|_{n=3} = \frac{a}{12\sqrt{2}} \cdot \frac{ca^2B_0^0}{Jl};$$

$$r_0^{\text{crit}}|_{n=4} = \frac{a}{4\sqrt[4]{3}} \sqrt{\frac{ca^2B_0^0}{Jl}} \text{ etc.} \quad (29)$$

When  $r_0 < r_0^{\text{crit}}$  the plasma will be unstable if its pressure decreases with radius.

Criterion (28) has a very simple physical interpretation, and can be obtained from the following considerations. Since  $v_{\parallel} \rightarrow 0$  the particles will not deviate much from the plane  $z = 0$ . Formula (6) and the parabolic approximation yield the following expression for the modulus of the field in this plane:

$$B(r) = B_0^0 \left\{ 1 + \frac{1}{2} \left[ -\frac{r^2}{l^2} + \left( \frac{4nJ}{ca^n} \right)^2 r^{2n-2} \right] \right\}. \quad (30)$$

The curve  $B(r)/B_0^0 = f(r)$  is shown in Fig. 2. The field decreases with  $r$  for small values of the latter but begins to increase at larger  $r$ , when the last term in (30) becomes important. The critical distance  $r_{\text{crit}}$  corresponding to the minimum field is found from the relationship  $\partial B / \partial r = 0$ , which yields

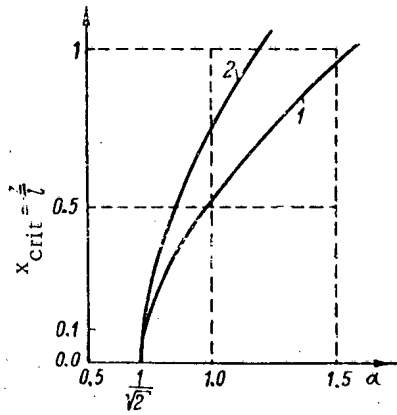


Fig. 3. Length of stable region  $z$  as a function of the parameter  $\alpha = 12Jl r_0 / ca^3 B_0^3$  for a system with six rods ( $n = 3$ ): 1) for given  $\nu^2$  and  $J_{\perp} = \nu^2 / B$ ; 2) for "cutoff" Maxwell distribution.

$$\frac{4nJl}{ca^n B_0^3} r_{\text{crit}}^{n-2} = \frac{1}{\sqrt{n-1}}, \quad (31)$$

the same result as formula (28).

For  $r > r_{\text{crit}}$  we have  $\partial B / \partial r > 0$ , which also leads to stability since the field increases from the plasma boundary towards the periphery. The particular case  $n = 2$ , when it is possible to have everywhere  $\partial B / \partial r > 0$  (see Fig. 2), was considered above. It is clear that for  $n = 2$  the plasma will be located near the axis of the system. When, however,  $n$  equals 3, 4, 5... and so on, the plasma must flow into the "hole" corresponding to the minimum in the field (see Fig. 2), so that the stable configuration takes the form of a plasma cylinder around  $r_{\text{crit}}$ ; the plasma pressure  $p(r)$  decreases both outwards from  $r_{\text{crit}}$  and also inwards from  $r_{\text{crit}}$  towards the axis (see the dotted curve in Fig. 2).

We now consider  $x \neq 0$ . Restricting ourselves to the case  $t \gg 1$  and neglecting terms of order  $t^2$ , we find from Eqs. (8)

$$\varphi - \varphi_0 = -\tilde{\alpha} \sin n\varphi_0 (1 - \tilde{\alpha} \cos n\varphi_0), \quad (32)$$

where  $\tilde{\alpha} = \alpha \int_0^{z/l} \frac{dt}{\beta^{n/2}(t)}$ , will be considered a small quantity of order  $t = z/l$ . Further, we have

$$\varrho = \frac{1}{\sqrt{\beta}} \left[ 1 + \tilde{\alpha} \cos n\varphi_0 + \frac{\tilde{\alpha}^2}{2} (n - \cos n\varphi_0) \right]. \quad (33)$$

Since  $\tilde{\alpha} \sim r_0^{n-2}$ , we find from (32) that

$$r_0 \frac{\partial \varphi}{\partial r_0} = -(n-2) \tilde{\alpha} \sin n\varphi_0 (1 - 2\tilde{\alpha} \cos n\varphi_0). \quad (34)$$

Inserting these expressions into formula (14), we find, to the same accuracy ( $\sim t^2$ ),

$$\begin{aligned} A_{\alpha}^{(n)}(t) &= (n-1)\alpha^2 - 1 + 3t^2 \\ &+ t^2 \alpha^2 (n-1) [1 - 4(n+1) + \alpha^2 n(2n-3)] \\ &+ \alpha^4 t^2 2(n-1)(n-2)(2n-3) \cos^2 n\varphi_0. \end{aligned} \quad (35)$$

Here we have dropped terms that are proportional to  $t$  since, being odd functions, they will drop out of integrals (15) and (16). The last term in (35) depends on  $\varphi_0$ , and consequently, the stable plasma shape for  $n \geq 3$  will no longer be axially symmetrical.

For simplicity we shall restrict ourselves to a system consisting of six rods ( $n = 3$ ):

$$\begin{aligned} A_{\alpha}^{(3)}(t) &= 2\alpha^2 - 1 \\ &+ 3t^2 [1 + 2\alpha^2(3\alpha^2 - 5) + 4\alpha^4 \cos^2 3\varphi_0]. \end{aligned} \quad (36)$$

Since  $t$  is taken to be small, this means that  $\alpha$  will be close to the value  $\alpha = 1/\sqrt{2}$ , corresponding to  $t = 0$ . Consequently, in the term with  $t^2$  in Eq. (36), we may put  $\alpha = 1/\sqrt{2}$ , which gives

$$A_{\alpha}^{(3)}(t)_{t \ll 1} = (2\alpha^2 - 1) - \frac{15}{2} t^2 \left( 1 - \frac{2}{5} \cos^2 3\varphi_0 \right). \quad (37)$$

Criterion (15) takes the following form, correct to within  $x^2$

$$2\alpha^2 - 1 - \frac{15}{4}x^2 \left(1 - \frac{2}{5} \cos^2 3\varphi_0\right) > 0. \quad (38)$$

This gives

$$x_{\text{crit}}^{(1)}|_{x \ll 1} = \sqrt{\frac{4(2\alpha^2 - 1)}{15 \left(1 - \frac{2}{5} \cos^2 3\varphi_0\right)}}. \quad (39)$$

The other criterion (16) with the pressure  $p_{\parallel} + p_{\perp}$  given by formula (24) leads to a result which is the same as (39) except for a factor  $\sqrt{2}$ :

$$x_{\text{crit}}^{(2)}|_{x \ll 1} = \sqrt{2} x_{\text{crit}}^{(1)}. \quad (40)$$

Figure 3 shows the curves  $x_{\text{crit}} = f(\alpha)$  plotted from formula (39) (curve 1) and formula (40) (curve 2) for  $\cos 3\varphi_0 = 0$ , (this is the worst case, since for  $3\varphi_0 \neq 0$  larger values of  $x$  are stabilized). These formulas are valid only for  $x \ll 1$ , but can be qualitatively applied even for  $x \approx 1$ . It is clear from Fig. 3 that  $x \approx 1$  is stabilized for  $\alpha \approx 1.5$  in the case of a plasma containing identical particles (curve 1), and for  $\alpha \approx 1.2$  in the case of the "cutoff" Maxwell distribution (curve 2).

We shall apply these results tentatively to the PR-5 device [2]. In this apparatus the mirror ratio  $B_{\text{max}}/B_{\text{min}} = 1.7$ . Assuming that the plasma extends right up to the mirrors and applying the parabolic approximation, we find the relationship  $1.7 = 1 + x^2$  that  $x = \sqrt{0.7} = 0.85$ . For this value of  $x$  and the "cutoff" Maxwell distribution (see Fig. 3, curve 2), we find that  $\alpha \approx 1.1$ , which corresponds to the stability condition

$$\alpha = \frac{12Jlr_{\text{crit}}}{ca^3B_0^0} > 1.1, \quad (41)$$

[in place of  $\alpha > 1/\sqrt{2} = 0.7$  in (28) as  $x \rightarrow 0$ ]. The above value of  $\alpha$  refers to the case of point rods. For the case of six rods in the shape of plates occupying each  $40^\circ$  arc of a circle, the coefficient 12 in formula (41) has to be replaced by  $18\sqrt{3}/\pi = 9.92$ . Moreover, we may assume that at the chamber walls  $B_{\perp} = 6.35 \text{ J/ca}$ , and consequently, taking  $a/l = 25/65 = 0.385$ , we have in place of (41).

$$\frac{r_{\text{crit}}}{a} = \frac{1.1 \cdot 6.35}{9.92} \cdot \frac{0.385}{B_{\perp}/B_0^0} = \frac{0.27}{\sqrt{\alpha_{\perp}^2 - 1}}, \quad (42)$$

where, as in [2],  $\alpha_{\perp} = \sqrt{1 + (B_{\perp}/B_0^0)^2}$ . This formula is close to the experimental relationship  $r_{\text{crit}} = f(\alpha_{\perp})$ , found from oscillograms taken with Langmuir probes (for  $r < r_{\text{crit}}$  the oscillograms show random oscillation, showing the plasma to be unstable; such oscillations are not observed for  $r > r_{\text{crit}}$  [3]).

In these experiments stable conditions were observed when  $\alpha_{\perp} > 1.08$ , which, from (42) for  $a = 25 \text{ cm}$ , corresponds to

$$r_{\text{crit}} = 25 \frac{0.27}{\sqrt{1.08^2 - 1}} = 17 \text{ cm}. \quad (43)$$

This result is in good agreement with the parameters of the device. The nitrous wall bounding the working volume of the trap is situated at  $r = 19 \text{ cm}$ , out of which  $2 \text{ cm}$  can be ascribed to the Larmor radius of the ions [2].

The author would like to thank V. G. Tel'kovskii for discussions on the results obtained in the article.

#### LITERATURE CITED

1. M. Rosenbluth and C. Longmire, *Ann. phys.*, 1, 120 (1957).
2. Yu. T. Baiborodov et al., *Atomnaya Énergiya*, 14, 443 (1963).
3. M. S. Ioffe and R. I. Sobolev, *Atomnaya Énergiya*, 17, 366 (1964).

## MAGNETIC MIRROR TRAP WITH A FIELD INCREASING IN ALL DIRECTIONS

(UDC 533.9)

A. I. Morozov and L. S. Solov'ev

Translated from *Atomnaya Énergiya*, Vol. 19, No. 5,  
pp. 420-423, November, 1965  
Original article submitted January 28, 1965

The existence of steady-state points of the square of the magnetic field's strength is considered, and the properties of the Andreoletti magnetic trap are investigated [1].

Topography of the Steady-State Points of the Square of the Field

The stability of confined plasma is favored by a configuration of the magnetic field  $\mathbf{B}$  where the modulus of  $\mathbf{B}$  increases in all directions from the center of the trap. The point of the minimum of  $B^2$  will be considered as the trap center, and the points where  $\nabla B^2 = 0$  will be referred to as steady-state points. After calculating the Laplacian of  $B^2$ , and considering that the Laplacians of the Cartesian components of  $\mathbf{B}$  vanish, we obtain

$$\Delta B^2 = 2 \sum_{i=1}^3 (\nabla B_i)^2, \quad i = x, y, z. \quad (1)$$

Since the sum of the second derivatives is nonnegative, the steady-state points of the field modulus can be either the points of the minimum of  $B^2$  or saddle points, while they cannot be maximum points. The conditions for the steady state of  $B^2$  are given by

$$\frac{\partial B^2}{\partial x_h} = 2 \sum_{i=1}^3 B_i \frac{\partial B_i}{\partial x_h} = 0. \quad (2)$$

If the field strength at the singular point of  $B^2$  is equal to zero, conditions (2) do not impose any additional limitations on the derivatives of the  $\mathbf{B}$  components. If  $B_i \neq 0$ , additional relationships between the first derivatives of  $\mathbf{B}$  follow from conditions (2).

The regions of the minimum field where the strength is different from zero are of interest for plasma traps. Let us consider the neighborhood of the steady-state point of  $B^2$  with the  $z$  axis oriented along the field at this point. Then, with an allowance for the equations

$$\operatorname{div} \mathbf{B} = 0, \quad \operatorname{rot} \mathbf{B} = 0, \quad (3)$$

and Eqs. (2), Eq. (1) will assume the following form:

$$\Delta B^2 = 4 \left[ \left( \frac{\partial B_x}{\partial x} \right)^2 + \left( \frac{\partial B_x}{\partial y} \right)^2 \right]. \quad (4)$$

The expansion of the scalar potential  $\Phi$  of the vacuum field near the  $z$  axis is given by

$$\begin{aligned} \Phi = & \int_0^z B_z(z) dz - \frac{B_z'(z)}{4} (x^2 + y^2) \\ & + \frac{k_1(z)}{2} (x^2 - y^2) + k_2(z) xy + \dots, \end{aligned} \quad (5)$$

where  $B_z$ ,  $k_1$ , and  $k_2$  are arbitrary functions of  $z$ . At the steady-state point of  $B^2$ , the derivative  $B_z(z)$  is equal to zero, and therefore, Eq. (4) yields

$$\Delta B^2 = 4(k_1^2 + k_2^2). \quad (6)$$

The latter equation implies the following:

- 1) there can be only saddle points of  $B^2$  on the axis of an axially symmetric field ( $k_1 = k_2 = 0$ );
- 2) in a two-dimensional field  $\Phi = \Phi(x, z)$ , since  $k_2 = 0$ ,  $k_1 = -B_z'/2$ , minimums of  $B^2$  do not exist either, as  $B_z' = 0$ ;
- 3) similarly, in an axially symmetric field, a minimum of  $B^2$  cannot exist at a point that does not lie on the axis if the field orientation at this point coincides with the symmetry axis  $z$ .

It can be shown that a helical field  $B_z = \text{const}$ ;  $k_1 = b \cos 2\alpha z$ ;  $k_2 = b_2 \sin 2\alpha z$  has a minimum on the  $z$  axis only if the field separatrix contracts to a point, i.e., if the lines of force depart from the  $z$  axis.

Two types of configuration of the magnetic field are used for plasma traps: toroidal, where the lines of force do not leave the trap region, and end-face traps is limited by the adiabatic invariant  $v_\perp^2/B$ .

An example of the configuration of a nonsymmetric field of the first type was given in [2]. This field had the property of the minimum of  $B^2$  in the averaging since:  $\int dl/B = \text{max}$ , which was sufficient for preventing the convective instability of low-pressure plasma.

If we limit our consideration to fields of the second type, the above relationship make it possible to produce traps with a region of minimum  $B^2$  values even in the case of fields with three-dimensional symmetry. A field described by the scalar potential

$$\Phi = B_0 z + b_1(x^2 - y^2), \quad (7)$$

constitutes an example of the corresponding two-dimensional field (with a nonvanishing longitudinal component  $B_z$ ). The longitudinal field  $B_z$  [see (5)] is of basic importance in this case. If this field is made to increase toward the end-faces (the field thus ceases to be a two-dimensional one), we shall obtain a simple model of a mirror trap with current rods [3].

According to what has been said above, axially symmetric traps with a minimum field region can be produced by using either azimuthal or radial fields as the basic fields. As an example of the first case, we can consider a trap formed by an azimuthal field  $B_\varphi = B_0 R/r$ , with a superimposed quadrupole field described by the scalar potential

$$\Phi_1 = b_1 \left( \frac{r^2}{2} - R^2 \ln \frac{r}{R} - z^2 \right) \approx b_1 [(r - R)^2 - z^2]. \quad (8)$$

The properties of fields with such a configuration are similar to the properties of fields of the anti-mirror type with a central current rod [4]. The other case, where a radial field is used as the basic one, was proposed by Andreoletti [1, 5]. Such a field has a very simple configuration of the lines of force; we shall analyze this field in greater detail.

### The Andreoletti System

The possibility of producing a radial mirror trap is obviously connected with the bunching of the radial field's lines of force in the vicinity of the  $z$  axis. Consider the configuration of a magnetic field whose median plane ( $z = 0$ ) contains only the radial field  $B_r$ .

The field near the median plane can be described by a scalar potential whose expansion with respect to powers of  $z$  is given by

$$\Phi = \int_0^r b(r) dr - \frac{1}{r} \left[ (rb)' \frac{z^2}{2} + \dots \right] \quad (9)$$

Here,  $\mathbf{B} = \nabla \Phi$ , while  $b(r)$  is the assigned field for  $z = 0$ . The corresponding flux function  $\psi = rA_\varphi$  is given by



$$\psi = -b(r)rz + r \left[ \frac{(rb)'}{r} \right]' \frac{z^3}{6} - \dots \quad (10)$$

Therefore, the equation of the lines of force  $\psi(r, z) = \text{const}$  near the  $z = 0$  plane can be approximately written thus:

$$z = \frac{\text{const}}{rb(r)}. \quad (11)$$

The square of the field strength is given by the expression:

$$B^2 = b^2 + \left\{ \frac{(rb)'^2}{r^2} - b \left[ \frac{(rb)'}{r} \right]' \right\} z^2 + \dots \quad (12)$$

Assume that the field modulus has a minimum at the point  $r = r_0, z = 0$ ; then,  $b'(r_0) = 0, b''(r_0) > 0$ . After denoting  $b(r_0)$  by  $b_0$ , we obtain the following expression for  $B^2(r_0, z)$ :

$$B^2 = b_0^2 + b_0 \left( \frac{2b_0}{r_0^2} - b_0'' \right) z^2 + \dots \quad (13)$$

Hence, it is obvious that if  $\partial^2 B^2 / \partial z^2$  is to be positive, it is necessary that the curvature of  $b = b(r)$  at the minimum be sufficiently small (Fig. 1). In the best case ( $b_0'' = 0$ ), we find:

$$B^2 = b_0^2 \left( 1 + 2 \frac{z^2}{r_0^2} \right). \quad (14)$$

Thus, the faster the field along  $z$  increases, the closer the field minimum to the axis. However, for small curvature of the  $[b = b(r)]$  curve, rather large distances  $b(r_1)/b(r_0)$  are required in order to secure a sufficiently large internal radial mirror ratio  $(r_0 - r_1)$ . Therefore, the radial dimensions will be comparatively larger, and the field increment along  $z$  smaller, in the case of traps with a larger radial mirror ratio. In order to secure the largest possible rise of the field along  $z$ , it is necessary to assign a  $b(r)$  function that diminishes rapidly along the axis, such, however, that  $\partial^2 B^2 / \partial z^2$  is everywhere positive.

As an illustration of the existing possibilities, we shall consider a field which, for  $z = 0$ , is assigned by the expression:

$$b(r) = c_1 r^{-m} + c_2 r^n \quad (m, n > 0). \quad (15)$$

The presence of the field minimum for  $r = r_0$  provides a relationship between  $c_1$  and  $c_2$ :

$$c_2 = \frac{m}{n} c_1 r_0^{-m-n}. \quad (16)$$

For  $r = r_0$ , we have

$$\frac{\partial^2 B^2}{\partial z^2} = 2c_1^2 r_0^{-2m-2} \left( 1 + \frac{m}{n} \right)^2 (2 - mn). \quad (17)$$

Hence follows the condition for the existence of the field minimum with respect to  $z$ :

$$mn < 2. \quad (18)$$

Calculation of  $\partial^2 B^2 / \partial z^2$  at an arbitrary point  $r$  yields

$$\begin{aligned} & \frac{1}{2} \frac{\partial^2 B^2}{\partial z^2} = 2c_1^2 r^{-2m-2} (1 - m) + 2c_2^2 r^{2n-2} (1 + n) \\ & \quad + c_1 c_2 r^{n-m-2} [4 - 2(m - n) - (m + n)^2] \\ & = c_1^2 r^{-2m-2} \left\{ 2(1 - m) + \frac{m}{n} [4 - 2(m - n) - (m + n)^2] \left( \frac{r}{r_0} \right)^{m+n} + \right. \\ & \quad \left. + \frac{2m^2}{n^2} (1 + n) \left( \frac{r}{r_0} \right)^{2(m+n)} \right\}. \end{aligned} \quad (19)$$

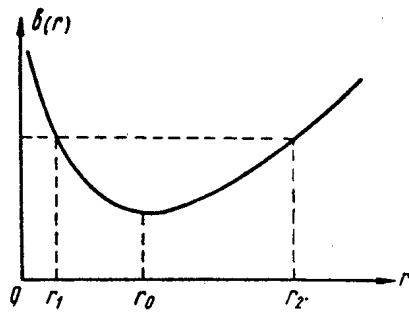


Fig. 1. Graph of the field in the median plane ( $z = 0$ ).

The latter expression, which is quadratic with respect to  $\left(\frac{r}{r_0}\right)^{m+n}$ , indicates that  $\frac{\partial^2 B^2}{\partial z^2}$  vanishes at the points  $r_s$ , which are determined by the expression:

$$\left(\frac{r_s}{r_0}\right)^{m+n} = \frac{n}{m} \left\{ -\frac{4-2(m-n)-(m+n)^2}{4(1+n)} \pm \sqrt{\left[\frac{4-2(m-n)-(m+n)^2}{4(1+n)}\right]^2 - \frac{1-m}{1+n}} \right\}. \quad (20)$$

Here, the expression under the radical sign will be negative if the following value is positive:

$$D \equiv 4 - 4(m-n) - (m+n)^2 > 0. \quad (21)$$

Thus, the requirement for the positive determinacy of the quadratic form (19) leads to the condition:

$$m < 2\sqrt{2(1+n)} - (2+n), \quad (22)$$

whence it follows that the maximum  $m$  value can occur for  $n = 1$ , in which case condition (22) becomes  $m < 1$ .

If  $m = n$ , inequality (21) is also reduced to the requirement for  $m < 1$ . In this case, the radii  $r_1$  and  $r_2$  (see Fig. 1) can be expressed simply in terms of the corresponding "mirror" field ratio  $\Pi = \frac{b(r_1)}{b(r_0)} = \frac{b(r_2)}{b(r_0)}$ :

$$\left. \begin{aligned} \frac{r_2}{r_0} &= (\Pi + \sqrt{\Pi^2 - 1})^{1/m}; \\ \frac{r_1}{r_0} &= (\Pi - \sqrt{\Pi^2 - 1})^{1/m}. \end{aligned} \right\} \quad (23)$$

If  $m = 1$ , the requirement (21) for the positive determinacy of the quadratic form (19) is too stringent, and it can be reduced by using  $m = 1$  and  $n = 1$ . It is readily seen that, even in this case,  $\partial^2 B^2 / \partial z^2$  never vanishes. If  $m = n = 1$ , the field under consideration exactly satisfies relationships (3) and is described by the scalar potential  $\Phi$  and the flux function  $\psi$ , which are respectively given by

$$\left. \begin{aligned} \Phi &= c_1 \ln \frac{r}{r_0} + c_2 \left( \frac{r^2}{2} - z^2 \right); \\ \psi &= -c_1 z - c_2 r^2 z. \end{aligned} \right\} \quad (24)$$

This field constitutes the superposition of a purely radial field on a quadripole field. The square of the modulus of the resultant field

$$B^2 = \left( \frac{c_1}{r} + c_2 r \right)^2 + 4c_2^2 z^2, \quad (25)$$

has a constant derivative  $\partial^2 B^2 / \partial z^2$ , while, at the field minimum, the derivatives  $\partial^2 B^2 / \partial r^2$  and  $\partial^2 B^2 / \partial z^2$  coincide. The position of the points  $r_1$ ,  $r_0$ , and  $r_2$  is defined in terms of  $\Pi$  by expression (23) for  $m = 1$ .

In principle, if the assigned field satisfies Eqs. (3), it can be produced by using two different methods. First, the iron poles of the magnets can be arranged along the equipotentials  $\Phi = \text{const}$ . The corresponding arrangement for the field (24) is shown in Fig. 2. Second, the surface currents  $i_\varphi (c/\pi) B$  can be arranged on the magnetic surfaces  $\psi = \text{const}$ . This method is equivalent to the use of ideally conducting surfaces. It is physically impossible to produce an infinitely strong field at the  $z$  axis. However, in the case of the field given by (24), instead of using the initial expression  $b(r) = \frac{c_1}{r} + c_2 r$  we can, for instance, assign the field for  $z = 0$  in the following form:

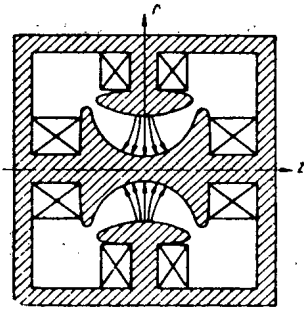


Fig. 2. A variant of the radial mirror trap with pole end-pieces.

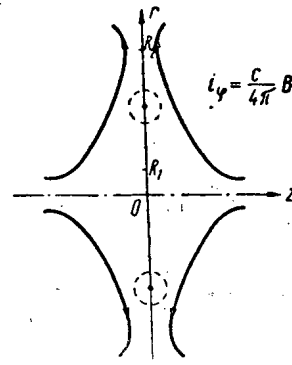


Fig. 3. Radial mirror trap, produced by means of surface currents.

$$b(r) = \frac{c_1 r}{R_1^2 + r^2} + \frac{c_2 r}{1 + r^2/R_2^2}, \quad (26)$$

where  $R_1 < r_0 < R_2$ . The change in the second term is not fundamental; it was made in order to reduce the currents necessary at large radii. It is readily seen that, if the condition  $R_1^2 \ll r_0^2 \ll R_2^2$  is satisfied, the field maximums in the median plane  $z = 0$  are secured for  $r_1 \approx R_1$  and  $r_2 \approx R_2$ , while, in the  $R_1 < r < R_2$  region, the corresponding field has about the same properties as the field (24). The arrangement of the surface currents necessary for producing such a field is shown schematically in Fig. 3.

#### LITERATURE CITED

1. J. Andreoletti, *Compt. rend Acad. sci., Paris*, 256, 1969 (1963).
2. H. Furth and M. Rosenbluth, *Phys. Fluids*, 7, 764, No. 5 (1964).
3. Yu. T. Baiborodov et al., *Atomnaya Énergiya*, 14, 443 (1963).
4. L. A. Artsimovich, *Controlled Thermonuclear Reactions* [in Russian], Moscow, Izd. AN SSSR (1961).
5. H. Furth, *Phys. Rev. Letters*, 11, 308 (1963).

SELF-CONSISTENT DISTRIBUTION OF PARTICLES  
AND LIMITING CURRENT IN A LINEAR ACCELERATOR

(UDC 621.384.62)

B. I. Bondarev and A. D. Vlasov

Translated from *Atomnaya Énergiya*, Vol. 19, No. 5,  
pp. 423-428, November, 1965

Original article submitted April 5, 1965

It is shown that the approximate representation of accelerated groups of particles as uniformly-charged ellipsoids is approximately self-consistent. This once more confirms the well-known expression for the limiting current in a linear accelerator on this concept. It is further shown that the approximation of the particle groups by cylinders, although not self-consistent, nevertheless gives an analogous expression for the limiting current, resulting in slightly overestimated values.

1. Statement of the Problem

The question of the limiting particle current attainable in the proton (or heavier-ion) linear accelerator has recently taken on special significance [1-4]. The current attainable is limited by the mutual repulsive effect of the space charge in the accelerated groups of particles. The simplest way to calculate this effect is that of representing the groups of particles as uniformly-charged ellipsoids, namely, ellipsoids of revolution for focusing by a longitudinal magnetic field (earlier papers of Ya. B. Fainberg, N. P. Selivanov, and others), and triaxial ellipsoids for quadrupole focusing (A. D. Vlasov [1]). This assumption leads to an expression for the limiting current closely agreeing with experiment [1, 4] and having the form [1, 2, 4].

$$I_M = \frac{3E_m R^2 \varphi_s \sin \varphi_s}{\gamma \lambda M_z} \cdot \frac{\tau S_M (1 - S_M)}{0.18} \quad (1)$$

Here  $I_M$  is the limiting current (averaged over the pulse) in A,  $E_m$  is the amplitude of the accelerating wave in kV/cm,  $\lambda$  and  $R$  are the wavelength and greatest radial dimension of the group of particles in cm;  $\gamma$  is the ratio of the largest and smallest semiaxes of the group,  $\varphi_s$  is the equilibrium phase,  $M_z$  is a coefficient depending on the form of the group,  $S$  is the ratio of the defocusing and phasing longitudinal forces for small phase oscillations, and  $S_M$  is the value of  $S$  at the maximum of  $S(1 - S)/M_z$ . Usually  $S_M = 0.3$  to  $0.4$ .

Certain doubts were expressed in [3] as to whether the assumption of a uniformly-charged ellipsoid were a sufficiently-close approximation to the self-consistent distribution of charge in the group, and also whether the relations derived from this assumption reflected the true behavior of the groups.

The charge distribution in the group depends on the form of the particle trajectories, which is determined not only by the external (accelerating and focusing) field but also by the internal field due to the charge in the group itself, i.e., the trajectories are determined by the space charge of the group of particles. In this respect the charge distribution should in fact be self-consistent (noncontradictory). Of course we are thinking of an established (stationary) distribution.

The problem of the self-consistent distribution of charge in the accelerated groups of particles is in general three-dimensional, and it is to this problem that the present paper is directed. As in [1-4], we shall neglect the fields due to neighboring groups, the effects of the sides of the accelerating system, and the charges on the electrons and ions of the residual gas. The longitudinal axes of the groups of particles will be regarded as coinciding with the axis of the accelerator.

## 2. Approximation of the Groups by Ellipsoids

We shall show that a uniform distribution of charge inside an ellipsoid is approximately self-consistent. Let  $X, Y, z$  be the accompanying system of coordinates, the axes of which coincide with the axes of the ellipsoid and the origin of which coincides with the equilibrium particle. A uniformly-charged triaxial ellipsoid is the only charge distribution for which the projections of the field on the coordinate axes  $X, Y,$  and  $z$  are independent of each other and are proportional to the individual coordinates. If the motion of the particles in the accelerating and focusing fields (in projection on the  $X, Y,$  and  $z$  axes) is described by linear, mutually-independent equations, then these equations remain the same on considering the field of the group itself as well.

We shall suppose approximately that the longitudinal oscillations of any of the particles are described by the equation:

$$z = z_m \cos(\Omega_1 t + \theta_z), \quad (2)$$

and the transverse oscillations for quadrupole focusing with a period  $L$  are described by the equations:

$$\left. \begin{aligned} X &= x_m \Phi_x(z_s) \cos(\Omega t + \theta_x); \\ Y &= y_m \Phi_y(z_s) \cos(\Omega t + \theta_y); \end{aligned} \right\} \quad (3)$$

in which the frequency of the transverse oscillations  $\Omega$  is the same for both  $X$  and  $Y$  axes and is not commensurable with the frequency of the longitudinal oscillations  $\Omega_1$ . In equation (3),  $z_s$  is the longitudinal coordinate of the center of the group in the laboratory system,  $\Phi_x$  and  $\Phi_y$  are periodic functions of  $z_s$  with period  $L$ , supposed normalized in such a way that  $\Phi_{x \max} = \Phi_{y \max} = 1$ . As usual, we suppose  $\Phi_y(z_s) = \Phi_x\left(z_s + \frac{L}{2}\right)$  and hence  $\Phi_{x \min} = \Phi_{y \min} = 1/\gamma$ . Equation (2) is approximately true if the amplitude of the phase oscillations is not too great. In Eq. (3) we neglect the dependence of the transverse on the longitudinal oscillations, and also the well-known periodic phase variation of the transverse oscillations with period  $L$  for quadrupole focusing [4]. This variation in phase is usually not large and vanishes as  $\gamma \rightarrow 1$ .

Since the transverse deviations of each particle are proportional to  $\Phi_x$  and  $\Phi_y$ , the transverse semi-axes of the group of particles may be written in the form

$$a_x = R\Phi_x(z_s); \quad a_y = R\Phi_y(z_s).$$

We shall consider that  $a_x a_y = R^2 \Phi_x \Phi_y \approx R^2 / \gamma = \text{const}$ ,  $a_z = \text{const}$  and  $\rho_0 = \text{const}$ , where  $\rho_0$  is the charge density in the group. Let us transform to variables  $x = X/\Phi_x(z_s)$  and  $y = Y/\Phi_y(z_s)$ . Then Eq. (3) takes on a simpler form:

$$x = x_m \cos(\Omega t + \theta_x); \quad y = y_m \cos(\Omega t + \theta_y). \quad (4)$$

In the variables  $x, y, z$ , the group of particles has the form of a uniformly-charged ellipsoid of revolution with constant radius  $R$ , length  $2a_z$ , and charge density  $\rho_0/\gamma$ . This ellipsoid is described by the equation

$$\frac{x^2 + y^2}{R^2} + \frac{z^2}{a_z^2} = 1. \quad (5)$$

The problem of self-consistency now reduces to finding a distribution of the particles following trajectories (2) and (4) with respect to the initial phases  $\theta_x, \theta_y, \theta_z$ , and amplitudes  $x_m, y_m, z_m$  such that the particles fill the ellipsoid with constant charge density  $\rho_0/\gamma$ .

Let us separate out of all the particles composing the group just those with a certain fixed value of  $z_m$ . These particles are enclosed within a circular cylinder inscribed in the ellipsoid and having length  $2z_m$  and radius  $R\sqrt{1 - (z_m/a_z)^2}$ . The probability of finding any of the particles in the section from  $z$  to  $z + dz$  is proportional  $|z|^{-1} dz \sim (z_m^2 - z^2)^{-1/2} dz$ . Let the particles be distributed uniformly with respect to phase  $\theta_z$ . Then the density of charge distribution for particles with given  $z_m$  is expressed (allowing for the axial symmetry of the ellipsoid) in the form:

$$\frac{N(r, z_m)}{\sqrt{z_m^2 - z^2}}, \quad (6)$$

where  $N$  is some function of  $r = \sqrt{x^2 + y^2}$  and  $z_m$ .

The total charge density  $\rho(r, z) = \rho_0/\gamma$  is expressed by the integral of the partial densities (6) with respect to all amplitudes  $z_m$  possible in ellipsoid (5) for given  $r$  and  $z$ :

$$N(r, z_m) = \frac{2Q_0}{\pi\gamma} \cdot \frac{z_m}{\sqrt{a_z^2 \left(1 - \frac{r^2}{R^2}\right) - z_m^2}}. \quad (7)$$

From this integral equation, which can easily be reduced to Abel's equation, we find:

$$\frac{Q_0}{\gamma} = \int_z^{a_z \sqrt{1 - (r/R)^2}} \frac{N(r, z_m) dz_m}{\sqrt{z_m^2 - z^2}}. \quad (8)$$

It remains to find a distribution of particles with given  $z_m$  with respect to the transverse-oscillation phases and amplitudes  $x_m, y_m, \theta_x, \theta_y$  such that the radial distribution of charge density is described by function (8). This problem has an infinite set of solutions. We shall now consider just two comparatively simple cases.

The first solution is that each of the particles, projected on the transverse plane, moves in a circle  $x^2 + y^2 = r^2$ . This occurs on condition that  $x_m = y_m = r_m, |\theta_x - \theta_y| = \pi/2$ , and also for a uniform distribution of particles with respect to phase  $\theta_x$  (and hence also  $\theta_y$ ), and for a distribution of particles with respect to  $r_m$  with a charge density  $2\pi r_m N(r_m, z_m)$ .

The second solution is less trivial. The transverse projection of the particle trajectory, according to (4), is an ellipse with semiaxes:

$$a, b = \frac{1}{2} \left( \sqrt{x_m^2 + y_m^2 + 2x_m y_m \sin |\theta_x - \theta_y|} \right. \\ \left. \pm \sqrt{x_m^2 + y_m^2 - 2x_m y_m \sin |\theta_x - \theta_y|} \right), \quad (9)$$

the angle between the largest of the axes of the ellipse and the  $x$  axis being

$$\eta = \frac{1}{2} \arctan \left[ \frac{2x_m y_m}{x_m^2 + y_m^2} \cos(\theta_x - \theta_y) \right]. \quad (10)$$

The probability of finding a particle in the cylindrical layer from  $r$  to  $r + dr$  equals  $4d(\Omega t)/2\pi = 2dr \frac{d(\Omega t)}{\pi dr}$ . Using Eqs. (4) and (9) we find:

$$\frac{2dr}{\pi dr/d(\Omega t)} = \frac{2r}{\pi \sqrt{a^2 - r^2} \sqrt{r^2 - b^2}}. \quad (11)$$

In view of the axial symmetry of the ellipsoid, the distribution of particles with respect to angle  $\eta$  [see expression (10)] should be uniform. Let us restrict the second solution by the condition that the large semiaxis  $a$  has the maximum value possible for the given  $z_m$  for all the particles:

$$a = R \sqrt{1 - \frac{z_m^2}{a_z^2}}. \quad (12)$$

Here the small semiaxes may vary from zero to  $a$ . Let the distribution of particles with respect to  $b$  be described by function  $n(b, z_m)$ . Then the charge density associated with particles of given  $z_m$  and fixed  $r$  is expressed by the integral of the product of function (11) and  $n(b, z_m)/2\pi r$  over all possible  $b$ . At the same time this density is expressed in the form (8) so that:

$$\frac{1}{\pi^2 \sqrt{a^2 - r^2}} \int_0^r \frac{n(b, z_m) db}{\sqrt{r^2 - b^2}} = \frac{2Q_0}{\pi \gamma} \cdot \frac{z_m}{\sqrt{a_z^2 \left(1 - \frac{r^2}{R^2}\right) - z_m^2}}$$

From this integral equation, which can also be easily reduced to Abel's equation we find, on taking account of expression (12):

$$n(b, z_m) = \frac{4Q_0 R}{\gamma a_z} z_m.$$

For focusing by a longitudinal magnetic field we can also find a self-consistent distribution analogous to that obtained here.

### 3. Self-Consistent Solution for Axial Particles Only

The following assumptions are made in [3]:

- 1) transverse oscillations of the particles may be neglected;
- 2) the group of particles forms a circular cylinder in which the charge density is constant with respect to  $r$  and depends only on  $z$  (on the phase  $\varphi$ );
- 3) the density of the distribution in the phase plane  $\psi = \varphi - \varphi_s$ ,  $q = \dot{\varphi} - \dot{\varphi}_s$  is constant within the separatrix;
- 4) the problem of self-consistency is formulated only for particles lying on the axis of the group.

The second and third assumptions limit the possible distributions of charge in the group so severely that a self-consistent (noncontradictory) distribution is impossible. In essence the authors themselves acknowledge this (see fourth assumption).

We note that the density of the stationary distribution in the phase plane  $\psi$ ,  $q$ , between any two neighboring phase trajectories is constant [5]. Hence it is more logical to operate not with a distribution in the  $\psi$ ,  $q$ , plane but with the distribution of particles with respect to the oscillation amplitudes  $\psi_m$  (see Section 2).

On the basis of the assumptions indicated, the authors of [3] obtained the following equation for the potential function of the longitudinal oscillations, denoted by  $\alpha\Phi(\psi)$ :

$$\alpha\Phi(\psi) = F(\psi) + k_0 \int_{\psi_c}^{\psi_k} \left[ \sqrt{b^2 + (\alpha - \psi)^2} - |\alpha - \psi| \right] \times \frac{\sqrt{1 - \Phi(\alpha)}}{\sqrt{1 - \Phi(\psi_0)}} d\alpha. \quad (13)$$

Here

$$F(\psi) = 1 - \cos \psi + (\psi - \sin \psi) \cotan \varphi_s \quad (14)$$

is the potential function in the absence of intrinsic charge,  $\varphi_s$  and  $\varphi_s + \psi_0$  are the equilibrium phases in the absence and presence of charge, respectively,  $\psi_c$  and  $\psi_k$  are the extreme values of  $\psi$  for the separatrix:

$$b = \frac{2\pi r_0 \sqrt{1 - \beta^2}}{\beta \lambda}; \quad k_0 = \frac{Q_0 \beta \lambda}{E_m \sin \varphi_s}, \quad (15)$$

where  $r_0$  is the radius of the group,  $\beta = v/c$  ( $v$  = velocity of the particle,  $c$  = velocity of light), and  $\rho_0$  is the charge density for  $\psi = \psi_0$  (in the laboratory system of coordinates). The values of  $\psi_0$ ,  $\psi_c$ ,  $\psi_k$  are determined from the equations:

$$\left. \begin{aligned} \Phi'(\psi_0) = \Phi'(\psi_c) = 0; \quad \Phi''(\psi_0) > 0; \\ \Phi''(\psi_c) < 0; \quad \Phi(\psi_k) = \Phi(\psi_c). \end{aligned} \right\} \quad (16)$$

The constant  $a$  for each value of current is determined from the equation

$$\Phi(\psi_k) = 1. \quad (17)$$

The average pulse current is expressed in the form

$$I = \frac{cQ_0}{\lambda} \pi r_0^2 \frac{\beta \lambda}{2\pi} \int_{\psi_c}^{\psi_k} \frac{\sqrt{1-\Phi(\alpha)}}{\sqrt{1-\Phi(\alpha_0)}} d\alpha. \quad (18)$$

In [3] Eq. (13) is solved on an electronic computer and only for the particular case

$$E_m = 15.6 \text{ kV/cm} \quad \lambda = 200 \text{ cm} \quad \varphi_s = 37^\circ; \\ \beta = 0.0387; \quad r_0 = 0.5 \text{ cm}. \quad (19)$$

In order to obtain a clearer, though approximate, solution of Eq. (13), let us represent the functions  $F(\psi)$ ,  $\Phi(\psi)$  and the integral in expression (13) by polynomials of the third degree:

$$F(\psi) \approx \frac{\psi^2}{2} + \frac{\psi^3}{6\varphi_s} = \frac{\psi_0^2}{2} + \frac{\psi_0^3}{6\varphi_s} + \left( \psi_0 + \frac{\psi_0^2}{2\varphi_s} \right) \\ \times (\psi - \psi_0) + \left( \frac{1}{2} + \frac{\psi_0}{2\varphi_s} \right) (\psi - \psi_0)^2 + \frac{(\psi - \psi_0)^3}{6\varphi_s}; \quad (20)$$

$$\Phi(\psi) \approx A_0 + A_1(\psi - \psi_0) + A_2(\psi - \psi_0)^2 \\ + \frac{A_3}{3\varepsilon\varphi_s}(\psi - \psi_0)^3; \quad (21)$$

$$\int_{\psi_c}^{\psi_k} \dots d\alpha \approx B_0 + B_1(\psi - \psi_0) + B_2(\psi - \psi_0)^2 + \frac{B_3}{3\varepsilon\varphi_s}(\psi - \psi_0)^3. \quad (22)$$

Here  $A_0 = \Phi(\psi_0)$ ,  $A_1$ ,  $A_2$ ,  $\varepsilon$ ,  $\psi_0$  are unknown constants. The function  $F(\psi)$  in the approximate form (20), just as in the exact expression (14), has a minimum at  $\psi = 0$ , a maximum at  $\psi = \psi_c = -2\varphi_s$ , and a value equal to the maximum at  $\psi = \psi_k = \varphi_s$ . Substituting (21) into Eq. (16), we find  $A_1 = 0$  and establish that the function  $\Phi(\psi)$ , which has a minimum at  $\psi = \psi_0$ , reaches a maximum at  $\psi = \psi_c = \psi_0 - 2\varepsilon\varphi_s$  and a value equal to the maximum at  $\psi = \psi_k = \psi_0 + \varepsilon\varphi_s$ . Thus the space charge leads to a shortening of the longitudinal dimensions of the separatrix, proportional to  $\varepsilon$  (for the ellipsoidal approximation to the groups of particles these diminish in proportion to  $1 - S$ ). Putting expressions (20)-(22) into (13) and (17), we obtain

$$\left. \begin{aligned} aA_0 &= k_0B_0 + \frac{\psi_0^2}{2} + \frac{\psi_0^3}{6\varphi_s}; \quad 0 = k_0B_1 + \psi_0 + \frac{\psi_0^2}{2\varphi_s}; \\ aA_2 &= k_0B_2 + \frac{1}{2} + \frac{\psi_0}{2\varphi_s} = k_0B_3 = \frac{\varepsilon}{2}; \\ 1 - A_0 &= \frac{4}{3} A_2 \varepsilon^2 \varphi_s^2. \end{aligned} \right\} \quad (23)$$

From these five equations it is not difficult to find  $a$ ,  $A_0$ ,  $A_2$ ,  $\varepsilon$ ,  $\psi_0$ . Then, using Eqs. (18), (21), and (23), we obtain

$$\frac{\sqrt{1-\Phi(\psi)}}{\sqrt{1-\Phi(\psi_0)}} = \left( 1 + \frac{\psi - \psi_0}{2\varepsilon\varphi_s} \right) \sqrt{1 - \frac{\psi - \psi_0}{\varepsilon\varphi_s}}; \\ I = \frac{2\sqrt{3}}{5} \beta cQ_0 \pi r_0^2 \frac{3\varepsilon\varphi_s}{2\pi}. \quad (24)$$

Expressing  $\rho_0$  in terms of  $k_0$  from expression (15) and  $k_0$  in terms of  $B_3 - B_2$  from (23), we have

$$I = \frac{3.12 E_m r_0^2 \varphi_s \sin \varphi_s}{\lambda M_z} \cdot \frac{\varepsilon \left( 1 - \varepsilon + \frac{\psi_0}{\varphi_s} \right)}{0.18}, \quad (25)$$

where  $M_z = B_3 - B_2$ . Equation (25) is written in the same system of units as (1); the coefficients in these expressions



differ by 4%. Otherwise these equations coincide, if we remember that  $\psi_0/\varphi_s$  is small in comparison with  $1 - \varepsilon$ , put  $r_0^2 = R^2/\gamma$ ,  $\tau = 1$ ,  $\varepsilon = 1 - S$ , and replace  $\varepsilon \left(1 - \varepsilon + \frac{\psi_0}{\varphi_s}\right)/M_z$  by its maximum value. In order to calculate the coefficients  $B_i$ , which depend on  $\varepsilon$ , we must substitute the value of  $\sqrt{1 - \Phi(\psi)}$  from (24) into the integrand of Eq. (13) or (22) and carry out the integration (preferably numerically) for four values of  $B_i$  equal to  $2\varepsilon\varphi_s$ ,  $-\varepsilon\varphi_s$ ,  $0$ ,  $\varepsilon\varphi_s$ . From the four values of the integral (for each value of  $\varepsilon$ ) the coefficients  $B_i$  in expression (22) are calculated. In particular, for  $\varphi_s = 37^\circ$  and  $b = 0.4$  we find that:

$$\begin{array}{cccccc} 1 - \varepsilon \approx S & . . . . . & 0 & 0.193 & 0.379 & 0.627 & 0.814 & 1 \\ M_z = B_3 - B_2 & . . . . . & 0.076 & 0.109 & 0.151 & 0.255 & 0.409 & 1 \\ \varepsilon \left(1 - \varepsilon + \frac{\psi_0}{\varphi_s}\right) / M_z & & 0 & 1.423 & 1.560 & 0.922 & 0.370 & 0. \end{array}$$

The expression for the limiting current (1) obtained on the basis of the elliptical approximation for the groups, applied to the case (19) with  $R^2/\gamma = r_0^2$  and  $\tau = 1$ , gives  $I_M = 127$  mA, with  $S_M = 0.34$  and  $M_z = 0.222$ . At the same time expression (25), based on the cylindrical (nonself-consistent) approximation, gives  $I_M = 210$  mA, i.e., 65% larger, with  $1 - \varepsilon_m = 0.3$  and  $M_z = 0.130$ . We note that in [3], for the same initial parameters, the obviously too-high value of  $I_M = 0.6 I_0 = 400$  mA was obtained. The calculations made on the electronic computer in [3] were not taken up to the value of  $h_\varphi = 1$  (corresponding to  $S = 1$ ,  $\varepsilon = 0$ ), and were only extrapolated to this value in an arbitrary fashion. Hence the conclusion drawn in [3] that the current reaches a maximum at  $h_\varphi = 1$  and that the space charge has little effect on the region of phase stability is unfounded. Actually at  $h_\varphi = 1$  ( $\varepsilon = 0$ ) the region of phase stability and the particle current vanish.

#### SUMMARY

The representation of accelerated groups of particles as uniformly-charged ellipsoids, used in deriving expression (1) for the limiting current, is approximately self-consistent, as shown in Section 2. In addition to its simplicity and computing advantages, this representation may be regarded as a fairly good approximation, and expression (1), confirmed as it is by experiment, is well-founded.

Naturally, further refinement of the form of the self-consistent charge distribution in the groups is required. For any charge distribution differing from the uniformly-charged ellipsoid, however, the equations of motion of the particles for the X, Y, and z axes are not only nonlinear but interlinked. This complicates the problem considerably. For example, attempts to consider the longitudinal motion independently of the radial (see Section 3) make self-consistency impossible and cannot be successful.

The solution of the self-consistency problem is not unique. At the very beginning certain arbitrary (more or less probable) assumptions were made regarding the distribution of charge in the group (see Section 2) or the distribution in the phase plane (see Section 3). Even then (as in Section 2 for example), an infinite set of self-consistent distributions is possible, rather than one only. Evidently this multiplicity of solutions is retained in the more general case when the motion along the three axes is interconnected.

In conclusion we note that the two extremely different approaches used in [1-3], one of them even excluding self-consistency (see Section 3), lead to expressions for the limiting current (1), and (25), coinciding in form and only slightly differing in the quantitative respect.

#### LITERATURE CITED

1. A. D. Vlasov, Limitation of Particle Current in a Linear Accelerator with Quadrupole Focusing [in Russian], RAIAN SSSR, NT 2460-33 (1960).
2. Theory and Calculation of Linear Accelerators [in Russian], Moscow, Gosatomizdat (1962), pp. 94, 114.
3. I. M. Kapchinskii and A. S. Kronrod, "Pribory i tekhnika éksperimenta," No. 3, 26 (1964).
4. A. D. Vlasov, Theory of Linear Accelerators [in Russian], Moscow, Atomizdat (1965).
5. C. Nielsen and A. Sessler, Rev. Scient. Instrum., 30, 80 (1959).

USE OF TIME INTEGRATION TO CALCULATE  
THE DIFFERENTIAL SCATTERING CROSS SECTIONS OF SLOW NEUTRONS

(UDC 539.125.525)

V. F. Turchin

Translated from *Atomnaya Énergiya*, Vol. 11, No. 5,  
pp. 428-432, November, 1965  
Original article submitted May 6, 1965

A method is suggested for calculating the differential cross sections for scattering of slow neutrons by bound atoms, by integrating the Van Hove formula with a cutoff factor under the integral sign, thus getting an average of the cross section over some energy range; this may in turn be used to compare the theoretical and experimental data. By this method it is possible to calculate the differential cross section for a liquid by means of a model previously suggested by the author. Calculations for water and ice near its melting point disclose the presence of a discontinuity in the total cross section at the ice-water transition; this agrees with the experimental data of Heinloth.

The Cutoff Factor

In the non-coherent Gaussian approximation, the twice-differentiated cross section for scattering of slow neutrons by bound atoms can be written as follows:

$$\frac{d^2\sigma}{d\Omega dE} = \sigma_0 \frac{(\mu + 1)^2}{4\pi\mu^2} \left(\frac{E}{E_0}\right)^{1/2} e^{\varepsilon/2T} \tilde{S}(q, \varepsilon). \quad (1)$$

Here  $\sigma_0$  is the cross section for scattering by a free nucleus,  $\mu$  is the mass of the atom as a multiple of the neutron mass,  $E_0$  and  $E$  are the energies of the neutron before and after scattering,  $T$  is the temperature of the scattering medium, and

$$\left. \begin{aligned} \varepsilon &= E_0 - E; \\ q &= \frac{1}{\mu} (E_0 + E - 2 \cos \theta \sqrt{E_0 E}), \end{aligned} \right\} \quad (2)$$

where  $\theta$  is the angle of scattering.

The symmetrized scattering law  $\tilde{S}(q, \varepsilon)$  can be written as a Fourier integral,

$$\tilde{S}(q, \varepsilon) = \frac{1}{2\pi} \int_{-\infty}^{\infty} e^{-q\gamma(t)} \cos \varepsilon t dt \quad (3)$$

in terms of the real even function  $\gamma(t)$ , which represents the dispersion of the Van Hove quantum autocorrelation function [1] in terms of the complex time  $t$ , the real part of which is the physical time, the imaginary part being  $1/2 T$  (putting Planck's constant  $\hbar = 1$ ).

For a symmetrical crystal,

$$\gamma_{cr}(t) = \gamma_{cr}(\infty) - \int_{-\infty}^{\infty} \frac{g_1(\omega)}{2\omega \operatorname{sh} \frac{\omega}{2T}} \cos \omega t d\omega. \quad (4)$$

Here

$$\gamma_{cr}(\infty) = \int_{-\infty}^{\infty} \frac{g_1(\omega)}{2\omega \operatorname{th} \frac{\omega}{2T}} d\omega, \quad (5)$$

$g_1(\omega)$  is the vibration spectrum of the atom, which [2] can be written as

$$g_1(\omega) = r \langle |\xi(\omega)|^2 \rangle g(\omega), \quad (6)$$

where  $r$  is the number of atoms in the unit cell,  $\langle |\xi(\omega)|^2 \rangle$  is the mean square modulus of polarization of the vibration vector with frequency  $\omega$ , and  $g(\omega)$  is the spectrum of normal vibrations of the crystal.

The conventional method for calculating the scattering law is as follows: for small  $q$  the exponential under the integral sign in (3) is expanded in powers of  $q$  (which is equivalent to expanding the cross section in the number of photons emitted or absorbed during scattering), while the large  $q$  (for which the expansion is poorly convergent) an asymptotic formula [3, 4] is used. Direct calculation of the scattering law by integration with respect to  $t$  in (3) would have a number of advantages which will be explained below; however, this operation meets certain difficulties due to the necessity of calculating the integrals over an infinite range of an oscillating and slowly decreasing function.

Let us try to improve the convergence: for this purpose we shall add the "cutoff factor"  $\exp\{-\delta^2 t^2/2\}$  under the integral sign in (3). We shall designate the scattering law thus found by

$$\tilde{S}'(q, \varepsilon) = \frac{1}{2\pi} \int_{-\infty}^{\infty} e^{-qV(t)} e^{-\delta^2 t^2/2} \cos \varepsilon t dt. \quad (7)$$

By the properties of the Fourier transform,  $\tilde{S}'(q, \varepsilon)$  will be a convolution of the true scattering law and the Fourier transform of the cutoff factor, i.e.,

$$\tilde{S}'(q, \varepsilon) = \int_{-\infty}^{\infty} \tilde{S}(q, \varepsilon') \frac{1}{\sqrt{2\pi\delta^2}} \exp\left\{-\frac{(\varepsilon - \varepsilon')^2}{2\delta^2}\right\} d\varepsilon'. \quad (8)$$

The addition of the cutoff factor considerably simplifies the evaluation of the integral. It is true that the result is not the true scattering law, but the law averaged over an energy range of order  $\delta$ . But this is not a very serious defect, because, if we choose  $\delta$  small by comparison with the smallest characteristic energies of the vibration spectrum, the averaging will not significantly alter the law of scattering. To calculate cross sections for use in neutron-spectrum calculations, a less restrictive requirement can be imposed on  $\delta$ , it need only be small by comparison with the mean square energy losses in inelastic scattering. And if we wish to calculate the second differential of the cross section for comparison of theory with experiment, this drawback becomes a positive advantage. In fact, the experimental cross section is always averaged over the resolution width of the apparatus. So if we choose an appropriate value of  $\delta$ , we can avoid having to average the theoretical cross section, and we can compare the theoretical results directly with experiment. This of course involves a certain approximation to the actual value, since, strictly speaking the experimentally found cross section

$$\sigma_{exp}(E_0 \rightarrow E, \theta) = \int \sigma(E'_0 \rightarrow E', \theta') \varphi_1(E_0 - E'_0) \varphi_2(E - E') \varphi_3(\theta - \theta') dE'_0 dE' d\Omega', \quad (9)$$

which cannot be expressed exactly in terms of  $\tilde{S}'(q, \varepsilon)$ . However, provided that the resolution is not too poor, and that  $\varphi_1$ ,  $\varphi_2$ , and  $\varphi_3$  are nearly Gaussian in form, we can always choose a value for  $\delta$  which adequately represents averaging over energy  $\delta$  in (9). Averaging over  $q$ , which of course occurs in (9), is usually much less important than averaging over  $\varepsilon$ , and if necessary can be performed in addition.

By calculating the scattering cross sections by direct integration w.r. to time, we can represent the scattering of neutrons in a liquid by means of a model suggested by the author in simplified form in [5] and in more complete form in [2]. This model is based on the assumption that the movement of atoms in a liquid is like a rapid vibration superimposed on continuous diffusion movement; it leads to the following form of  $\gamma(t)$  for a liquid:

$$\frac{1}{\gamma_{cr}(t)} = \frac{1}{\gamma_{cr}(t)} - \frac{1}{\gamma_{cr}(\infty)} + \frac{1}{\gamma_{cr}(\infty) + \frac{4MD}{h} \left( t^2 + \frac{1}{4T^2} \right)^{1/2}} \quad (10)$$

Here  $M$  is the mass of the atom,  $D$  the self-diffusion coefficient of the liquid, and the function  $\gamma_{crit}(t)$  is found from (4) and (5), where  $g_1(\omega)$  must be understood as the spectrum of vibracy motion of atoms in the liquid.

To calculate the spectra of slow neutrons, we must know the differential w.r.t. energy of the scattering cross section,

$$\sigma(E_0 \rightarrow E) = \int \frac{d^2\sigma}{d\Omega dE} d\Omega \quad (11)$$

and the first angular moment,

$$\sigma_1(E_0 \rightarrow E) = \int \frac{d^2\sigma}{d\Omega dE} \cos \theta d\Omega \quad (12)$$

In calculating the cross section by integration with respect to time, the integration with respect to  $d\Omega$  can be performed analytically. From (1) and (3) we find:

$$\sigma(E_0 \rightarrow E) = \sigma_0 \frac{(\mu+1)^2}{4\pi\mu E_0} e^{\varepsilon/2T} \times \int_0^\infty \frac{[e^{-a\gamma(t)} - e^{-b\gamma(t)}]}{\gamma(t)} \cos \varepsilon t dt; \quad (13)$$

$$\begin{aligned} \sigma_1(E_0 \rightarrow E) &= \frac{E_0 + E}{2\sqrt{E_0 E}} \sigma(E_0 \rightarrow E) - \sigma_0 \frac{(\mu+1)^2}{8\pi E_0 \sqrt{E_0 E}} e^{\varepsilon/2T} \\ &\times \int_0^\infty \frac{1}{\gamma(t)} \left\{ \left[ a + \frac{1}{\gamma(t)} \right] e^{-a\gamma(t)} - \left[ b + \frac{1}{\gamma(t)} \right] e^{-b\gamma(t)} \right\} \cos \varepsilon t dt. \end{aligned} \quad (14)$$

Consequently the evaluation of these cross sections, like that of the second-differential cross section, reduces to evaluation of a Fourier integral, which can be performed by introducing a "cutoff factor."

#### Brief Description of the Algorithm

For calculating  $\frac{d^2\sigma}{d\Omega dE}$ ,  $\sigma(E_0 \rightarrow E)$  and  $\sigma_1(E_0 \rightarrow E)$  by the above method, an algorithm has been devised and is known as Program for Calculating Cross Section by Integration with Respect to Time [Russian acronym "PRASSIV\*"]: it begins with calculation and storage of the function  $\gamma(t)$  and its derivative  $\gamma'(t)$  at  $N_t$  reference points with constant spacing  $h_t$ . In calculating  $\gamma(t)$ , provision is made for possible approximate allowance for Einstein vibrations with high frequency  $\omega_0$ , which are not excited during scattering. The influence of these vibrations on  $\gamma(t)$  is eliminated firstly by adding a term (variation of thermal factor) which is constant for a crystal and varies smoothly for a liquid; and secondly by adding a small-amplitude "flicker" with frequency  $\omega_0$  which leads to a transition with an energy change which is a multiple of  $h\omega_0$ . If  $T \ll h\omega_0$  and we are interested in energy changes below  $h\omega_0$ , this "flicker" can be removed from consideration.

The spectrum of vibrations to which the exact calculation is applicable is given at  $N_\omega$  reference points with constant spacing  $h_\omega$ . It can be given as a function  $g_1(\omega)$ , or alternatively as a function

$$\tilde{f}(\omega) = \frac{g_1(\omega)}{2\omega \operatorname{sh} \frac{\omega}{2T}} \quad (15)$$

In calculating  $\gamma(t)$  it is assumed that  $f(\omega)$  is a broken line consisting of straight segments joining the values of

\*Publisher's Note.

$\tilde{f}(\omega)$  at the reference points. This enables us to calculate  $\gamma(t)$  and  $\gamma'(t)$  at the reference points analytically in terms of  $t$ . The value of  $\gamma(t)$  at an arbitrary point  $t$  is calculated by means of a special interpolation subroutine which replaces  $\gamma(t)$  by a third-degree polynomial which has the same value and the same derivative as  $\gamma(t)$  at two neighboring reference points.

The value of  $\delta$ , which characterizes the range of averaging over energy, is determined in calculating  $d^2\sigma/d\Omega dE$  by the formula

$$\delta = A_1^2 + (A_2 E_0^{3/2})^2 + (A_3 E^{3/2})^2, \quad (16)$$

where  $A_1$ ,  $A_2$ , and  $A_3$  are arbitrary coefficients. This determination of  $\delta$  enables us to carry out the calculation either with constant resolution, or with resolution proportional to  $E^{3/2}$ , which corresponds to a real spectrometer (the coefficients  $A_2$  and  $A_3$  are determined from the resolution of the spectrometer at the initial and final neutron energies).

In calculating  $\sigma(E_0 \rightarrow E)$  and  $\sigma_1(E_0 \rightarrow E)$  the value of  $\delta$  is given by the formula:

$$\delta = B_1 + B_2 E_0 + B_3 E, \quad (17)$$

which allows for  $\delta$  increasing proportionally to the energy. This is reasonable, because at high neutron energies the energy scale is determined by the value of the energy itself, and not by the frequencies of the vibration spectra, and therefore it is not necessary to choose such small values of  $\delta$  as at low energies.

Integration with respect to  $t$  is performed in one of two ways, depending on the relation between the characteristic time  $1/|\varepsilon|$  of the cosine curve and the characteristic time  $t_1$  of the integrand.  $t_1$  is taken as the least out of the following three quantities: 1)  $1/\omega_{\max}$  = minimum characteristic time of  $\gamma(t)$ ; 2)  $[q \gamma''(0)]^{-1/2}$  = characteristic time of  $\exp\{-q\gamma(t)\}$  at very large  $q$ ; 3)  $1/\delta$  = characteristic time of cutoff factor

$$\frac{1}{|\varepsilon|} > \alpha t_1, \quad (18)$$

we can integrate by Simpson's rule with interval  $t_1/H$  ( $H$  can be varied). If (18) does not hold, the integral is evaluated as a sum of integrals of half-wave cosine curve, each of which is calculated from Gauss's formula with  $n = 6$ . To shorten the calculations,  $\alpha$  (which is of order unity) can be varied.

For economy in the use of subroutines, the cutoff factor and  $\cos \varepsilon t$  are calculated from values of the trigonometrical and exponential functions at the preceding point.

Integration with respect to  $t$  is terminated when the cutoff factor becomes less than a given value  $\varepsilon$  or when  $t$  reaches its maximum value  $t_{\max} = N_t \cdot h_t$ . The limitation imposed on the length of the main part which stores the function  $\gamma(t)$ , i.e., on  $N_t$ , imposes a limitation from below on  $\delta$  (it assumed that the cutoff factor continues to operate to the end of the main part).

For a crystal ( $D = 0$ , for which  $\gamma(t)$  tends to its ultimate limit as  $t \rightarrow \infty$ ), we subtract from the integrand its limiting value and thus calculate only the cross section for inelastic scattering. The cross section for elastic scattering is found separately. For a liquid ( $D > 0$ ) all scattering is inelastic.

This algorithm was used as a basis for the "PRASSIV-1" computer program for calculating  $\sigma(E_0 \rightarrow E)$  and  $\sigma_1(E_0 \rightarrow E)$ , and for the "PRASSIV-2" program for computing  $d^2\sigma/d\Omega dE$ .

#### Changes in Scattering Cross Section Due to Melting of a Crystal

The author of [6] measured the total cross section for scattering of neutrons by water as a function of the temperature and state of aggregation. He found that when ice undergoes transition to water at  $0^\circ\text{C}$ , there is a discontinuous change in the total cross section for very slow neutrons; on further increase of temperature this cross section increases nonlinearly, rising very rapidly by comparison with the weak linear dependence of the total scattering cross section for ice.

When ice melts, its temperature remains constant, and thus the motions of its atoms (which can be typified as "rapid" or "crystalline") should not change very much. The essential changes are the disappearance of long-range

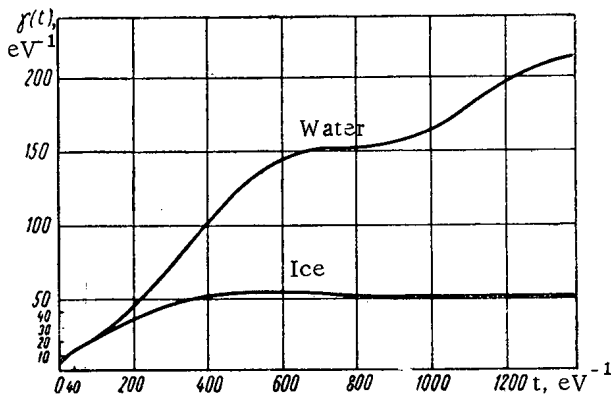


Fig. 1.  $\gamma(t)$  for motion of hydrogen atom in water at  $0^\circ\text{C}$  in the solid and liquid states.

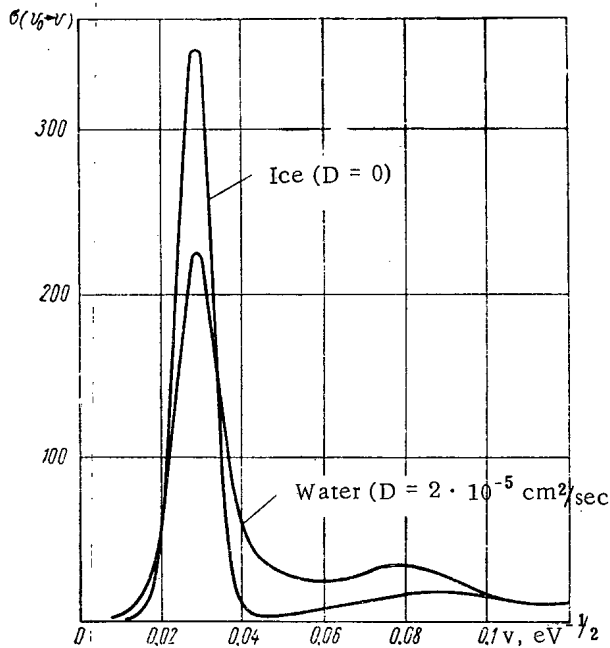


Fig. 2. Differential cross sections for scattering of neutrons by water and ice.

We deliberately chose a resolution comparable with the quasi-elastic broadening  $\Delta$ , and in the second place, to the appearance of marked additional scattering with final neutron velocity  $0.05\text{--}0.1\text{ eV}^{1/2}$ , which corresponds to acquisition by the neutron of energy averaging about  $0.005\text{ eV}$ . It is this additional scattering which leads to the step-wise increase of total cross section during melting. The appearance of additional inelastic scattering with low energy transfer is explained by the fact that in the presence of diffusion motion  $\gamma(t)$  rises rapidly with time (see Fig. 1), i.e., the atoms become as it were less rigidly bonded, in contrast to their firm bonding in the crystal.

We calculated that the increase on melting of the total scattering cross section should be about 18 barn: the experimental value is about 25 barn. There is thus a qualitative agreement between theory and experiment. Considering that the vibration spectrum and autodiffusion coefficient are very approximate, we cannot expect more than this qualitative agreement. Further experimental and theoretical work is undoubtedly needed on the scattering of neutrons by liquids.

#### LITERATURE CITED

1. L. Van Hove, Phys. Rev., 95, 249 (1954).
2. V. F. Turchin, Slow Neutrons [in Russian], Moscow, Gosatomizdat (1963).

order in the positions of the molecules and the appearance of diffusion motion leads to an abrupt change in the total cross section for neutron scattering; this cannot be ascribed to transition from elastic to quasi-elastic scattering, since, in the first place, the integral is unaffected by replacing the  $\delta$  function by the Lorentz function, and, in the second place, the magnitude of the discontinuity in the total cross section varies markedly with the initial neutron energy (approximately as  $1/v$ ), showing that it is due to inelastic scattering.

By means of our model of diffusion motion of atoms in in a liquid (as used in the PRASSIV algorithm), we can study the effect of diffusion on inelastic neutron scattering without the interference of other factors. For this purpose we need only calculate the differential and total scattering cross sections at a given temperature  $T$  and either with  $D \neq 0$  (liquid) or  $D = 0$  (crystal). Such calculations were made for water-ice at  $0^\circ\text{C}$  by means of the PRASSIV-1 program. The vibration spectrum of the hydrogen atom was taken from [7], and the coefficient of self-diffusion for water was taken, following [8], as  $2 \cdot 10^{-5}\text{ cm}^2/\text{sec}$ .

Figure 1 plots  $\gamma(t)$  for ice and water. To make it easier to assess the effect of scattering times on the scattering law, the times are plotted in reciprocal electron volts. It is seen that for  $t \leq 50\text{ eV}^{-1}$  diffusion has practically no effect on the form of  $\gamma(t)$ , and consequently with  $\delta \geq 0.02$  there will be no detectable effect of diffusion. For a crystal,  $\gamma(t)$  tends to a constant limit at large  $t$ , while for a liquid it is roughly proportional to  $t$ .

Figure 2 plots the differential cross sections  $\sigma(v_0 \rightarrow v)$  for ice and water. The scale is of velocities  $v = \sqrt{E}$  instead of the more usual energies, so as to cover a wide energy range on the same graph. For the initial energy  $E_0 = 0.00078\text{ eV}$ ,  $v_0 = 0.028\text{ eV}^{1/2}$ . The breadth of the resolution function  $\delta$  was taken as  $0.0002\text{ eV}$ . It will be seen that the appearance of diffusion motion of the atoms leads, in the first place, to shortening and broadening of the elastic peak (in our case these effects are slight because we

3. M. Nelkin and D. Parks, Phys. Rev., 119, 1060 (1960).
4. P. Egelstaff and P. Schofield, Nucl. Sci. Engng, 12, 260 (1962).
5. V. F. Turchin, Inelastic Scattering of Neutrons in Solids and Liquids, Vienna (1961), p. 259.
6. K. Heinloth, Z. Phys., 163, 218 (1961):
7. P. Egelstaff et al., Inelastic Scattering of Neutrons in Solids and Liquids, Vienna (1963), V. I, p. 343.
8. D. Cribier and B. Jackrot, J. phys. et radium, 21, 69 (1960).

## THE HYDRATION OF CATIONS IN HEAVY WATER

(UDC 542.934 : 546.212.02)

V. M. Vdovenko, Yu. V. Gurikov, and E. K. Legin

Translated from *Atomnaya Énergiya*, Vol. 19, No. 5,

pp. 433-437, November, 1965

Original article submitted January 28, 1965

The authors use a molecular-kinetic description of the two-layer hydration model to analyze the isotopic differences of free energy and enthalpy of solution in aqueous and heavy-water solutions of alkali-metal halides. They discuss the lifetimes and water-molecule densities in the secondary hydration layer. They show that the ions undergo dehydration in heavy-water solutions. They show that the differences between the free energies and enthalpies of solution in light and heavy water should increase with the cation radius, i.e., from  $\text{Li}^+$  to  $\text{Cs}^+$ . Their results agree with the experimental data.

Practical and theoretical interest attaches to the changes in the physicochemical properties of water occasioned by substituting deuterium for hydrogen: so far there has been no complete explanation of the observed differences between the thermodynamic properties of light and heavy water. Special attention is deserved by the marked difference between the solvent capacities of light and heavy water—the solubilities of salts are lower in heavy water, the isotope effect sometimes reaching 25-30% [1], while the heats of solution have greater absolute values in heavy water [2]. Ions are more easily extracted and sorbed from heavy water by ion-exchange media [3, 4].

The explanation seems to lie in the structural differences between  $\text{H}_2\text{O}$  and  $\text{D}_2\text{O}$ . The thermodynamic properties and structure of water are well represented by Samoilov's model [5, 6], in which the arrangement and short-range order of the molecules in water are regarded as identical with those in ice [1]. In heavy water, as compared with light water, there is a smaller proportion of unfilled vacancies, the molecules have lower mobility, and the deuterium bonds are stronger [7, 8]. On the whole, heavy water is more like ice in its structure and the nature of the thermal motion of its molecules. In this sense we can say that it is more structured than light water.

In considering the thermodynamic equilibrium between the two states of water in a salt solution (i.e., as ionic hydration shells or in the main residual bulk which is not disturbed by the ionic field), it is easy to see that strengthening of the structure will displace the equilibrium by removing water molecules from the hydration shells. The isotope effects mentioned above can be explained by the weakened ionic hydration in heavy water.

The connection between hydration and solvent structure is easily established on the basis of Samoilov's molecular-kinetic ideas [6]. An important characteristic of hydration is the ratio between the time during which water molecules remain as nearest neighbors of an ion ( $\tau_1$ ) to the lifetime around the equilibrium position ( $\tau$ ), in the undisturbed solvent:

$$\frac{\tau_1}{\tau} = e^{\frac{E_i - E_H}{RT}}, \quad (1)$$

where  $E_i$  is the energy barrier separating the equilibrium positions within and without the hydration shell, and  $E_H$  is the activation energy of self-diffusion in pure water. In  $\text{D}_2\text{O}$  (a more structured solvent), the activation energy of self-diffusion is greater [8], i.e.,

$$E_D = E_H + \delta E_w.$$

The barrier  $E_i^D = E_i^H + \delta E_i$ , which determines the emergence of  $\text{D}_2\text{O}$  molecules from the hydration shells, can vary for two reasons: either owing to the different interactions of  $\text{H}_2\text{O}$  and  $\text{D}_2\text{O}$  molecules with the ion, or



because of the difference between their moments of inertia (the libration frequency of the D<sub>2</sub>O molecule is less than that of the H<sub>2</sub>O molecules).

According to Rabinovich [7], the mean energy of rotational oscillations of the D<sub>2</sub>O molecule is lower than that for H<sub>2</sub>O, while the corresponding activation energy is higher. The difference between the libration frequencies largely determines the isotope shift in pure water [9]. In an ionic field the libration frequencies and the values of  $\delta E_i$  should be higher. However, we must remember that D<sub>2</sub>O has a lower polarizability [7]. This causes some decrease in  $\delta E_i$ , but on the whole  $\delta E_i > 0$ . The increased strength of the hydrate complexes on replacing H<sub>2</sub>O by D<sub>2</sub>O confirms the results of [10] for the shift of the bands in the electron absorption spectra of Fe<sup>3+</sup>, Ni<sup>2+</sup>, Co<sup>2+</sup>, and Cr<sup>3+</sup> in the short-wave region.

Applying (1) to a heavy-water solution, we get

$$\frac{(\tau_i/\tau)_D}{(\tau_i/\tau)_H} = e^{\frac{\delta E_i - \delta E_W}{RT}} \quad (2)$$

If the libration frequencies were unaltered near the ion, the isotope shifts would be the same inside and outside the hydration shell. Increase in the libration frequencies in the ionic field does not reduce  $\delta E_i$ , and therefore we always have

$$\delta E_i \geq \delta E_W. \quad (3)$$

It then follows from (2) that for all ions

$$\frac{(\tau_i/\tau)_D}{(\tau_i/\tau)_H} > 1, \quad (4)$$

i.e., the relative lifetime of a D<sub>2</sub>O molecule in a hydration shell is greater both near a positively and near a negatively hydrated ion.

From (4) it follows that hydration is reinforced in heavy water. However, this contradicts the experimental data mentioned above. The dependence of the isotope effect on the nature of the ion determines the value of  $\delta E_i$ . Clearly  $\delta E_i$  is greater when there is a stronger field created by the ion at the positions of its nearest-neighbor water molecules. Since the electrostatic field of the ion in its primary hydration layer decreases with increasing ionic radius  $r_i$ , the value of  $\delta E_i$  for alkali-metal cations must increase from Cs<sup>+</sup> to Li<sup>+</sup>. From (2) it follows that the difference between the lifetimes of H<sub>2</sub>O and D<sub>2</sub>O molecules in a hydration shell will be greatest for Li<sup>+</sup>.

However, the experimental data indicate that the isotopic differences in the heats and free energies of solution of salts vary regularly in just the opposite sense. Figure 1 plots data from [2] for  $\delta L = L_D - L_H$ , the difference between the heats of solution of alkali chlorides in heavy and light water. It is seen that the absolute value of the effect increases from Li<sup>+</sup> to Cs<sup>+</sup>. Figure 2 shows a similar variation in the free energy change  $\delta F$  on transfer of a salt molecule from heavy to light water [11]. From the figure it is seen that the free energy of solution of the salt in heavy water is greater than in light water, and increases from Li<sup>+</sup> to Cs<sup>+</sup>.

According to Born's thermodynamic equation for the free energy of hydration

$$\Delta F = \frac{\text{const}}{\epsilon r_i}, \quad (5)$$

where  $\epsilon$  is the dielectric constant of the solvent: this equation also fails to explain the way in which the isotope effects of hydration [12] depend on the nature of the ion. In fact, from (5) it follows that

$$\delta \Delta F = \frac{\text{const}}{r_i} \left( \frac{1}{\epsilon_D} - \frac{1}{\epsilon_H} \right) > 0.$$

This equation gives the sign of the effect correctly. However, according to (5), the free energy of hydration ought to decrease with increasing ionic radius from Li<sup>+</sup> to Cs<sup>+</sup>.

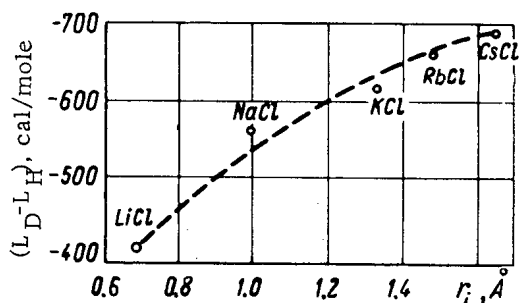


Fig. 1. Difference between heats of solution of alkali chlorides in heavy and light water, plotted versus cation radius.

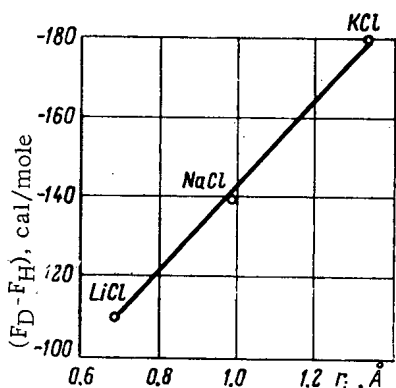


Fig. 2. Difference between free energies of solution of alkali chlorides in heavy and light water, plotted versus cation radius.

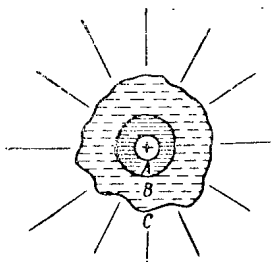


Fig. 3. Two-layer model of hydrated cation.

the properties of pure water at a higher temperature. As the structural disruption is localized in layer B, it is in this layer that the effective structural temperature appears to be raised.

We must bear in mind that the differences between the properties of  $\text{H}_2\text{O}$  and  $\text{D}_2\text{O}$  decrease with rising temperature. This is seen, for instance, in the temperature dependences of the heats of evaporation (Fig. 5)  $\Delta H_{\text{D}_2\text{O}}/\Delta H_{\text{H}_2\text{O}}$ , and of the vapor pressure [1, 17]. The enthalpy characterizes the depth of the potential well in which the molecule is located. Consequently the deepening of the potential well on transition to  $\text{D}_2\text{O}$  must be less marked in layer B than in pure water. In other words,

$$\Delta < \delta E_w \quad (6)$$

Furthermore, we can assert that  $\Delta$  will be the less, the stronger is the disruption of the water structure in layer B,

This particle shows how to explain the above facts on the basis of a two-layer hydration model [13, 14]. In this model it is supposed that, in addition to the primary hydration layer immediately next to the ion in which the solvent molecules are tightly bonded to the ion by nondipole forces, there is also a more remote layer B (Fig. 3) in which the mobility of the water molecule is greater than in the remaining main bulk of the water (layer C), where they are not disturbed by ionic fields. Vdovenko et al. [14] suggest a molecular-kinetic treatment of the two-layer model. They introduce two barriers  $E_A$  and  $E_B$  which determine the equilibrium positions of molecules in layers A and B and the corresponding relative lifetimes,

$$\frac{\tau_A}{\tau} = e^{\frac{\Delta E_A}{RT}} \quad \text{and} \quad \frac{\tau_B}{\tau} = e^{\frac{\Delta E_B}{RT}},$$

where  $\Delta E_A = E_A - E_W > 0$  and  $\Delta E_B = E_B - E_W < 0$ .

Figure 4 shows the relation between the energy barriers. It was demonstrated above that the potential barriers in layers A and C are higher in heavy water. It is thus natural to suppose that in  $\text{D}_2\text{O}$ —the more structured liquid—the degree of structural irregularity in layer B is less than in light water. Therefore, as a whole, the potential curve of  $\text{D}_2\text{O}$  lies lower.

Since the observed relation between the isotope effect and the nature of the ions cannot be explained by means of the changes in the barriers in layers A and C, it is natural to seek an explanation in the way in which the activation energy and lifetime in layer B vary with the isotopic composition of the water. In fact, the region B of broken structure near each ion appears as a result of competition [15] between the orienting effects of the ion's field and the tendency for the ice-like skeleton to retain its former, more economical configuration. Thus, the mutual interrelationship between the two mechanisms of disturbance of the water structure (i.e., electrostatic interaction with the ion and strengthening of the skeleton on transition to  $\text{D}_2\text{O}$ ) should be more intense in layer B.

Let us consider the expected relationship between  $\Delta = E_B^D - E_B^H$  and  $\Delta E_B = E_B - E_W < 0$ , the characteristic disruptive effect of the ion on layer B. We shall base our discussion on Bernal and Fowler's concept of the structural temperature [16], according to which the water in a salt solution has

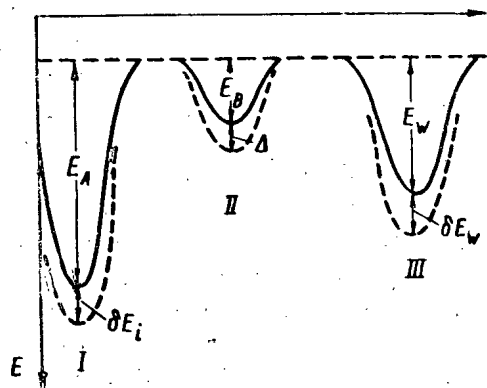


Fig. 4. Potential energy of water molecules near an ion: I and II) equilibrium positions in layers A and B, respectively; III) equilibrium position nearest to ion in layer C.

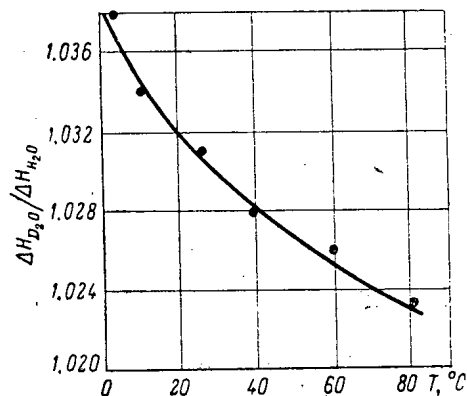


Fig. 5. Temperature dependence of the ratio between the heats of evaporation of light and heavy water.

Approximate Barrier Potential of Hydration of Ions in H<sub>2</sub>O

Barrier potential of layers, kcal/mole	Li+	Na+	K+	Cs+
$\Delta E_A$	1.19	1.07	1.14	0.99
$\Delta E_B$	-0.81	-0.97	-1.27	-1.28

i.e., the greatest is the absolute value of  $\Delta E_B$ . The table gives tentative values of  $\Delta E_A$  and  $\Delta E_B$ . It is seen that the absolute value of  $\Delta E_B$  increases in the order  $Li^+ \rightarrow Cs^+$ . The value of  $\Delta$  should decrease in the same direction. Let us now see how the differences in lifetimes  $\tau_B$  in layer B alter on going from  $Li^+$  to  $Cs^+$ . For  $D_2O$  we can write (see Fig. 4):

$$\tau_B^D = \tau_B^H e^{\frac{E_B + \Delta - E_W - \delta E_W}{RT}} = \tau_B^H e^{\frac{\Delta E_B + \Delta - \delta E_W}{RT}}$$

whence

$$\frac{(\tau_B/\tau)_D}{(\tau_B/\tau)_H} = e^{\frac{\Delta - \delta E_W}{RT}} \quad (7)$$

Consequently, since the difference  $\Delta - \delta E_W < 0$  also increases in absolute value on going from  $Li^+$  to  $Cs^+$ , for any ion the ratio

$$\frac{(\tau_B/\tau)_D}{(\tau_B/\tau)_H} < 1, \quad (8)$$

also increases from  $Cs^+$  to  $Li^+$ , being nearer to unity for  $Li^+$  than for  $Cs^+$ . Thus the isotope effect is greatest for  $Cs^+$  and decreases on going to  $Li^+$ . This result can be extended to the thermodynamic properties of heavy and light water.

Since the lifetimes are connected with the thermodynamic probabilities, it follows from (7) that the density of  $D_2O$  molecules is lower in layer B, and consequently the ions are less markedly hydrated in heavy water. This is easily demonstrated, remembering that the current of substance through the potential barrier is proportional to the concentration of molecules and inversely proportional to the lifetime of water molecules in the equilibrium position. Considering the transfer of molecules from layer B to layer C and back, we can write

$$\frac{I_{B \rightarrow C}}{I_{C \rightarrow B}} = \frac{Q_B \tau_C}{Q_C \tau_B},$$

where  $\rho_B$  and  $\rho_C$  are the densities of molecules in layers B and C. In equilibrium, the currents through the barrier are equal in either direction, and hence

$$\frac{Q_B}{Q_C} \cdot \frac{\tau_C}{\tau_B} = 1.$$

Hence

$$\left(\frac{\rho_B}{\rho_C}\right)_D = \left(\frac{\rho_B}{\rho_C}\right)_H \frac{(\tau_B/\tau)_D}{(\tau_B/\tau)_H} \quad (9)$$

By (8) we get

$$\left(\frac{\rho_B}{\rho_C}\right)_D < \left(\frac{\rho_B}{\rho_C}\right)_H \quad (10)$$

On the other hand, the molecular density of heavy water is less than that of light water [1, 17]. Thus, by (10),

$$\frac{\rho_B^D}{\rho_B^H} < \frac{\rho_C^D}{\rho_C^H} < 1.$$

Thus D<sub>2</sub>O has a reduced density of molecules in layer B. Thus, the ions are dehydrated in heavy water.

Let us rewrite (9) in the form:

$$\frac{\rho_B^D}{\rho_B^H} = \frac{\rho_C^D}{\rho_C^H} \cdot \frac{(\tau_B/\tau)_D}{(\tau_B/\tau)_H} = \frac{\rho_C^D}{\rho_C^H} e^{\frac{\Delta - \delta E_{IV}}{RT}}.$$

Since  $\rho_C^D/\rho_C^H < 1$ , dehydration in heavy-water solutions must be most marked for Cs<sup>+</sup>. On going to Li<sup>+</sup>, there is a decrease in the difference between the molecular densities of light and heavy water.

When H is replaced by D, the thermodynamic properties (e.g., free energy and enthalpy of solution) of a salt solution can alter for two reasons; either because of displacement of the molecular energy levels in the hydration shells, or by decrease in the coordination number (or, more generally, the density of molecules near the ion). If we assume that the second mechanism predominates for alkali-metal cations, we can easily explain all the observed effects—the weakened interaction of alkali-metal cations with water on going over to D<sub>2</sub>O, and the increase in this effect in the direction Li<sup>+</sup> → Cs<sup>+</sup>. However, in the case of strongly hydrated ions there is an increased contribution to the isotope effect from the primary hydration layer. For multiply charged ions of small radius we can therefore expect increased hydration in heavy water.

#### LITERATURE CITED

1. A. I. Brodskii, Isotope Chemistry [in Russian], Moscow, Izd-vo AN SSSR (1952).
2. E. Lange and W. Martin, Z. phys. Chem., **A180**, 233 (1937).
3. V. M. Vdovenko and E. K. Legin, Radiokhimiya, No. 3 (1966).
4. V. M. Vdovenko, E. K. Legin, and A. V. Zharkov, Radiokhimiya, No. 3 (1966).
5. Yu. V. Gurikov, Zh. strukturn. khimii, **4**, 824 (1963).
6. O. Ya. Samoilov, Structures of Aqueous Solutions of Electrolytes and Hydration of Ions [in Russian], Moscow, Izd-vo AN SSSR (1957).
7. I. B. Rabinovich, Isotope Effects in the Physicochemical Properties of Liquid Deuterium Compounds [in Russian], Doctorate dissertation, Gor'kii (1963).
8. Yu. V. Gurikov, Zh. strukturn. khimii (1966).
9. C. Swain and R. Bader, Tetrahedron, **10**, 182 (1960).
10. J. Bigeleisen, J. Chem. Phys., **32**, 1583 (1960).
11. J. Greyson, J. Phys. Chem. **66**, 2218 (1962).
12. J. Hepler, Austral. J. Chem., **17**, 587 (1964).
13. H. Frank and M. Evans, J. Chem. Phys., **13**, 507 (1945); H. Frank and Wen-Yang-Wen, Disc. Faraday Soc., **24**, 133 (1957).
14. V. M. Vdovenko, Yu. V. Gurikov, and E. K. Legin, Radiokhimiya, No. 3 (1966).
15. Yu. V. Gurikov, Zh. strukturn. khimii, **1**, 286 (1960).
16. J. Bernal and R. Fowler, J. Chem. Phys., **1**, 531 (1933).
17. I. Kirshenbaum. Heavy Water [Russian translation], Moscow, Izd-vo inostr. lit., (1953).

\*  $\rho_C = 1/V_C$ , where  $V_C$  is the molecular volume of water;  $\rho_B$  has a similar meaning.

THE BINARY SYSTEM  $UF_4-UCl_4$ 

(UDC 546.791.4)

L. A. Khripin, Yu. V. Gagarinskii, G. M. Zadneprovskii  
and L. A. Luk'yanova

Translated from *Atomnaya Énergiya*, Vol. 19, No. 5,  
pp. 437-441, November, 1965

Original article submitted December 2, 1964

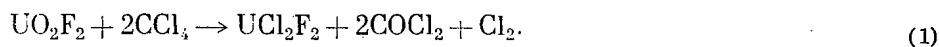
Resubmitted in revised form May 31, 1965

The authors study the binary system  $UF_4-UCl_4$  by DTA and x-ray diffraction and plot its phase diagram. Three compounds are formed in this system: uranium dichlorodifluoride  $UCl_2F_2$ , uranium monochlorotrifluoride  $UClF_3$  and (obtained for the first time) uranium trichloromonofluoride  $UCl_3F$ . These compounds melt incongruently at  $460 \pm 3$ ,  $530 \pm 6$  and  $444 \pm 2^\circ C$ , respectively. The optimal conditions for obtaining these compounds in pure form from melts of the system have been determined in general form.

Using the phase diagram of the system  $UF_4-UCl_4$ , the authors explain the contradictory results obtained by other authors in the synthesis of  $UCl_2F_2$  and  $UClF_3$ .

Of the U(IV) halides, mixed halides have been least studied although their preparation and properties are of considerable interest. Of the six possible types of mixed U(IV) halides containing two different halogens, only one is examined here, namely the chlorofluorides. Two chlorofluorides are described in the literature:  $UCl_2F_2$  and  $UClF_3$  [1-3]. The dichlorodifluoride has been obtained by two methods. In one method an equimolar mixture of  $UCl_4$  and  $UF_4$  was fused in a quartz tube at  $800^\circ C$  [1] or at  $600^\circ C$  [4] in pure helium. The composition of the solidified melt was determined by chemical analysis and corresponded to the formula  $UCl_{1.85}F_{2.05}$ . The x-ray diffraction pattern of this product was unintelligible and was not deciphered by the authors of [1]. In [4] the melting point of the dichlorodifluoride was found to be  $460^\circ C$ ; according to this report, the compound undergoes slow disproportionation to  $UCl_4$  and  $UF_4$  when heated to  $600^\circ C$ . An analysis of [1, 4] does not confirm that these authors obtained  $UCl_2F_2$ . This was also noted in [2], where attempts to reproduce experiments described in [4] on synthesis of  $UCl_2F_2$  by fusing  $UCl_4$  and  $UF_4$  were unsuccessful,  $UClF_3$  being obtained instead of the target compound.

The second method of obtaining uranium dichlorodifluoride [5] consists in reacting uranyl fluoride with  $CCl_4$  vapor at  $450^\circ C$ :



Analysis of the product showed that its formula was  $UCl_{1.63}F_2$ , i.e., not that of the dichlorodifluoride. The authors of [2, 3] indicate that Gates et al. [5] obtained  $UClF_3$ , not  $UCl_2F_2$ .

The author of [2] obtained uranium monochlorotrifluoride by several methods, but only three will be discussed here. It was apparently first obtained from uranium trifluoride by the reaction



which is mentioned in [1]. The reaction product contained about 67%  $UClF_3$ , the remainder consisting of  $UF_3$  and  $UF_4$ . In [2]  $UClF_3$  was obtained by the action of  $CCl_4$  vapor on uranyl fluoride, and by fusing a 1 : 3 molar mixture of  $UCl_4$  and  $UF_4$  in a quartz tube at  $600^\circ C$  in argon. In the latter case the product contained 80-90%  $UClF_3$ . Discussing syntheses of  $UClF_3$  performed in [2], the authors of [3] note that none of the methods used in [2] gave a homogeneous product. It is clear from the above that it is very difficult to obtain pure uranium chlorofluorides.

The aim of the present work is to study the reaction of  $\text{UCl}_4$  with  $\text{UF}_4$  at high temperatures, construct the phase diagram of the system, determine the possibility of formation of uranium chlorofluorides in the melts, establish their compositions and determine the optimal conditions for obtaining pure compounds from the melt.

#### EXPERIMENTAL

The initial components were anhydrous  $\text{UCl}_4$  and  $\text{UF}_4$ , purified by sublimation in vacuum. The tetrachloride contained 99.9%  $\text{UCl}_4$ , the tetrafluoride had an impurity of  $\sim 1\%$   $\text{UO}_2\text{F}_2$ .

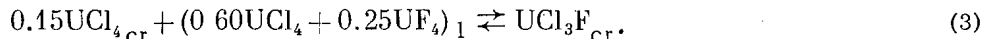
The system was studied by DTA and x-ray diffraction analysis. The heating-cooling curves were recorded in an FPK-59 pyrometer.  $\text{UCl}_4 - \text{UF}_4$  mixtures, prepared in a dry chamber, were heated in pure helium at temperatures 100-200°C higher than their melting points, held at the maximum temperature for 25-40 min, and the cooling curves recorded. The cooling rate was 4-7 deg/min, the temperature measurement error  $\pm 3^\circ$ . The experimental procedure and the apparatus used for DTA are described in detail in [6].

X-ray diffraction analysis of the specimens was performed in a URS-50I diffractometer with an SI-4R ionization counter (Cu radiation, Ni filter, anode voltage 27 kV, current 10 amps). The recordings were made with counter speed 1 deg/min and time constant of the integrating device 4 sec. All conditions and geometry were kept constant throughout recording. The specimens were powders, packed tightly in transparent plastic cells (diameter of the powder layer 20 mm, depth 0.3 mm), rotated at 30 rev/min. Preparation of the specimens was performed in the dry chamber because these compounds are very hygroscopic. The cells were sealed at the top with a thin Teflon film; its "background" was taken into account when the diffraction patterns were processed.

Some of the uranium tetrachloride sublimed from the melt and was deposited on the cold lid of the apparatus, so the compositions of the specimens after DTA did not agree with those of the initial mixtures; the compositions of the cooled fusions were therefore checked by chemical analysis. The contents of uranium and chlorine were determined by quantitative analysis; the fluorine content was found by subtraction. We also determined the content of  $\text{UO}_2$ , formed by partial hydrolysis of the halides by the residual moisture in the apparatus; it was less than 0.5 to 0.6%. The analytical methods are described in [6]. When it was necessary for the diffraction analysis specimens to have specific compositions (for example, containing 25, 50, or 75%  $\text{UF}_4$ ), the mixture of the components was fused in evacuated nickel ampoules, which were then sealed. This eliminated volatilization of  $\text{UCl}_4$  and the composition of the specimen remained unchanged.

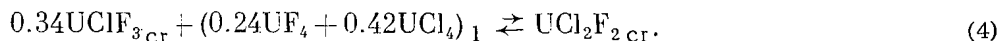
#### DISCUSSION

Figure 1 gives the phase diagram of the system  $\text{UCl}_4 - \text{UF}_4$ , constructed from DTA and x-ray diffraction data. It has 12 fields, the phase designation of each of these being indicated in the figure. The liquidus curve has seven sectors, corresponding to crystallization of the  $\alpha$ - and  $\beta$ -forms of uranium tetrachloride and tetrafluoride and three mixed compounds. The individual sectors of the liquidus intersect at six invariant points. It will be seen from the phase diagram that the following compounds are formed in the system: the trichloromonofluoride  $\text{UCl}_3\text{F}$ , dichlorofluoride  $\text{UCl}_2\text{F}_2$  and monochlorotrifluoride  $\text{UClF}_3$ . The trichloromonofluoride is formed from the melt at  $444 \pm 2^\circ\text{C}$  by the peritectic reaction



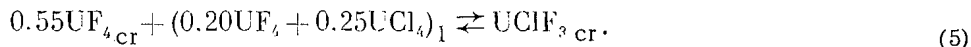
When the system is heated, crystalline  $\text{UCl}_3\text{F}$  is formed; it melts incongruently at this temperature, decomposing by the reverse reaction to solid  $\text{UCl}_4$  and a melt containing 28.0 mole %  $\text{UF}_4$ .

Uranium dichlorodifluoride crystallizes from the melt at  $460 \pm 3^\circ$ , due to the peritectic reaction



When the system is heated, the  $\text{UCl}_2\text{F}_2$  formed melts incongruently, leading to formation of crystalline uranium monochlorotrifluoride and a melt containing 38.5 mole %  $\text{UF}_4$ .

Finally, uranium monochlorotrifluoride is formed from the melt at  $530 \pm 6^\circ\text{C}$ , as follows:



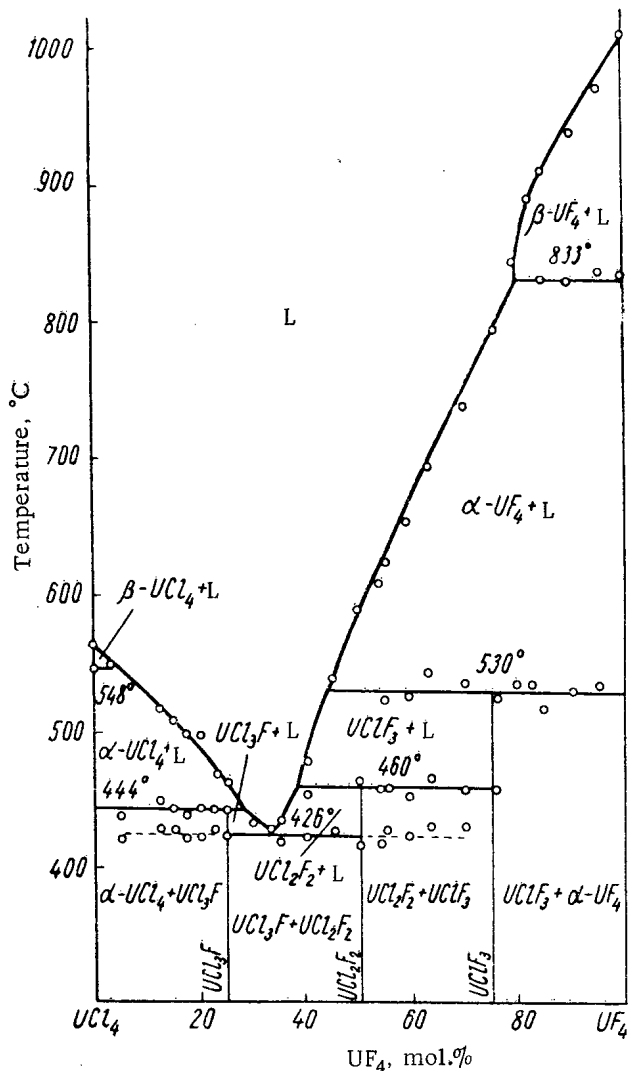


Fig. 1. Phase diagram of the system  $UCl_4 - UF_4$ .

By analogy, specimens with 25 mole %  $UF_4$  contained not only  $UCl_3F$  but also  $UCl_4$  and  $UCl_2F_2$  (10-30 wt. %). This explains why (3) is a slow reaction and why some of the  $UCl_4$  and the melt were not converted. The residual melt solidified at the eutectic temperature. The eutectic line may therefore be prolonged into the region of compositions with less than 25%  $UF_4$ , which is metastable for the eutectic. The composition of specimens with 75 mole %  $UF_4$  contained not only  $UCl_3F$  but also  $UF_4$  and  $UCl_2F_2$  as impurities.

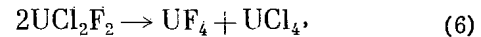
Figure 2 gives x-ray diffraction patterns of the initial salts, melts with compositions  $3UCl_4 + UF_4$ ,  $UCl_4 + UF_4$ ,  $UCl_4 + 3UF_4$ , and the protective Teflon film. The figure also gives the most characteristic reflections of the compounds formed in the system. The structural characteristics of the pure compounds  $UCl_2F_2$  and  $UCl_3F$ , formed in this system, have not been fully determined; however, our data on the interplanar spacings and lattice constants of  $UCl_3F$  agree with data in [3].

We can thus draw the following practical conclusion: to obtain pure  $UCl_3F$ ,  $UCl_2F_2$  and  $UCl_3F$  the melts must be kept at the appropriate peritectic temperatures for a time sufficient to allow the reaction to proceed to completion.

The phase diagram of the system  $UCl_4 - UF_4$  enables us to explain why other authors have obtained contradictory data on the preparation of  $UCl_2F_2$ . As already mentioned, the authors of [1, 4] discuss the preparation of this compound by fusing equimolar amounts of  $UCl_4$  and  $UF_4$ . Reference [2] indicates that fusion of a 1 : 1 molar mixture of  $UCl_4$  and  $UF_4$  does not give  $UCl_2F_2$ , but a product consisting mainly of  $UCl_3F$ . It would appear that this

When the system is heated to  $530 \pm 6^\circ$ ,  $UCl_3F$  melts incongruently with formation of crystalline  $UF_4$  and a melt containing 44 mole %  $UF_4$ .

All three uranium chlorofluorides and therefore thermally unstable and decompose at elevated temperatures; the thermal stability decreases as follows:  $UCl_3F \rightarrow UCl_2F_2 \rightarrow UCl_3F$ . The phase diagram of the system  $UCl_4 - UF_4$  shows that Katz et al. [7, p. 541] did not give the correct scheme of thermal decomposition of uranium dichlorodifluoride, and their equation



is incorrect. In fact, this compound does not decompose into the tetrafluoride and tetrachloride, but forms  $UCl_3F$  in accordance with (4); this equation indicates a hitherto undetected close genetic relationship between uranium dichlorodifluoride and the monochlorotrifluoride, these compounds being linked by mutual transitions.

X-ray diffraction analysis showed that the solidified melts containing 50 mole %  $UF_4$  did not consist of  $UCl_2F_2$  alone, but also variable amounts of  $UCl_3F$  and another phase (evidently  $UCl_3F$ , the content reaching as much as 25-30 wt. %) and very small amounts of the initial components. The reasons for this were the excessive cooling rates (4-7 deg/min) and incompleteness of the peritectic formation reaction (4), which was evidently slow (due to participation of the solid phase  $UCl_3F$ ). In consequence, the specimen contained unreacted  $UCl_3F$ , and the liquid phase, which was not fully converted, solidified at the eutectic temperature. This also explains the prolongation of the eutectic into the region of compositions with more than 50 mole %  $UF_4$ . In this region the eutectic is evidently metastable, so that in this part of the phase diagram the eutectic line is expressed by a dashed line (cf. Fig. 1).

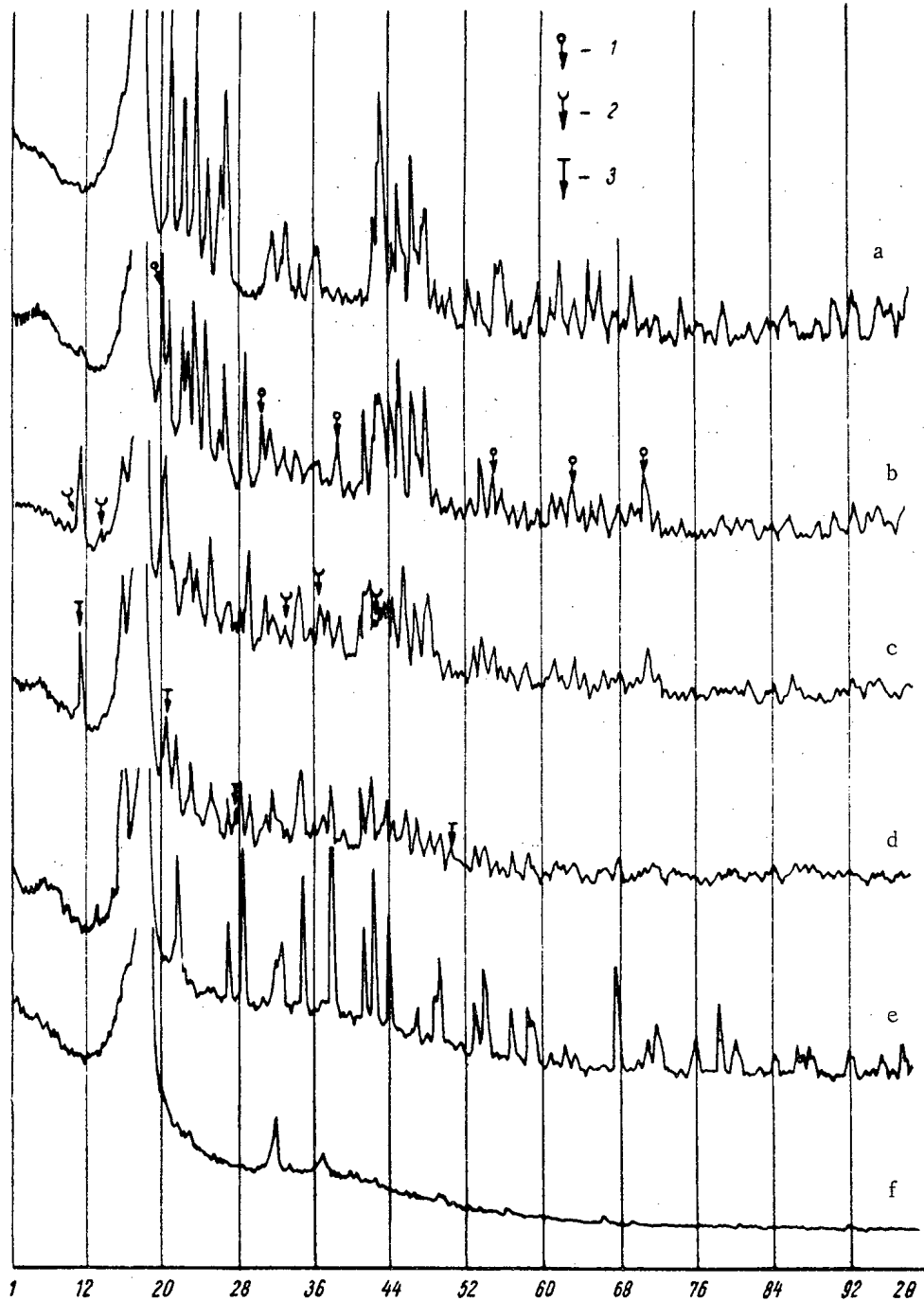


Fig. 2. X-ray diffraction patterns of  $UF_4$  (a),  $UCl_4 + 3UF_4$  (b);  $UCl_4 + UF_4$  (c);  $3UCl_4 + UF_4$  (d);  $UCl_4$  (e); Teflon film (f). The arrows indicate reflections of the compounds: 1)  $UClF_3$ ; 2)  $UCl_2F_4$ ; 3)  $UCl_3F$ .

discrepancy is due simply to the fact that these authors used different cooling rates of the melts; in one case the rate was too high and the bulk of the previously crystallized  $UClF_3$  was therefore not converted to  $UCl_2F_2$ ; in the other case cooling was slower, so that  $UCl_2F_2$  accumulated in the specimen. Furthermore, since the process was performed at  $450^\circ C$ , which is virtually the same as the temperature of incongruent melting of  $UCl_2F_2$ , an increase in temperature of only  $10^\circ$  led to decomposition of  $UCl_2F_2$ ; the principal reaction product could then be  $UCl_3F$ .

The phase diagram of the system also explains why, at equal cooling rates of the melt, the dichlorodifluoride is the only one of the three chlorofluorides obtained in the pure form. The point is that whereas  $UCl_3F$  and  $UClF_3$



are formed by a single peritectic reaction the formation of  $UCl_2F_2$  is more complex; when a melt containing 50 mole %  $UF_4$  is cooled the first stage is crystallization of  $UF_4$  alone (this begins at  $585^\circ C$ ); then  $UClF_3$  is formed from the solid tetrafluoride and the melt, and, finally,  $UCl_2F_2$  is obtained from  $UClF_3$  and the melt. The dichlorodifluoride is thus formed by two successive peritectic reactions, neither of which proceeds to completion if the cooling rate is too fast. Furthermore, since the region of existence of the dichlorodifluoride begins in the center of the diagram, specimens obtained contain both trichloromonofluoride and monochlorotrifluoride, whereas specimens of these two compounds contain only an admixture of the next nearest chlorofluoride.

#### SUMMARY

1. The authors have studied the binary system  $UCl_4 - UF_4$  by DTA and by chemical analysis, and have constructed the phase diagram.

2. Three uranium chlorofluorides are formed in this system:  $UClF_3$ ,  $UCl_2F_2$ , and  $UCl_3F$  (which is described for the first time). All three chlorofluorides melt incongruently at  $530 \pm 6$ ,  $460 \pm 3$ , and  $444 \pm 2^\circ$ , respectively. No solid solutions were observed in this system.

3. The optimal conditions for obtaining uranium (IV) chlorofluorides from binary melts of the system  $UCl_4 - UF_4$  have been basically determined.

#### LITERATURE CITED

1. J. Warf and N. Baenziger, *The Chemistry of Uranium*. Ed. by J. Katz, E. Rabinovitch USAEC, TID-5290 (1958), p. 120.
2. A. Savage, *J. Amer. Chem. Soc.*, **78**, (12), 2700 (1956).
3. E. Staritzky and R. Douglas, *Analyt. Chem.*, **28**, (7), 1210 (1956).
4. N. Gregory, Report RL-4.6.905 (1945). Quoted in [7].
5. J. Gates et al., Report CD-460 (1944). Quoted in [1].
6. L. A. Khripin, Yu. V. Gagarinskii, and L. A. Luk'yanova, *Izv. SO AN SSSR, Ser. khim. n.*, No. 3, 14 (1965).
7. J. Katz and E. Rabinovitch, *The Chemistry of Uranium*, National Nuclear Energy Series. Division VIII, Vol. 5, McGraw-Hill Book Co., Inc., (1951).

## NOTES ON ARTICLES RECEIVED

CONSTRUCTION OF A SECTORED 300 keV CYCLOTRON  
WITH EXTERNAL INJECTION

(UDC 621.384.611)

V. A. Gladyshev, L. N. Katsaurov, A. N. Kuznetsov,  
E. M. Moroz, and L. P. NechaevaTranslated from *Atomnaya Énergiya*, Vol. 19, No. 5,  
p. 442, November, 1965  
Original article submitted February 9, 1965

The efficiency of utilization of accelerated particles with a thin target can be improved by using additional acceleration after passage through the target [1]. To test the feasibility of additional acceleration, a small sectored cyclotron with deuteron energy  $\sim 300$  keV has been constructed at the Physics Institute of the USSR Academy of Sciences. It is proposed to perform a number of investigations with this cyclotron: in particular, it has been fitted with external ion injection in its median plane [2]. The magnet is made of three separate C-shaped magnets. This ensures appreciable depth of azimuthal variation of the magnetic field without the need for additional windings between the sectors, and permits easy access to the chamber. The magnet diameter is 70 cm. Each pole piece is a sector with straight edges and angle  $66^\circ$ . The magnet current is stabilized to within  $3 \cdot 10^{-6}$ . In addition, the field of each of the three magnets is stabilized by an independent proton stabilization system.

The pole pieces form part of the lid of the vacuum chamber, while the chamber itself consists of several sections. The main section consists of three triangular chambers made of brass, each of which is bolted to the side walls of the pole-piece sectors of two neighboring magnets. The vacuum seal is of lead wire which is attached to the slits between the individual components of the chamber and squeezed against them by special fastenings. The oil vapor diffusion pump of type N-5T yields a vacuum of  $\sim 2 \cdot 10^{-6}$  mm Hg.

Observation of the beam is by movable probes which can be positioned in any part of the accelerator chamber at the required angle to the beam by means of a spherical vacuum joint with Teflon packing and a movable arm, also with Teflon packing of the Wilson type.

The source and accelerator tube can be moved in the median plane of the magnet, so that the point of injection of the beam into the chamber can be varied.

To get the accelerating voltage to the dees, voltage from a generator is fed to a quarter-wave spiral line made of copper tubing wound on a cylindrical glass frame. The accelerating voltage on the dees is up to 20 kV.

In addition to its constructional features (divided magnet, sectional vacuum chamber, spiral quarter-wave line), the cyclotron is distinguished by external ion injection, which opens up new possibilities for the use of sources of polarized particles and other complex sources.

## LITERATURE CITED

1. L. N. Katsaurov and V. G. Latysh, *Trudy FIAN SSSR*, XXXIII, 235 (1965).
2. V. A. Gladyshev et al., *Proc. of International Conference on Accelerators, Dubna (1963)*, [in Russian], Moscow Atomizdat (1964), p. 658.

MAGNETIC FIELD OF A 300-keV SECTOR CYCLOTRON  
WITH EXTERNAL INJECTION

(UDC 621.384.611)

V. A. Gladyshev, L. N. Katsaurov, A. N. Kuznetsov,  
E. M. Moroz, and L. P. Nechaeva

Translated from *Atomnaya Énergiya*, Vol. 19, No. 5,  
p. 443, November, 1965  
Original article submitted May 29, 1965

This article provides data on the magnetic field of a sector cyclotron with a split magnet, calculated for the acceleration of deuterons to an energy of 300 keV. The cyclotron sectors are shifted away from the magnet's center along the radius, while the center contains cylindrical core. The required field was secured by experimentally determining the magnet parameters.

The field was measured by means of a coil, which was moved in steps. The coil was connected to the circuit of a ballistic galvanometer. Passing through the check points in the sectors, the coil was moved in steps of 2° along the azimuth and steps of 1 cm along the radius. The field at the check points was measured by means of the nuclear resonance method.

The focusing properties of the field of an isochronous cyclotron depend on the azimuthal variation depth and are determined by the frequencies of betatron oscillations. The azimuthal variation depth is characterized by the

"flutter," defined as

$$F = \frac{\langle B^2 \rangle - \langle B \rangle^2}{\langle B \rangle^2}$$

In this cyclotron, the flutter smoothly increases from 0.2 to 0.45 as the radius changes from 10 to 30 cm. The amplitudes of the field's first and second harmonics, which characterize the departure of the magnetic field from symmetry, are smaller than the amplitudes causing radial instability by approximately one order of magnitude.

The equations of motion were integrated by means of an electronic computer, while the measured field was assigned in the form of tables. This made it possible to obtain complete information on the behavior of particles and the orbit parameters in the actual field.

We plotted the equilibrium orbits for different energies and calculated the mean magnetic field along the equilibrium orbits. The thus obtained field differed only slightly from an isochronous field, while the phase shift in acceleration from 40 to 300 keV was equal to 6° for an energy increment of 10 keV per revolution. The properties of the orbits are especially clearly revealed in the so-called phase ellipses, which close after N revolutions. The number N is related to the frequencies  $Q_r$  and  $Q_z$  of betatron oscillations by the following expressions:

$$N_r = (Q_r - 1)^{-1} \text{ and } N_z = (Q_z - 1)^{-1}.$$

By plotting the ellipses for different energies and betatron oscillation amplitudes, it was found that the maximum allowable amplitude of radial oscillations, which was equal to 3 cm at 50 keV, increased with an increase in the energy and attained 5-6 cm at energies above 100 keV. The frequencies of betatron oscillations calculated with respect to the phase ellipses by means of a computer indicated that the focusing was sufficiently effective throughout the entire energy range.

The betatron oscillation frequencies calculated by means of the computer were compared with the frequency values calculated under the assumption of circular orbits. This comparison showed that the frequencies calculated by means of the "smooth approximation" expression, the expression based on harmonic field analysis, and the expressions derived under the assumption of a step field differed from the results obtained by means of the computer by 5-7%.

An analysis of the magnetic field shows that the split-magnet cyclotron design makes it possible to produce an isochronous field with great azimuthal variation depth, whereby good focusing in all orbits is secured.

IMPROVEMENT OF THE SENSITIVITY  
OF ALPHA-SCINTILLATION CHAMBERS

(UDC 543.52)

L. V. Gorbushina and V. G. Tyminskii

Translated from *Atomnaya Énergiya*, Vol. 19, No. 5,  
pp. 443-444, November, 1965

Original article submitted March 1, 1965

Original abstract submitted April 22, 1965

The standard  $\alpha$ -scintillation chambers presently used for  $\alpha$ -radiation measurements have a cylindrical shape with a volume of 350-2000  $\text{cm}^3$ . Even with the maximum chamber volumes, the sensitivity of the instruments does not exceed  $3.7 \cdot 10^{-13}$  Ci/pulse/min, which is insufficient for emanation measurements in dosimetry work and emanation determinations of the percentage of radioactive elements in water.

The article provides the results obtained in experiments on improving the sensitivity of instruments with  $\alpha$ -scintillation chambers by increasing the utilization factor of alpha radiation and using chambers with the optimum dimensions.

Figure 1 shows the dependence of the utilization factor of  $\alpha$ -radiation ( $K$ , %) on the scintillation chamber's volume ( $v$ ,  $\text{cm}^3$ ). Curve 1 was plotted by using the available data obtained in experimental determinations of the utilization factors in chambers with different volumes [1, 2], while curve 2 was plotted on the basis of the approxi-

mate expression  $K = \frac{3.9}{\sqrt{v}} \cdot 100\%$ , which is convenient for approximate estimates of the utilization factor of

$\alpha$ -scintillation chambers of various sizes where the height and the diameter are approximately equal. The table contains experimental data, from which it is seen that the utilization factor of alpha radiation has different values in different sections of the chamber's sensing surface (Fig. 2).

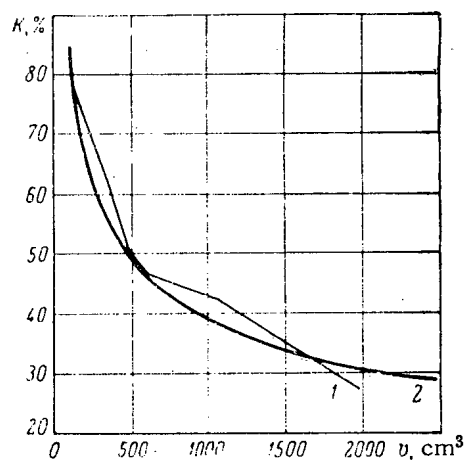


Fig. 1. Dependence of the utilization factor of  $\alpha$ -radiation on the scintillation chamber's volume: 1) experiment; 2) calculation.

It was found that the radiation utilization factor has the largest value at the chamber's bottom and that it sharply increases if a negative voltage is supplied to this section.

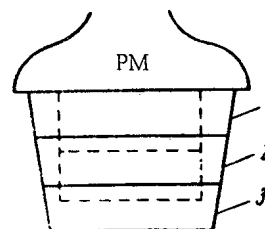


Fig. 2. Schematic diagram of the chamber: 1) zone 1; 2) zone 2; 3) zone 3; ———) conical chamber; - - - -) standard chamber.

## Results of Activity Measurements

Operating surface	Area of the sensing surface		Measured activity, % of total activity	
	cm <sup>2</sup>	percentage of over-all area	without a field	with electro-static field
Bottom	88.2	21	35	56
Wall				
zone 1	106.1	25	27	17
zone 2	112.0	26	22	14
zone 3	118.2	28	16	13

If  $\alpha$ -scintillation chambers are used for measurements with respect to thoron (in through flow), the optimum voltage value is equal to  $-400$  V. The counting rate produced by a control specimen in this case increases from 450 to 535 pulses/min. Thus, the factor of radiation utilization in the chamber increases by 19%.

## LITERATURE CITED

1. V. L. Shashkin, Methods for Analyzing Natural Radioactive Elements [in Russian], Moscow, Gosatomizdat (1961).
2. E. I. Zheleznova and A. A. Popova, Byulleten' Nauchno-Tekhnicheskoi Informatsii ONTI (Gosgeoltekhizdat), No. 6 (50), 70 (1963).

CERTAIN METHODS FOR REDUCING THE FLUXES  
OF PENETRATING SECONDARY  $\gamma$ -RADIATION

(UDC 539.121.73 : 539.122)

D. L. Broder, A. P. Kondrashov, and A. V. Kudryavtseva

Translated from *Atomnaya Énergiya*, Vol. 19, No. 5,  
pp. 444-445, November, 1965

Original article submitted October 26, 1964

Original abstract submitted August 5, 1965

Secondary  $\gamma$ -radiation, which contributes greatly to the resulting dose rate beyond the shield, arises in the radiative capture of neutrons in the materials of the screens, the vessel, and the biological shield of reactors. The largest portion of capture  $\gamma$ -quanta, which determines the radiation fluxes, is formed in the immediate vicinity of the core.

The present article is concerned with certain experimental assemblies used for simulating the screens and the reactor vessel, which consisted of alternating layers of steel and a hydrogenous material as well as one-piece monoliths. The yield of capture  $\gamma$ -radiation from such compositions and methods for radiation suppression were investigated.

There is a very efficient method for reducing the fluxes of penetrating secondary  $\gamma$ -radiation from screens and reactor vessels which consists in reducing the fluxes of thermal and epithermal neutrons that return from the light components of the biological shield. This reduction can be secured in two ways: 1) by adding to the materials of the reactor's thermal shield a substance which intensively absorbs neutrons without producing high-energy secondary  $\gamma$ -radiation (for instance, boron carbide); 2) by placing a layer of this material between the vessel and the hydrogenous component of the biological shield.

We calculated and measured the reduction of fluxes of  $\gamma$ -quanta with energies  $E > 6$  MeV that were formed in mock-ups of four screen and reactor vessel variants, where the vessel was blocked with layers of boron carbide and boron steel with boron concentrations of 0.5, 0.8, and 2% by weight.

The fluxes of capture  $\gamma$ -radiation can also be reduced by installing immediately beyond the vessel a layer of a heavy substance with a small neutron radiative capture cross section, for instance, a layer of lead.

The main purpose of our experiments was to determine the variation of the reduction factor for capture  $\gamma$ -radiation fluxes in the case of vessel blocking in dependence on the biological shield's thickness. The blocking factor was calculated and measured for different shield thicknesses. Good agreement between the theoretical and experimental values was observed.

The results of calculations and measurements are given in the form of graphs and tables.

Our investigations led to the following conclusions: 1) good materials for reducing the yield of capture  $\gamma$ -radiation are lead (thickness, 60 mm), boron carbide, and boron steel (2-3% boron by weight); 2) the blocking factor decreases with an increase in the shield thickness up to 4 mean free path lengths, while it changes only slightly with a further increase in thickness.

## LETTERS TO THE EDITOR

MEASUREMENTS OF THE PRESSURE DISTRIBUTION  
BEHIND THE FRONT OF A STRONG SHOCK WAVE

(UDC 533.9)

V. I. Fedulov and V. D. Borman

Translated from *Atomnaya Énergiya*, Vol. 19, No. 5,  
pp. 446-448, November, 1965

Original article submitted April 14, 1965

According to the one-dimensional theory of shock tubes, where it is assumed that the gas in the tube's channel is ideal, while the friction between the gas and the tube walls is neglected, a region of uniformly heated gas, which is separated from the thrusting gas by a contact surface, develops behind the front of the shock wave. We shall refer to this region as the plug of the shock wave. The experimentally measured length of the plug is smaller than the length calculated according to the idealized theory. For relatively low velocities of the shock wave ( $M < 8$ ), this discrepancy can be explained by the effect of the boundary layer on the gas flow in the shock tube [1-3]. Moreover, the presence of the boundary layer leads to a slight increase in the pressure, density, and temperature of the gas along the plug's length. With an increase in the wave velocity, this effect diminishes. However, the radiation losses increase, which, in turn, may be the cause of the plug's nonuniformity as a result of the different times of deexcitation of the plasma sections located at various distances from the wave front. Therefore, it is of interest to measure the plasma parameters along the entire length of the plug and not only at the wave front.

The pressure distribution along the length of shock wave plugs was investigated in [4]. These experiments, which were performed with an ordinary shock tube, showed that the pressure in the plug is constant during the first  $50 \mu\text{sec}$ , after which it drops, attaining a value of 80% of the initial value at the contact surface.

The aim of the experiment described here was to investigate the pressure distribution in the plugs of shock waves produced in electric-discharge shock tubes. The specific feature of such tubes (Fig. 1) is the fact that the energy of electric discharge is used for raising the temperature of the thrusting gas. In connection with this, there arise at least two additional factors which promote nonuniformities in the plug of the shock wave: 1) the electric discharge time is commensurable with the diaphragm's opening time; 2) the discharge power is not constant in time.

## EXPERIMENTAL METHOD

For pressure measurements, we prepared a data unit whose design was similar to that described in [5-8]. The distinctive features of the piezoelectric transducer used in our experiments were the following:

- 1) For the sensing element, we used disks of TsTS-19 piezoelectric ceramic (lead zirconate titanate), whose parameters were much superior to those of barium-titanate piezoelectric ceramic; the disk diameter was 7 mm, while the thickness was 0.5 mm;
- 2) the piezoelectric ceramic disks were soldered by using Wood's low-temperature alloy, which made it possible to improve the quality of the mechanical joining of the disks to each other and to the end-face of the zinc acoustic cylinder;
- 3) for insulation from plasma, the data unit was coated with an epoxide resin layer, which made it possible to mold the data unit's end-face on the inside surface of the tube; the leakage resistance of the piezoelectric transducer amounted to a few thousands of megohms.

The entire measuring circuit (see Fig. 1) transmitted without distortion pulses with a duration of up to  $700 \mu\text{sec}$ .



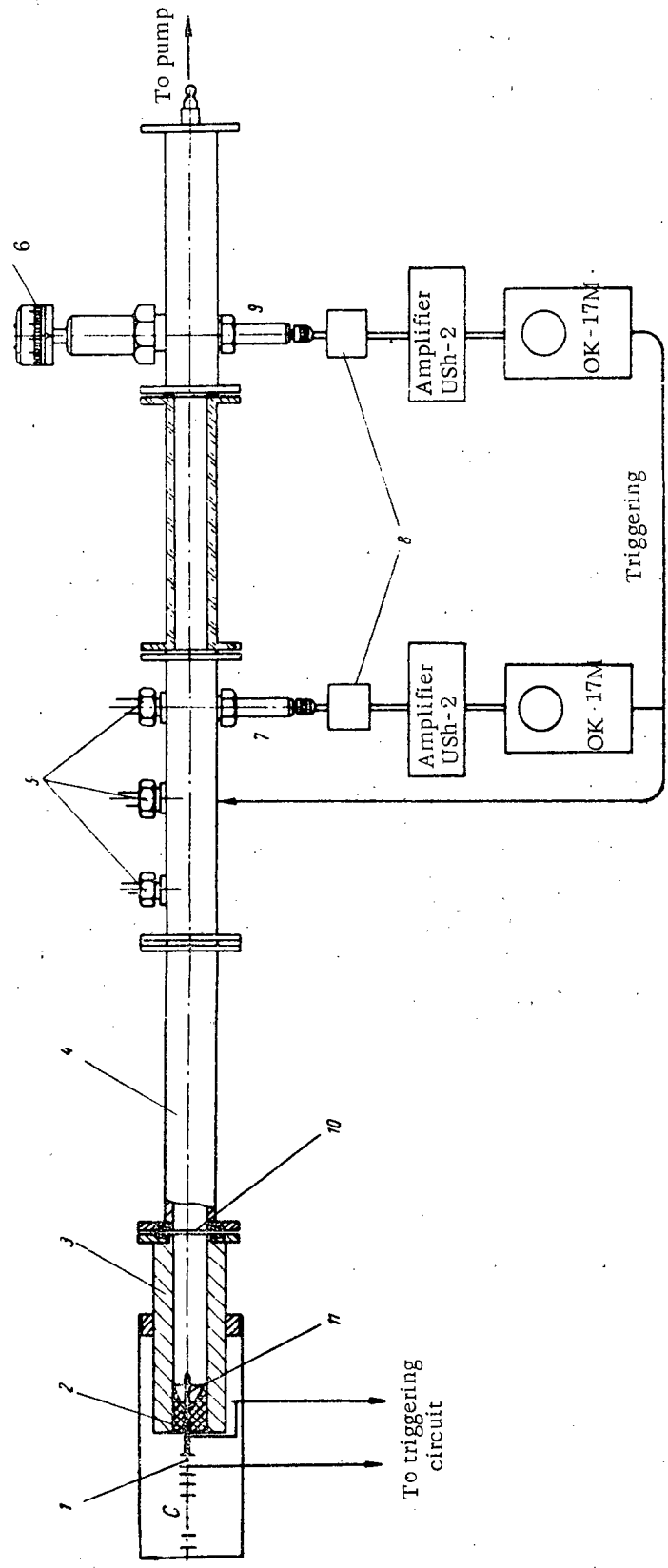


Fig. 1. Schematic diagram of the electric-discharge shock tube: 1) spark gap; 2) insulator; 3) high-pressure chamber; 4) channel; 5) ionization gauges; 6) diaphragm data unit; 7) first piezoelectric transducer; 8) second piezoelectric transducer; 9) second piezoelectric transducer; 10) diaphragm; 11) central electrode.

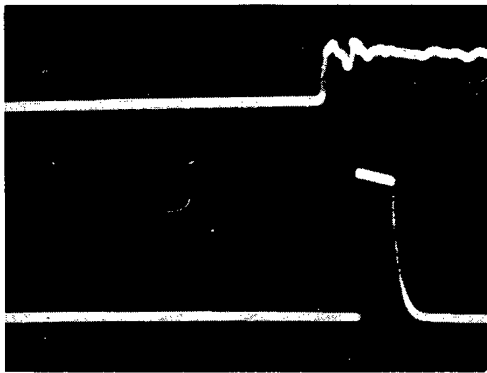


Fig. 2. Oscillogram of the calibration experiment. (The pulse from the piezoelectric transducer was supplied to the upper beam, and the signal from the diaphragm data unit was supplied to the lower beam.)

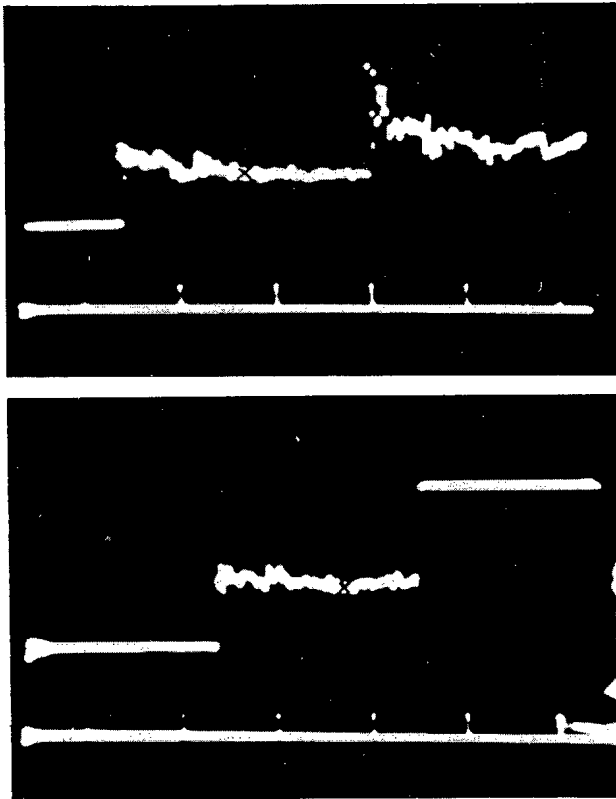


Fig. 3. Oscillograms of signals from two piezoelectric transducers, located at different points of the tube ( $x$  is the position of the contact surface).

fect of the boundary layer on the basis of data from [3], is marked on the oscillograms. It is seen that the pressure behind the wave front drops over a distance reaching the contact surface, where it amounts to approximately 85% of the pressure at the front, after which it remains constant until the second shock wave appears. A comparison of the oscillograms of signals from the first and the second transducers shows that the pressure drop at the shock tube's section where the first transducer is located is larger than the pressure drop at the location of the second transducer.

The piezoelectric transducers were calibrated by means of a diaphragm data unit [5]. The operating principle of the diaphragm data unit consisted in the following: Under the action of a pressure pulse, the diaphragm, which is fastened along its rim, is deflected until it comes into contact with a needle, whose end can be positioned at a certain given distance from the diaphragm's center by means of a micrometric screw. In [5], the diaphragm data unit was used under conditions where the duration of the pressure pulse was much shorter than the time necessary for the diaphragm to reach the needle, while the diaphragm was considered to be unrestrained in calculating the magnitude of the pressure pulse with respect to the time of the diaphragm's movement.

If a constant pressure  $p$  acts for a certain time on a diaphragm whose surface density is  $\rho$ , which corresponds to the conditions in the shock tube, a relationship between the needle-diaphragm gap  $u$  and the time  $t$  in which the diaphragm covers this gas can be obtained by taking into account the fastening of the diaphragm:

$$u = \frac{1}{2.7Q} p t^2.$$

It follows from this relationship that the value of  $p t^2 / u$  is constant. This was confirmed in our experiments. The value of  $p t^2 / u$  was equal to  $273 \pm 7 \cdot 10^{-8} \text{ mm} \cdot \text{sec/cm}$ . A typical calibration oscillogram is shown in Fig. 2. The experiments on pressure measurement were performed in the 6-10 range of Mach numbers. Argon plasma was investigated for an initial argon pressure of 10 mm Hg in the channel. For the propelling gas, we used helium under a pressure of 3 atm, which was heated by discharge from a battery of capacitors, which were charged to 5-6 kV. The pressure in the shock wave's plug was measured by means of two piezoelectric transducers, which were located at distances of 263 and 303 cm from the diaphragm (see Fig. 1). Both oscilloscopes were started simultaneously, which made it possible to measure the shock wave's velocity in the channel section between the two piezoelectric transducers with respect to the time interval between the signals from these transducers.

#### EXPERIMENTAL RESULTS

The oscillograms of the signals obtained from the two piezoelectric transducers are given in Fig. 3. The position of the contact surface relative to the shock wave's front, calculated with an allowance for the ef-

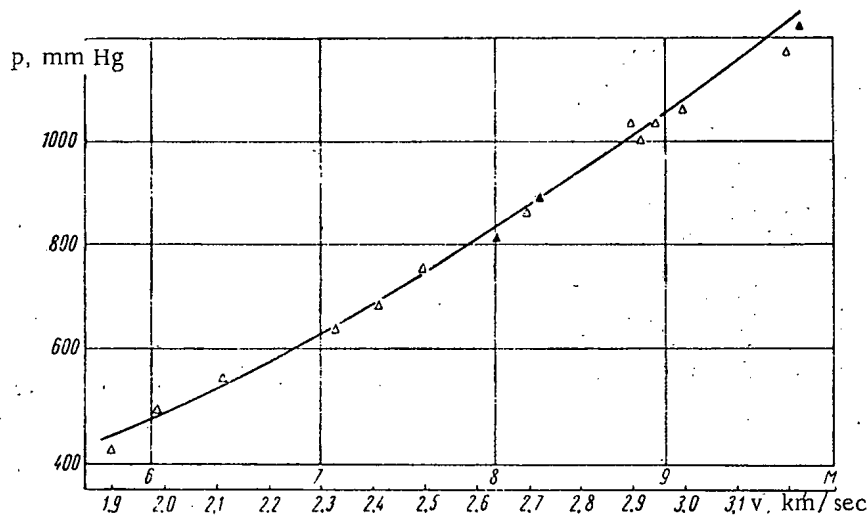


Fig. 4. Dependence of the pressure at the front of the first shock wave on its velocity  $v$  (the argon pressure was  $p_1 = 10$  mm Hg).  $\Delta$ ) First piezoelectric transducer;  $\blacktriangle$ ) second piezoelectric transducer.

The smoothness of the lower-beam pulse after the second pressure rise could be explained by the fact that the oscilloscope beam had left the linear characteristic region.

The dependence of the pressure at the front of the first shock wave on its velocity is shown in Fig. 4. For the sake of comparison, this figure also shows the theoretical velocity dependence of the pressure (solid curve), which was calculated with an allowance for the ionization [9]. Good agreement was observed between the measured and calculated pressure values not only in the region where the ionization effect on the plasma parameters can be neglected ( $M < 8$ ), but also in the region of considerable ionization ( $M > 8$ ).

A characteristic feature of the oscillograms of signals from the piezoelectric transducers is the presence of two pressure jumps, corresponding to two shock waves, which move it in the same direction along the channel of the shock tube. In order to explain the causes of the development of the second wave, we performed a series of experiments where the helium pressure  $p_4$  in the chamber was measured. In each experiment, we determined the velocities of the first and the second shock waves and also the time interval between these waves.

On the basis of these experiments, we reach the conclusion that the distance between the first and the second shock waves diminishes with a reduction in  $p_4$ ; for a pressure  $p_4 = 1$  atm, the second wave overtakes the first at the location of the first transducer. If we know the distribution of the shock wave's velocity along the length of the tube (which was actually measured in these experiments) and the time interval between the waves at the observation points, we can estimate their time separation at the diaphragm. This time diminished from 700 to 550  $\mu$ sec with a reduction in the pressure  $p_4$  from 3 to 1.5 atm. The measured half-period of the discharge current was equal to 100  $\mu$ sec. A comparison of these time values indicates that the development of the second shock wave cannot be explained by the heating of the gas during the second and the subsequent half-periods of the discharge current.

Considering the dependence of the characteristic times on the pressure  $p_4$ , it can be assumed that the second shock wave develops in the following manner. The shock wave that had developed during the first half-period of discharge is reflected from the diaphragm back toward the chamber. Then, after repeated reflection from the chamber's end-face, it appears as the second shock wave. A reduction in the pressure  $p_4$  leads to an increase in the specific energy input in the discharge region, which increases the velocity of waves in the high-pressure chamber. This could explain the fact that the second shock wave overtakes the first at  $p_4 = 1$  atm.

In conclusion, the authors extend their thanks to N. A. Kolokol'tsov for his interest in this project, N. V. Filippov for his useful advice at the initial stages of the work, and D. S. Derkbukov, who performed the precision mechanical work.

LITERATURE CITED

1. A. Roshko, *Phys. Fluids*, 3, 835 (1960).
2. W. Hooker, *Phys. Fluids*, 4, 1451 (1961).
3. H. Mirels, *Phys. Fluids*, 6, 1201 (1963).
4. O. Laport and T. Wilkerson, *J. Opt. Soc. America*, 50, No. 12 (1960).
5. N. V. Filippov, In the collection: *Plasma Physics and the Problem of Controlled Thermonuclear Reactions* [in Russian], Vol. 3, Moscow, Izd. AN SSSR (1958), p. 231.
6. W. Willmart, In the collection: *Shock Tubes* [Russian translation], Moscow, Izd. Inostr. Lit., (1962), p. 364.
7. G. Knight, In the collection: *Shock Tubes* [Russian translation], Moscow, Izd. Inostr. Lit., (1962), p. 374.
8. S. G. Zaitsev, *Pribory i Tekhnika Éksperimenta*, No. 6, 97 (1958).
9. E. Resler, S. C. Lyn, and A. Kantrowitz, In the collection: *Shock Tubes* [Russian translation], Moscow, Izd. Inostr. Lit., (1962), p. 218.

USE OF SURFACE-BARRIER SILICON DETECTORS  
FOR MEASURING FAST-PARTICLE SPECTRA

(UDC 539.16.07)

G. F. Bogdanov and B. P. Maksimenko

Translated from Atomnaya Énergiya, Vol. 19, No. 11,  
p. 449, November, 1965

Original article submitted April 26, 1965

Surface-barrier silicon detectors of nuclear radiation made it possible to reduce considerably the recording threshold in the energy analysis of charged particles. A linear dependence of the amplitude of detector pulses on the proton energy in the 18-250 keV range was obtained in [1]. The aim of our experiments was to check the possibility of using detectors of this type for measuring the spectra of neutral charge-exchange ions and of ions with energies of 10-200 keV emerging from the Ogra machine [2].

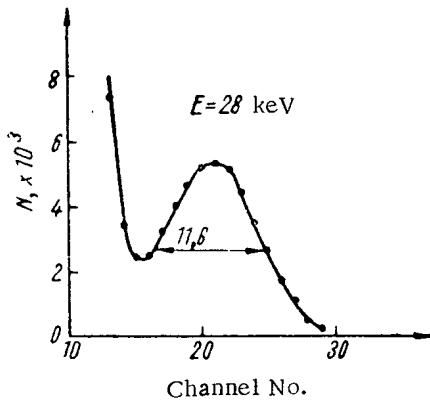


Fig. 1. Amplitude distribution of counter pulses in recording protons with an energy of 28 keV.

The counters which we used were made of n-type silicon with a resistivity of 700  $\Omega$ cm and a lifetime of the minority carriers of 2100  $\mu$ sec; the operating surface area of the counters was 5 mm<sup>2</sup>, while the thickness of the gold plating was  $\sim 25 \mu$ g/cm<sup>2</sup>. With a bias of 50 V, the back current did not exceed  $3.4 \cdot 10^{-8}$  A.

The detectors were checked by means of a magnetic separator in proton beams with energies of 28; 29.7; 49.5; 69.3 keV. The dependence of the amplitude of detector pulses on the energy  $E$  was linear within the accuracy of the calibration of the separator.

The amplitude distribution of the detector pulses in recording protons with an energy of 28 keV is shown in Fig. 1. The total width at the half-maximum was equal to 11.6 keV; to a considerable extent, it was due to the preamplifier noise.

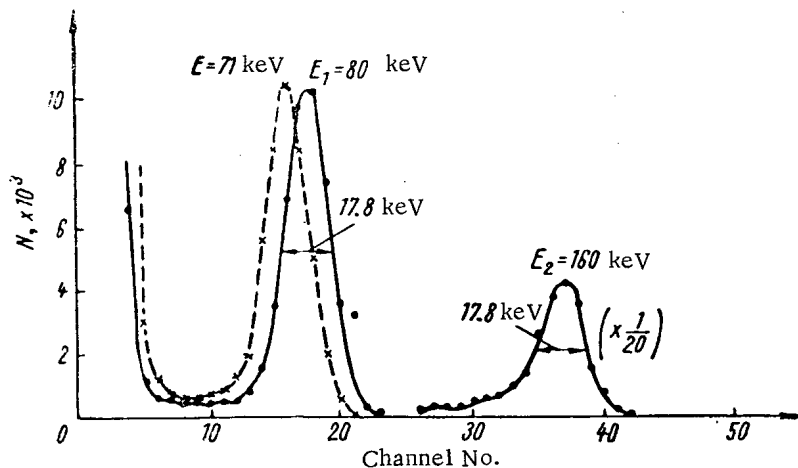


Fig. 2. Spectrum of neutral ions reaching the walls of the Ogra chamber (the dashed curve marks the spectrum obtained when the slit was covered with an aluminum foil).

Figure 2 shows the spectrum of neutral molecular ions reaching the walls of the Ogra chamber. It was measured under conditions where the energy spread of atomic ( $E_1 \approx 80$  keV) and molecular ( $E_2 \approx 160$  keV) neutral ions did not exceed 10% (according to measurements performed by means of an electrostatic analyzer with a foil). In order to ascertain that the peak  $E_2$  corresponds to neutral molecular ions, the slit in front of the detector was covered with aluminum foil, which caused the dissociation of  $H_2^0$ . The angular spread of the dissociation products of a single  $H_2^0$  molecule precluded the possibility of their reaching the counter simultaneously. The thus obtained spectrum is indicated by the dashed curve without the second peak. The energy loss in the foil was equal to 9 keV. Thus, the peak  $E_2$  in fact corresponds to neutral molecular ions.

The results obtained were in good agreement with the data given in [1]. They show that surface-barrier silicon detectors are suitable for measuring the spectra of particles emerging from plasma.

The authors hereby express their gratitude to Yu. S. Maksimov for his help in practical work and the useful discussions, É. Z. Ryndina and V. F. Kushniruk for the consultation on the counter preparation technology, and A. T. Vinogradova and V. V. Strulev for their help in preparing the counters.

#### LITERATURE CITED

1. R. Ewing, IRE Trans., NS-9, No. 3, 207 (1962).
2. G. F. Bogdanov, P. I. Kozlov, and B. P. Maksimenko, In the collection: Plasma Diagnostics [in Russian], Edited by B. P. Konstantinov, Moscow, Gosatomizdat, (1963), p. 175.

DEPENDENCE OF THE ENERGY LOSS AVERAGED WITH RESPECT  
TO THE ELECTRON SPECTRUM ON THE END-POINT ENERGY  
OF THE  $\beta$ -SPECTRUM, THE ATOMIC NUMBER OF THE  $\beta$ -RADIATOR,  
AND THE TRANSITION TYPE

(UDC 577.391.087)

V. F. Baranov

Translated from *Atomnaya Énergiya*, Vol. 19, No. 5,

pp. 450-451, November, 1965

Original article submitted January 28, 1965

Final version submitted April 7, 1965

The dose  $D$  due to  $\beta$ -radiation can be determined from the relationship

$$D = 1.6 \cdot 10^{-8} N t \bar{S} \text{ rad}, \quad (1)$$

where  $N$  is the density of the flux of  $\beta$ -particles ( $\text{cm}^{-2} \cdot \text{sec}^{-1}$ ),  $t$  is the irradiation time (sec), and  $\bar{S}$  is the ionization loss per single  $\beta$ -particle, averaged with respect to the electron spectrum ( $\text{MeV} \cdot \text{cm}^2 \cdot \text{g}^{-1}$ ). The  $\bar{S}$  value depends on the absorber material, the end-point energy, and the shape of the electron spectrum; it is calculated by means of the expression:

TABLE 1. Calculated Values of Ionization Losses per Single  $\beta$ -Particle for Aluminum and Tissue (water)

$E_0$ , MeV	Allowed $\beta$ -transition					Absolutely forbidden first-order $\beta$ -transitions		
	Z = 10	Z = 20	Z = 40	Z = 60	Z = 80	Z = 10	Z = 40	Z = 80
In aluminum								
0,1	13,2	14,4	16,3	16,8	17,2	8,45	9,70	11,5
0,2	7,85	8,55	9,65	9,95	10,1	5,85	6,58	7,70
0,3	5,75	6,30	7,10	7,35	7,50	4,70	5,25	6,05
0,4	4,63	5,10	5,70	5,90	6,00	4,03	4,45	5,15
0,6	3,42	3,73	4,20	4,35	4,45	3,25	3,55	4,05
0,8	2,83	3,05	3,41	3,55	3,65	2,79	3,05	3,43
1,0	2,48	2,65	2,95	3,05	3,15	2,50	2,73	3,03
1,5	2,02	2,13	2,30	2,38	2,44	2,08	2,25	2,42
2,0	1,80	1,88	1,98	2,04	2,08	1,85	1,99	2,11
3,0	1,62	1,66	1,70	1,73	1,77	1,69	1,75	1,82
In tissue (water)								
0,1	17,1	18,6	21,1	21,7	22,2	10,9	12,5	14,9
0,2	10,1	11,0	12,4	12,8	13,0	7,51	8,45	9,90
0,3	7,35	8,05	9,06	9,39	9,57	6,00	6,70	7,72
0,4	5,88	6,47	7,24	7,50	7,61	5,11	5,65	6,54
0,6	4,30	4,70	5,29	5,47	5,60	4,09	4,46	5,10
0,8	3,54	3,81	4,26	4,44	4,56	3,48	3,81	4,29
1,0	3,08	3,30	3,67	3,80	3,92	3,11	3,40	3,77
1,5	2,48	2,62	2,83	2,93	3,00	2,56	2,77	2,98
2,0	2,20	2,29	2,42	2,49	2,54	2,26	2,43	2,57
3,0	1,96	2,01	2,06	2,09	2,14	2,04	2,12	2,20

$$\bar{S} = \frac{\int_0^{E_0} S(E, Z_{\text{abs}}) n(E) dE}{\int_0^{E_0} n(E) dE}, \quad (2)$$

where  $n(E) dE$  is the number of electrons with energies in the interval from  $E$  to  $E + dE$ ;  $E_0$  is the end-point energy of the spectrum, and  $S(E, Z_{\text{abs}})$  is the ionization loss of electrons with the energy  $E$  in an absorber whose atomic number is  $Z_{\text{abs}}$ . In [1, 2], the  $\bar{S}_{\text{ti}}$  values for tissue were calculated on the basis of the  $\beta$ -spectra of certain radioactive isotopes, which were measured by means of a scintillation spectrometer. Unfortunately, such analyzers distort the shape of the  $\beta$ -spectrum in the energy range below 200-300 keV. Moreover, the dependence of  $\bar{S}$  on the spectral shape has not yet been determined in a wide range of the spectral end-point energies  $E_0$ .

We shall calculate here the energy losses of  $\beta$ -radiation in aluminum and tissue, averaged with respect to the electron spectrum, for radiators with allowed transitions and with absolutely forbidden first-order transitions. The  $Z$  values for the  $\beta$ -radiators were equal to 10, 20, 40, 60, and 80; the end-point energies of the spectrum were in the range  $0.1 \leq E_0 \leq 3.0$  MeV. The electron energy distribution  $n(E) dE$  was calculated in the same manner as in [3]. In calculating  $\bar{S}$ , we used the data given in [4, 6]

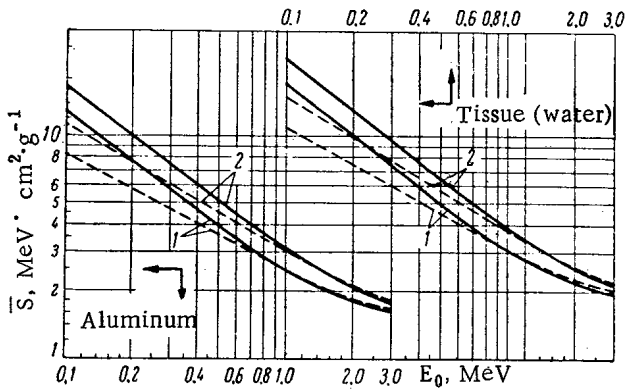


Fig. 1. Averaged energy losses of  $\beta$ -radiation in aluminum and tissue (water) in dependence on the end-point energy of the  $\beta$ -spectrum: 1)  $Z = 10$ ; 2)  $Z = 80$ ; —) allowed transitions; - - -) absolutely forbidden first-order transitions.

TABLE 2. Accuracy of  $\bar{S}$  Determinations Based on Expression (4)

Allowed $\beta$ -transitions		Absolutely forbidden first-order $\beta$ -transition	
$E_0$ , MeV	$\delta$ , %	$E_0$ , MeV	$\delta$ , %
0,1—1,0	+2; -18	0,2—0,4	$\pm 8$
1,0—2,0	$\pm 8$	0,4—1,5	0; -12
2,0—3,0	+9; -2	1,5—3,0	$\pm 5$

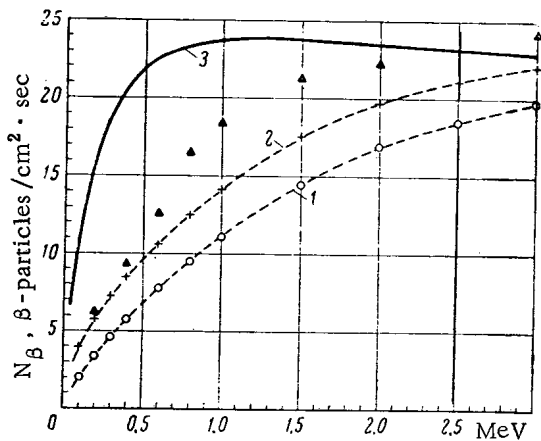


Fig. 3. Dependence of the maximum allowable flux of  $\beta$ -particle on the end-point energy of the  $\beta$ -spectrum.

The  $\bar{E}$  value can be determined on the basis of data from [3], while the  $R(E)$  values for different absorbers are given [4-6]. Table 2 provides the upper and lower values of the error  $\delta$  in determining  $\bar{S}$  by means of (4).

The calculated  $S$  values are necessary for determining the dose due to the  $\beta$ -radiation of radioactive specimens when the shape of the electron spectrum is close to the shape of the emission spectrum and for determining

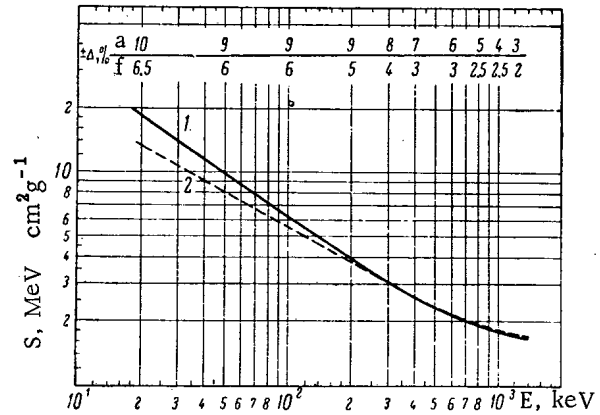


Fig. 2. Dependence of the averaged energy losses of  $\beta$ -radiation in aluminum on the mean energy of the  $\beta$ -spectrum: 1) allowed transitions (a); 2) absolutely forbidden first-order transitions (f).

for the ionization losses of the electron energy in aluminum, water, and tissue in the energy range  $1 \leq E \leq E_0$  keV. The contribution of electrons with energies of  $1 - 10$  keV to the  $S$  value is considerable for small  $E_0$  values and large  $Z$  values of the radiator; it attains 30%. In determining  $\bar{S}$  on the basis of the experimentally measured  $\beta$ -spectra, this energy range is usually neglected [1]. The results obtained in calculating  $\bar{S}$  by means of expression (2) for aluminum and tissue (water) are given in Table 1 and Fig. 1. The relationship between  $\bar{S}_{ti}$  and  $\bar{S}_{Al}$  for the corresponding  $E_0$  and  $Z$  values in the case of allowed transitions and absolutely forbidden first-order transitions in the range  $0.1 \leq E_0 \leq 3$  MeV is given by

$$\bar{S}_{ti} = (1.25 \pm 0.04) \bar{S}_{Al}. \quad (3)$$

For  $E_0 = 0.1$  MeV, in dependence on the radiator's value and the transition type, the difference between the  $\bar{S}$  values attains 50% (for  $E_0 = 3.0$  MeV, it amounts to 11%). Figure 2 shows the dependence of  $\bar{S}_{Al}$  on the mean energy  $\bar{E}$  of the  $\beta$ -spectrum and also the errors  $\pm \Delta \%$  with which the  $\bar{S}_{Al}$  values can be determined if  $\bar{E}$  and the transition type are known, but the  $Z$  value of the radiator is not known. It was found that the ratio  $\bar{E}/\bar{S}$  is very close to the value of the maximum range  $R(\bar{E})$  of monoenergetic electrons with the energy  $E = \bar{E}$ . On the basis of this, the  $\bar{S}$  value can be calculated by using the approximate expression:

$$\bar{S} = \frac{\bar{E}}{R(\bar{E})}. \quad (4)$$



the specific activity of thick-layer  $\beta$ -sources. Moreover, by means of  $\bar{S}$ , the maximum allowable fluxes  $N_{\beta}$  of  $\beta$ -particles can be determined with greater accuracy. For an absorbed dose rate of 0.1 rad/week and an irradiation time  $t = 40$  h per week,

$$N_{\beta} = \frac{43.4}{\bar{S}_{ti}} \quad (5)$$

Figure 3 shows the dependence of  $N_{\beta}$  and  $E_0$ , calculated by means of expression (5) for radiators with  $Z = 80$  (curve 1) and  $Z = 10$  (curve 2). For the sake of comparison, the figure also provides the  $N_{\beta}$  values for monoenergetic electrons with the energy  $E = E_0$  borrowed from [7] and converted for  $t = 40$  h (curve 3), and the data from [1] for the experimentally measured  $\beta$ -spectra, which were reduced to an absorbed dose rate of 0.1 rad/week and  $t = 40$  h (triangles).

#### LITERATURE CITED

1. K. K. Aglintsev and V. P. Kasatkin, Collection of Papers on Certain Problems in the Dosimetry and Radiometry of Ionizing Radiation [in Russian], Edited by Yu. V. Sivintsev, Vol. 1, Moscow, Gosatomizdat (1960), p. 59; *Atomnaya Énergiya*, 7, 138 (1959).
2. K. K. Aglintsev and V. P. Kasatkin, *Atomnaya Énergiya*, 12, 51 (1952).
3. N. S. Shimanskaya and É. G. Zaletskii, *Atomnaya Énergiya*, 17, 9 (1964).
4. L. Spencer, *Phys. Rev.*, 98, 1597 (1955).
5. A. Nelms, NBS Circular 577, Washington (1956).
6. R. Eger, *Dosimetry and Radiation Protection* [Russian translation], Moscow, Gosatomizdat (1961), p. 75.
7. N. G. Gusev, *Maximum Allowable Levels of Ionizing Radiation* [in Russian], Moscow, Medgiz (1961), p. 110.

COEFFICIENTS OF SECONDARY  $\gamma$  - RADIATION  
FOR ALUMINUM, COPPER, AND TUNGSTEN

(UDC 539.122)

S. P. Belov, V. P. Demin, Yu. A. Kazanskii, A. P. Lobakov,  
and V. I. Popov

Translated from *Atomnaya Énergiya*, Vol. 19, No. 5,  
pp. 452-453, November, 1965

Original article submitted March 10, 1965

The coefficient  $\beta$  of secondary  $\gamma$ -radiation was introduced in [1] as the ratio of the total number of capture  $\gamma$ -quanta with an energy above  $E_{thr}$  emerging from the shield's surface (the integral flux of  $\gamma$ -quanta) to the total number of neutrons leaving this surface (the integral neutron flux). The experimental method for determining  $\beta$ , which has been described in detail in [1], does not require the determination of the absolute yield of  $\gamma$ -quanta and neutrons from the shield. For determining  $\beta$ , it is necessary to measure the ratio of the number ( $N_\gamma$ ) of  $\gamma$ -quanta emerging from the shield's surface to the number ( $N_\gamma^*$ ) of  $\gamma$ -quanta in the case where there is a water layer on the shield's surface. Then, as was shown in [1],

$$\beta = \frac{\delta k \eta}{\frac{N_\gamma^*}{N_\gamma T} - 1} \cdot \frac{G'(R, \theta)}{G(R, \theta)}$$

where  $\delta$  is the ratio of the number of neutrons returned by the water layer to the shield and trapped in it to the number of neutrons emerging from the shield without an aqueous reflector,  $k$  is the self-absorption factor of capture  $\gamma$ -quanta which are generated in the shield material by the neutrons reflected by water,  $\eta$  is the number of  $\gamma$ -quanta with an energy exceeding  $E_{thr}$  per single absorbed neutron ( $\eta$  can be determined by using the data from [2]),  $T$  is the factor of attenuation of  $\gamma$ -quanta in the water layer, and  $G'(R, \theta)$  and  $G(R, \theta)$  are geometric factors which take into account the spatial and angular distributions of the capture  $\gamma$ -radiation emerging from the shield in the presence and absence of an aqueous reflector, respectively. By introducing the geometric factors according to the method described in [1], we can calculate the integral flux of  $\gamma$ -quanta beyond the shield by using the radiation flux measured at a certain distance  $R$  from the shield at the angle  $\theta$  (for instance,  $\theta = 0^\circ$ ) with respect to the normal passing through the center of the neutron source and the calculated angular distribution of  $\gamma$ -radiation beyond the shield. The methods for determining the  $\delta$ ,  $k$ ,  $T$  and  $G'(R, \theta)/G(R, \theta)$  values were also described in detail in [1].

Values of the  $\beta$  Coefficients

Material	Thick- ness, cm	$\delta$	$k$	$\eta$ for $E > 5$ MeV	$N_\gamma^*/N_\gamma T$	$G'(R, \theta)/G(R, \theta)$	$\beta$ , %
Aluminum	20	0,21	0,64	0,40	12,4	0,19	0,09
	9,5	0,36	0,71	0,66	6,0	0,63	2,2
Copper	28,5	0,43	0,71	0,66	4,8	0,54	2,9
	48	0,44	0,71	0,66	4,5	0,54	3,2
Tungsten	5	0,44	0,60	0,14	5,0	0,73	0,68
	10	0,49	0,56	0,14	5,4	0,71	0,62
	13	0,47	0,62	0,14	5,6	0,71	0,63
	17	0,52	0,59	0,14	6,5	0,71	0,56

Earlier, papers [1, 3] provided the experimentally determined coefficients of secondary  $\gamma$ -radiation for iron, nickel, and nickel with boron on the basis of the neutron spectra of a Po- $\alpha$ -Be-source and of the reactor of the RIZ stand.

In our experiments, we determined the coefficient of secondary  $\gamma$ -radiation for aluminum, copper, and tungsten. The measurements were performed on the RIZ stand. The RIZ stand and the experimental devices were described in detail in [3]. A single-crystal scintillation spectrometer with sodium iodide, whose diameter and length were equal to 40 mm, served as the  $\gamma$ -radiation detector.

The values of the  $\beta$  coefficients and of the intermediate quantities necessary for calculating  $\beta$  are given in the table.

The  $N_{\gamma}^*/N_{\gamma}$  ratio was determined with respect to the instrumental distributions of  $\gamma$ -quanta by summing the counts in each channel, beginning with the amplitudes corresponding to a  $\gamma$ -quantum energy of 5 MeV. The  $(N_{\gamma}^*/N_{\gamma})$  ratio was thus determined for aluminum and tungsten. The shapes of the instrumental distributions  $N_{\gamma}^*(E)$  and  $N_{\gamma}(E)$  and, consequently, the spectral distributions for these media differ only slightly from each other, so that this operation was justified. For copper, the above distributions differ considerably. It was shown in [4] that the spectra of  $\gamma$ -radiation in the case of radiative capture of neutrons whose energies exceed 50 keV differ considerably from the  $\gamma$ -radiation spectrum in the case of thermal neutron capture. Therefore, the  $N_{\gamma}^*/N_{\gamma}$  ratios for copper were determined with respect to the spectral distributions obtained by transforming the amplitude distributions by means of the matrix used in [4]. It should be noted that the values of these ratios were only by 10-20% lower than those obtained with respect to the instrumental distributions. The error in determining the  $\beta$ -coefficients was 10-20%. It was calculated as the root-mean-square value of the errors in individual factors in the expression for  $\beta$ .

#### LITERATURE CITED

1. A. T. Bakov et al., *Atomnaya Énergiya*, 13, 31 (1962).
2. L. V. Groshev et al., *Atlas of Spectra of Thermal-Neutron Radiative-Capture  $\gamma$ -Radiation* [in Russian], Moscow, Atomizdat (1958).
3. S. P. Belov et al., *Atomnaya Énergiya*, 18, 136 (1965).
4. A. T. Bakov and Yu. A. Kazanskii, *ZhÉTF*, 46, 1163 (1964).

---

All abbreviations of periodicals in the above bibliography are letter-by-letter transliterations of the abbreviations as given in the original Russian journal. *Some or all of this periodical literature may well be available in English translation. A complete list of the cover-to-cover English translations appears at the back of this issue.*

---

VISCOSITY COEFFICIENT OF HYDROGEN (H<sub>2</sub>, D<sub>2</sub>), NEON (Ne<sup>20</sup>, Ne<sup>22</sup>)  
AND HELIUM (He<sup>3</sup>) ISOTOPES IN THE TEMPERATURE RANGE -195 TO +25°C

(UDC 533.16 : 546.117)

N. E. Menabde

Translated from *Atomnaya Énergiya*, Vol. 19, No. 5,  
pp. 553-454, November, 1965  
Original article submitted February 3, 1965

In studying transfer phenomena, data on the viscosity coefficient of gaseous isotopes and isotopic compounds are of particular interest in order to obtain additional information on the mechanism of intermolecular interactions. It is well known that experimental values of the viscosity as a function of temperature may be used to calculate the force parameters of the interatomic-interaction potential function, in particular the Lennard-Jones function:

$$\varphi(r) = 4\varepsilon \left[ \left( \frac{\sigma}{r} \right)^{12} - \left( \frac{\sigma}{r} \right)^6 \right], \quad (1)$$

where  $\varepsilon$  is the depth of the potential well and  $\sigma$  is the collision diameter of low-energy molecules.

At the present time the parameters of function (1) have only been determined and calculated for hydrogen isotopes H<sub>2</sub> and D<sub>2</sub>. Since the differences in intermolecular interaction for the isotopes of heavier gases are small, high measuring accuracy is needed in order to detect them. The present measurements were made on a vibrating-disk viscosimeter at pressures of 40 to 50 mm Hg, graduated with respect to the viscosity of helium [1]. A special cryostat made it possible to keep the experimental temperature constant to 0.01°C over the whole temperature range measured.

TABLE 1. Viscosity Coefficient  $\eta$ ,  $\cdot 10^6$  g/cm $\cdot$ sec

He <sup>3</sup>		Ne <sup>20</sup>		Ne <sup>22</sup>		H <sub>2</sub>		D <sub>2</sub>	
T, °C	$\eta$	T, °C	$\eta$	T, °C	$\eta$	T, °C	$\eta$	T, °C	$\eta$
22,1	171,6	21,6	311,7	23,3	327,8	26,5	90,2	25,9	125,2
21,6	171,2	18,9	309,6	19,0	324,4	24,3	89,7	24,1	124,7
18,0	170,0	-10,3	288,7	20,0	325,2	20,0	88,8	20,0	123,6
17,6	169,8	-50,5	258,0	17,5	323,5	-35,6	77,0	-28,1	109,8
-20,0	154,4	-80,8	233,3	-20,3	294,2	-73,1	68,4	-44,1	104,8
-53,5	140,5	-90,2	225,8	-33,3	283,6	-96,9	62,7	-73,0	95,8
-58,0	138,8	-102,3	215,6	-38,2	280,1	-118,5	57,4	-107,1	83,3
-68,0	134,2	-110,3	208,5	-75,2	249,4	-139,6	51,8	-154,3	66,1
-93,4	123,3	-122,2	206,8	-100,6	227,6	-162,1	45,3	-183,0	54,1
-121,7	110,6	-130,2	190,3	-119,0	210,3	-183,0	39,1	-195,8	48,3
-123,7	109,7	-155,0	166,2	-146,7	182,4	-195,8	35,2	—	—
-147,5	98,0	-156,6	164,8	-150,0	178,7	—	—	—	—
-159,4	91,8	-156,8	164,5	-154,2	174,8	—	—	—	—
-160,0	91,7	-161,5	159,6	-156,0	173,0	—	—	—	—
-174,6	83,6	-174,3	145,3	-160,0	168,2	—	—	—	—
-179,1	81,2	-179,0	140,1	-177,3	148,4	—	—	—	—
-195,8	71,7	-195,8	120,3	-181,5	143,6	—	—	—	—
—	—	—	—	-195,8	125,0	—	—	—	—

TABLE 2. Viscosity Ratios of Isotopes at Various Temperatures

T°, C	$\eta_{D_2}/\eta_{H_2}$	$\eta_{Ne^{22}}/\eta_{Ne^{20}}$	$\eta_{He^4}/\eta_{He^3}$
20	1,392	1,047	1,148
0	1,391	1,047	1,149
-20	1,394	1,047	1,150
-40	1,396	1,047	1,151
-60	1,398	1,047	1,151
-80	1,397	1,047	1,151
-100	1,397	1,047	1,151
-120	1,395	1,048	1,152
-140	1,388	1,046	1,152
-160	1,386	1,045	1,152
-180	1,382	1,045	1,152
-195,8	1,372	1,039	1,152

TABLE 3. Force Parameters of Potential (1)

Isotope	$r/k, ^\circ K$	$\sigma, \text{ \AA}$
He <sup>3</sup>	11,2	2,561
He <sup>4</sup>	10,2	2,582
Ne <sup>20</sup>	34,9	2,796
Ne <sup>22</sup>	34,4	2,802
H <sub>2</sub>	36,8	2,928
D <sub>2</sub>	35,4	2,960

The accuracy of measuring the relative viscosity was around 0.03% at room temperature and 0.02% at the boiling point of liquid nitrogen. The deuterium was obtained by the electrolysis of heavy water, D<sub>2</sub>O. The isotopes of neon enriched in a separator (Ne<sup>20</sup> to 99.75% and Ne<sup>22</sup> to 99.88%) and helium isotope He<sup>3</sup> (99.8% concentration) were freed from air impurities by means of activated charcoal cooled in liquid nitrogen.

The measured viscosities of the isotopes in question are shown in Table 1. We see from Table 2 that the viscosity ratio of the isotopes,  $\eta_H/\eta_L$ , differs from  $(M_H/M_L)^{1/2}$ , where  $M_H$  and  $M_L$  are the molecular weights of the heavy and light isotopes, respectively. Moreover, starting from a particular temperature for each substance, the ratio diminishes, except in the case of helium, for which the ratio rises between room temperature and -110°C, reaching 1.152 at the latter and thereafter remaining constant.

The viscosity of the isotopes H<sub>2</sub> and D<sub>2</sub> has been measured by many workers over a fairly wide temperature range.

Comparison of our own results with those of others at two temperatures shows that, at 20°C, our value for  $\eta_{D_2}/\eta_{H_2}$  (equal to 1.392) is quite close to the 1.388 given in [1], 1.39 in [2], and 1.40 in [3]. At -190.0°C our value of  $\eta_{D_2}/\eta_{H_2}$  is 1.375; that given elsewhere is 1.380 [4] and 1.37 [5].

Using the method described in [6], we calculated the force parameters of potential (1) from the temperature dependence of the viscosity. Table 3 gives the values of these parameters.

## LITERATURE CITED

1. A. Rietveld and A. Van Itterbeek, *Physika*, 25, 205 (1959).
2. A. Van Itterbeek and A. Claes, *Physika*, 5, 938 (1938).
3. J. Kestin and W. Leidenfrost, *Physika*, 25, 1033 (1959).
4. J. Coremans et al., *Physika*, 24, 557 (1958).
5. A. Van Itterbeek and Van Paemel, *Physika*, 7, 263 (1940).
6. J. Hirschfelder et al., *Molecular Theory of Gases and Liquids* [Russian translation], Moscow, IL (1961), p. 443.

DETERMINATION OF THE SPECTRAL CHARACTERISTICS  
OF ISOTOPIC NEUTRON SOURCES BY PAIRED SCINTILLATION CRYSTALS  
OF THE LiI(Eu) TYPE

(UDC 539.16.08)

P. L. Gruzin, A. Z. Kichev, V. M. Minaev, V. T. Samosadnyi,  
and Su Ch'ang-sung

Translated from *Atomnaya Énergiya*, Vol. 19, No. 5,  
pp. 454-456, November, 1965

Original article submitted February 25, 1965 and final form May 31, 1965

Existing methods of determining the spectral characteristics of neutron sources require expensive equipment and considerable time. The determination of the spectral characteristics of isotopic neutron sources by scintillation crystals of the LiI(Eu) type is based on a method of nuclear reactions induced by neutrons in which only charged particles are formed [1]. By determining the over-all energy of the charged particles, we can calculate the energy of the neutrons [2]. The advantage of the scintillation method over-all the rest is its high sensitivity to neutrons. Owing to the high energy of the  $\text{Li}^6(n, \alpha)T$  ( $Q = 4.78$  MeV) reaction, the effect of  $\gamma$ -background on the energy spectrum of the neutrons is relatively slight.

The energy of  $\gamma$ -quantum creating the same light scintillation as that of a thermal neutron equals 3 MeV for LiI(Eu)-type crystals. Since the number of  $\gamma$ -quanta with energy greater than 3 MeV may in most cases be compared with the number of neutrons, the  $\gamma$ -background must be taken into account. In this paper we consider the method of subtracting the  $\gamma$ -background by means of paired scintillation crystals of the LiI(Eu) type [3].

The neutron spectrum of isotopic sources was recorded by means of two LiI(Eu)-type crystals of the same thickness and diameter, one enriched with isotope  $\text{Li}^6$  and the other with  $\text{Li}^7$ . The recording efficiency for  $\gamma$ -radiation was considered to be the same for both crystals, while that for fast neutrons was 150 times greater in the  $\text{Li}^6\text{I}(\text{Eu})$  crystal than the  $\text{Li}^7\text{I}(\text{Eu})$ , since the ratio of the number of  $\text{Li}^6$  nuclei in these crystals was 150. This enables us to regard the  $\text{Li}^7\text{I}(\text{Eu})$ -type crystal as practically insensitive to the recording of fast neutrons. The difference between the numbers of pulses in the same analyzer channels corresponding to the two crystals gives the number of neutrons recorded by the crystals. Thus the  $\gamma$ -background is eliminated.

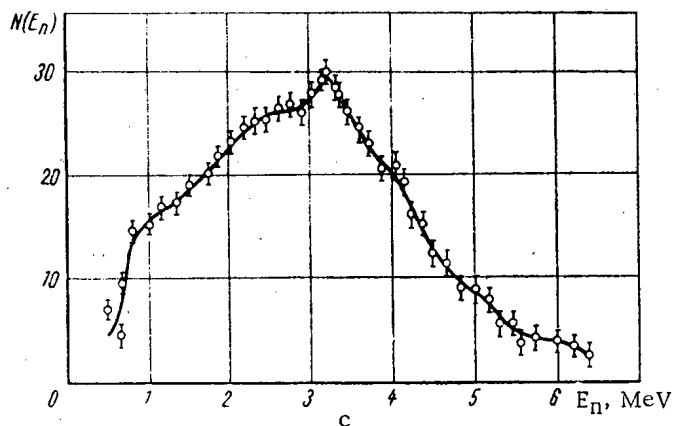
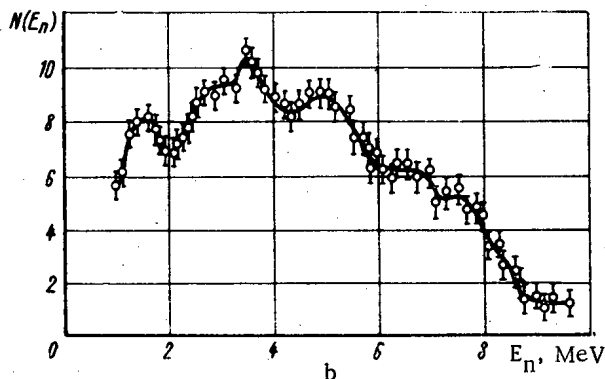
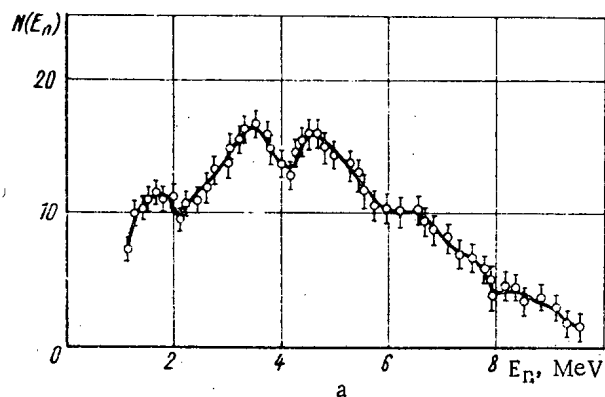
We used  $\text{Li}^6\text{I}(\text{Eu})$  and  $\text{Li}^7\text{I}(\text{Eu})$  crystals 39 mm in diameter and 16 mm thick; the  $\text{Li}^6$  enrichment,  $f$ , for  $\text{Li}^6\text{I}(\text{Eu})$  was 0.90 and the  $\text{Li}^7$  enrichment for the  $\text{Li}^7\text{I}(\text{Eu})$  0.994.

The presence of a small amount of isotope  $\text{Li}^6$  (0.6%) in the  $\text{Li}^7\text{I}(\text{Eu})$  crystal enabled us to correct the energy scales with respect to the thermal-neutron peaks present in the apparatus spectra of both crystals. The resolving power of the LiI(Eu) crystals was only determined with respect to the thermal neutrons and equaled 11%.

The calibration of the crystal was effected with respect to two points, its light output being linearly dependent on the kinetic energy of the neutron recorded. One reference point was the energy corresponding to thermal neutrons and the other was 4.16 MeV. Neutrons of energy 4.16 MeV were obtained in a Van-de-Graff linear accelerator.

Differential neutron spectra of Po-Be, Pu-Be, and Po-B sources were obtained by the method indicated. These spectra are shown in the figure. The spectrum of the Po-Be source is similar to that obtained by the photoemulsion method [4]. The upper limit of the neutron spectra of the Po-Be and Pu-Be sources lies at approximately 11 MeV, and for the Po-B source at 6 MeV, as we should expect.

From the neutron spectra obtained, relative determinations of the neutron yields may be made; by using a source such as Pu-Be ( $T_{1/2} = 2 \cdot 10^5$  years) we can also obtain the absolute neutron yields of the Po-Be and Po-B



Differential spectra of the a) Po-Be, b) Pu-Be, and c) Po-B neutron sources obtained by the authors.

sources. Our experimental data on strength was in good agreement with the standard values. The experimental data on the neutron yield for the Po-Be neutron source differed by 35% from the standard value, this source being experimental; it may well be that its initial strength was determined incorrectly. For the Po-B neutron source the difference between rated and experimental values of neutron yield was 5%.

Our neutron-yield results for the Po-Be source were supported by experiments on the  $\gamma$ -radiation of the neutron sources. By comparing the radiation intensities of Po-Be and Pu-Be 4.5-MeV neutron sources it was found that the neutron yield of the Po-Be source was some 1.35 times smaller than the rated value; this agrees with the direct comparison of neutron yields from the neutron spectra.

Comparison of the 0.8-MeV  $\gamma$ -radiation intensities showed that the neutron yield of the Po-Be source was 5.5 times greater than that of the Po-B source.

Our investigations have thus shown that the proposed method gives fairly reliable differential spectra of isotopic neutron sources; this gives grounds for believing that the method is quite applicable for determining certain characteristics of isotopic neutron sources.

The authors wish to thank B. M. Gokhberg and G. W. Yan'kov for collaboration in the experiments on calibrating the LiI(Eu) crystals, and also I. A. Velichko and E. O. Lyalin who kindly supplied the crystals.

#### LITERATURE CITED

1. R. Murray, Nucl. Instru., 2, 237 (1958).
2. E. Segré, Experimental Nuclear Physics [Russian translation], Vol. II, Moscow, IL (1955).
3. V. V. Matveev et al., "Pribory i tekhnika éksperimenta," No. 4 (1963).
4. B. Whitmore and W. Baker, Phys. Rev., 78, 799 (1950).



CROSS SECTIONS FOR THE INELASTIC INTERACTION  
 OF NEUTRONS WITH NUCLEI OF  $\text{Li}^7$ ,  $\text{C}^{12}$ ,  $\text{N}^{14}$ ,  $\text{Al}^{27}$ ,  $\text{Fe}^{56}$ ,  
 $\text{Cu}$ ,  $\text{Pb}$ ,  $\text{U}^{235}$ ,  $\text{U}^{238}$ , and  $\text{Pu}^{239}$

(UDC 529.125.5 : 539.17.02)

Yu. G. Degtyarev

Translated from *Atomnaya Énergiya*, Vol. 19, No. 5,  
 pp. 456-457, November, 1965  
 Original article submitted February 20, 1965

This article contains data additional to the results published in [1] for  $\text{Al}^{27}$ ,  $\text{Fe}^{56}$ ,  $\text{Cu}$ ,  $\text{Pb}$ ,  $\text{U}^{235}$ ,  $\text{U}^{238}$ , and  $\text{Pu}^{239}$ , and also the cross sections corresponding to the inelastic interaction of neutrons with the nuclei of  $\text{Li}^7$ ,  $\text{C}^{12}$ , and  $\text{N}^{14}$ .

The neutron transmission coefficients for spherical samples of the materials studied were measured in "reciprocal geometry" [2]. This method is as follows. The intensity of the flow of neutrons from an external monochromatic source is measured by means of a detector insensitive to inelastically-scattered neutrons, both inside the spherical sample and in its absence. Owing to the compensation of the elastically-scattered neutrons [2], the transmission coefficient of a sphere,  $T = (\text{intensity with sample}) / (\text{intensity without sample})$ , is simply a measure of the inelastic-interaction cross section.

Inelastic Neutron-Interaction Cross Sections

Isotope	Neutron energy, MeV	$x = r_2 - r_1^*$ , cm	$h = \frac{r_1}{r_2}$	$T$	$\sigma_{ne}$ , barn	$M$ , %
$\text{Li}^7$	16,7	6,35	0,11	$0,881 \pm 0,007$	$0,42 \pm 0,03$	1,8
	18,2	6,35	0,11	$0,867 \pm 0,010$	$0,47 \pm 0,04$	1,6
	20,7	6,35	0,11	$0,916 \pm 0,008$	$0,30 \pm 0,03$	1,4
$\text{C}^{12}$	15,2	3,8	0,28	$0,810 \pm 0,004$	$0,62 \pm 0,02$	2,8
	19,8	3,8	0,28	$0,800 \pm 0,002$	$0,65 \pm 0,02$	2,4
$\text{N}^{14}$	15,2	9,5	0,14	$0,792 \pm 0,004$	$0,70 \pm 0,03$	2,0
	19,8	9,5	0,14	$0,792 \pm 0,010$	$0,69 \pm 0,05$	1,7
$\text{Al}^{27}$	8,1	3,0	0,4	$0,830 \pm 0,012$	$1,02 \pm 0,08$	2,3
$\text{Fe}^{56}$	8,1	3,0	0,4	$0,700 \pm 0,010$	$1,34 \pm 0,06$	5,3
	19,7	2,9	0,42	$0,738 \pm 0,007$	$1,22 \pm 0,04$	2,2
$\text{Cu}$	8,1	3,0	0,4	$0,675 \pm 0,010$	$1,47 \pm 0,07$	5,5
$\text{Pb}$	8,1	3,0	0,4	$0,793 \pm 0,008$	$2,28 \pm 0,08$	3,5
$\text{U}^{235}$	8,1	1,82	0,5	$0,760 \pm 0,012$	$3,11 \pm 0,20$	3,6
$\text{U}^{238}$	8,1	2,95	0,5	$0,633 \pm 0,008$	$3,10 \pm 0,10$	5,2
	17,5	2,95	0,5	$0,679 \pm 0,020$	$2,71 \pm 0,21$	2,5
$\text{Pu}^{239}$	13,4	1,5	0,7	$0,851 \pm 0,011$	$2,72 \pm 0,20$	2,3
	15,4	1,5	0,7	$0,853 \pm 0,011$	$2,70 \pm 0,20$	2,0
	18,4	1,5	0,7	$0,861 \pm 0,006$	$2,57 \pm 0,07$	1,5

\*  $r_1$  and  $r_2$  are the internal and external radii of the spherical sample, respectively.

Neutrons with energies of 8.1 and 13 to 21 MeV, respectively were obtained in an electrostatic accelerator, using the  $\text{Be}^9(\alpha, n)\text{C}^{12}$  and  $\text{T}(d, n)\text{He}^4$  reactions. The neutron-flux intensity was measured from the edge of the spectrum of recoil protons from a scintillation plastic detector. The height and diameter of the crystal were 14 mm, ensuring fair discrimination of  $\gamma$ -quanta for neutron energies above 13 MeV. In order to secure discrimination of  $\gamma$ -quanta for neutron energies of 8.1 MeV, a stilbene single crystal was used as scintillator and a pulse-shape discrimination scheme was employed [3]. The main information regarding the samples used in the measurements is shown in the table, together with the results of the measurements. For light nuclei (from  $\text{Li}^7$  to  $\text{Al}^{27}$ ) a correction for the fall in the recording efficiency of elastically-scattered neutrons was introduced into the measured transmission coefficients. The table shows values of  $T$  with due allowance for this correction.

The inelastic-interaction cross sections  $\sigma_{ne}$  were determined with allowance for multiple scattering from the relation

$$T = T_0 + (1 - T_0) \frac{\sigma_{et} + P_m}{\sigma_{ne} + \sigma_{et} P_m}, \quad (1)$$

and from the formula

$$T = e^{-n\sigma_{ne}x}, \quad (2)$$

where  $x$  is the thickness of the spherical sample,  $T_0 = e^{-n\sigma_{tr}x}$ ,  $\sigma_{tr}$  is the total transport cross section,  $\sigma_{et}$  the elastic-scattering transport cross section, and  $P_m$  the probability of a neutron escaping from the sphere after elastic collision. In no case did the value of the multiple scattering  $M$  (see table) exceed 5.50%. This was due to the strong anisotropy of the elastic scattering and to the sample dimensions chosen.

The results obtained for  $\sigma_{ne}$  are very precise and partly fill up the gap in the neutron-energy range from 8 to 21 MeV.

#### LITERATURE CITED

1. Yu. G. Degtyarev and V. G. Nadochii, "Atomnaya Énergiya," 11, 397 (1961).
2. H. Bethe, J. Beyster, and R. Carter, J. Nucl. Energy, 3, 207 (1956).
3. F. Brooks, Nucl. Instrum., 4, 151 (1959).

CROSS SECTIONS FOR THE RADIATIVE CAPTURE  
OF FAST NEUTRONS IN RHENIUM AND TANTALUM

(UDC 539.17.02 : 539.172.4)

V. N. Kononov and Yu. Ya. Stavisskii

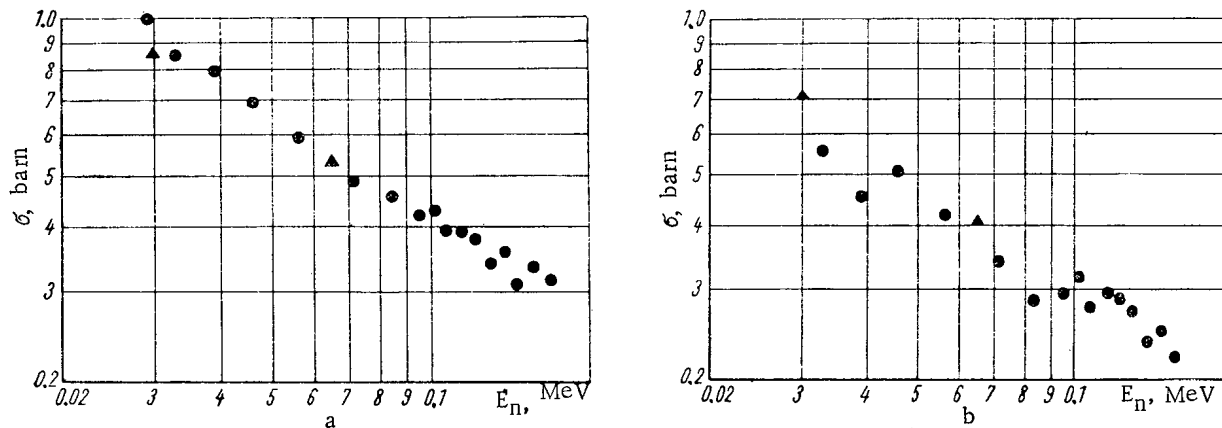
Translated from *Atomnaya Énergiya*, Vol. 19, No. 5,  
pp. 457-458, November, 1965

Original article submitted May 6, 1965

The cross sections for the radiative capture of neutrons in rhenium and tantalum were measured in the energy range 30 to 170 keV. The neutrons were provided by the  $T(p, n)He^3$  reaction on the target of a pulse accelerator with a maximum proton energy of 1.2 MeV. For recording cases of capture with respect to prompt  $\gamma$ -rays, a liquid scintillation detector of dimensions  $0.5 \times 0.5 \times 0.5$  m was used. The neutron energy was measured from the time of flight with a time resolution of 20 to 30 nsec and a base of 1.5 m.

The figure shows the energy dependence of the cross sections for the radiative capture of neutrons by rhenium and tantalum nuclei. The cross sections were measured to an accuracy of 10 to 12% with an energy resolution of 10%. The behavior of the cross sections as a function of neutron energy was determined relative to that of the capture cross section in indium [1], and the absolute cross sections fixed by means of new data on the absolute cross sections for the absorption of 24-keV neutrons [2]. The reference cross sections used in our calculations were 10% smaller than those used in [1]. The data of [1], however, require renormalization, all the cross sections being reduced 5%, in view of a change in reference cross sections [3]. Thus the difference between our reference cross sections and those of [1] is effectively 5%.

Our cross sections agree closely with the results of [1, 4] (these results are shown partly in the figures). In the tantalum capture cross sections there is competition with inelastic neutron scattering at levels 136 and 159 keV; this was not observed in [1]. The considerable difference between the results of [5] and the cross sections obtained by ourselves and in [1, 4] is evidently due to the large indeterminacy in fixing the absolute value of the cross sections by using the  $U^{235}$  neutron-absorption cross section as reference. This indeterminacy was due to the considerable difference in the spectra and number of emitted  $U^{235}$  neutron-absorption cross section as reference, and this led



Variation of the cross section for the radiative capture of neutrons in (a) rhenium and (b) tantalum with neutron energy: ●) present work; ▲) results taken from [1].

to a 1.7-times rise in the capture cross sections. Hence in choosing the reference cross section preference was given to the results obtained by measuring the neutron-absorption cross sections in spherical geometry.

LITERATURE CITED

1. J. Gibbons et al., Phys. Rev., 122, 182 (1961); R. Macklin et al., Phys. Rev., 129, 2659 (1963).
2. T. S. Belanova et al., "Atomnaya énergiya," 19, 3 (1965).
3. H. Schmitt, WASH-1044 (1963).
4. V. A. Konks, Yu. P. Popov, and F. L. Shapiro, ZhÉTF, 46, 80 (1964).
5. B. Diven et al., Phys. Rev., 120, 556 (1960).

PRODUCING STABLE ISOTOPES OF KRYPTON  
AND XENON BY IRRADIATING ALUMINUM HALIDES IN A REACTOR

(UDC 621.039.3)

A. N. Murin, L. K. Levskii, and A. E. Zakharova

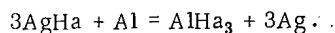
Translated from *Atomnaya Énergiya*, Vol. 19, No. 5,  
pp. 458-459, November, 1965  
Original article submitted March 1, 1965

Much work has been done in various fields of analytical and nuclear chemistry, geochemistry, and cosmochemistry in determining small concentrations (up to  $10^{-13}$  or  $10^{-14}$  g) of elements or their isotopes [1]. For solving this kind of problem, mass spectrometers (extremely accurate and sensitive instruments) and isotope dilution are used [2]. The accuracy of the method is determined mainly by the presence of a monoisotope of the element being studied (the best case) or an isotopic mixture greatly enriched with respect to one isotope. Obtaining monoisotopes of inert gases by classical methods of thermodiffusion is an expensive and laborious process. A more promising method is that of producing the isotopes by means of an  $(n, \gamma)$  reaction followed by  $\beta$ -decomposition, and also that of irradiating the corresponding halides in a reactor. \* Despite the wide application of stable isotopes of inert gases, however, there is no detailed description of the irradiation procedure and sample preparation in the literature.

For a variety of reasons aluminum halides are convenient for irradiation. The advantages of these are: 1) insignificant radiation hazard; 2) high specific halogen content; 3) crystalline state of the substance irradiated; 4) comparatively low melting point.

Despite the simplification in the separation process, however, there are some difficulties connected with the necessity of working with sealed ampoules previously evacuated to a low pressure, since during irradiation the melting point is 300 to 400°C, so that there may be partial degassing of the sample as a result of diffusion. Attempts have been made to use crystalline organic halogen compounds (e.g., tetrabromomethylene,  $C_2Br_4$ ) together with the aluminum halides, but these proved unsuccessful. The radiolysis taking place during irradiation raised the pressure in the quartz ampoules and burst them.

The aluminum halides were obtained by reducing the corresponding silver halides with aluminum according to the reaction



The apparatus for the reaction consisted of two quartz ampoules connected by a crosspiece. The reagent mixture was placed in one of the ampoules and the system was pumped out to a high vacuum. The ampoule containing the mixture was heated to some 400°C; the  $AlX_3$  condensed in the second (cooled) ampoule. The whole process lasted 10 to 15 sec. The ampoule containing the  $AlX_3$  was sealed off and placed in a container for irradiation. Spring shock absorbers were used in the packing; these pressed against the ends of the ampoule, which otherwise would be broken in removing from the irradiation zone.

Yield of Krypton and Xenon Isotopes on Irradiation  
with an Integral Neutron Flux of  $2.16 \cdot 10^{17}$

Iso- tope	Reaction	Cross section, mb	Gas yield, cm <sup>3</sup>
Kr <sup>80</sup>	$Br^{79} + n \rightarrow$ $\xrightarrow{\beta^-} Br^{80} \xrightarrow{18 \text{ min}} Kr^{80}$	10,1	$\sim 2,4 \cdot 10^{-2}$
Kr <sup>82</sup>	$Br^{81} + n \rightarrow$ $\xrightarrow{\beta^-} Br^{82} \xrightarrow{35,7 \text{ h}} Kr^{82}$	2,6	$\sim 0,6 \cdot 10^{-2}$
Xe <sup>132</sup>	$J^{127} + n \rightarrow$ $\xrightarrow{\beta^-} J^{128} \xrightarrow{25 \text{ min}} Xe^{128}$	0,25	$6,8 \cdot 10^{-4}$

When using  $AlBr_3$  and  $AlI_3$ , 2 g of the material were placed in the ampoules. The resultant yield of krypton and xenon isotopes appears in the table. In

\* When a natural mixture of bromine isotopes is irradiated, a bi-isotopic krypton specimen results.

working with a sensitive mass-spectral apparatus [3], sufficient quantities of krypton and xenon were obtained for several thousand determinations.

After holding for three weeks, the ampoules were placed in an apparatus for separating and purifying the inert gases. After opening under vacuum, the ampoules were heated, and the released gases were subjected to the purification usual for inert gases [3]. The apparatus contained liquid-nitrogen traps (solid carbon dioxide was used for working with xenon), and traps containing KOH, CuO ( $t = 600^{\circ}\text{C}$ ), and Ca ( $t = 600^{\circ}\text{C}$ ). The purified krypton and xenon were transferred to ampoules containing activated charcoal, which were then sealed.

The isotope analysis of krypton and xenon was effected in the MV-2302 mass spectrometer (high resolving power), the peaks corresponding to the krypton and xenon isotopes and those corresponding to possible hydrocarbon contamination being completely resolved. One xenon peak corresponding to  $\text{Xe}^{128}$  appeared on the mass spectrogram. The atmospheric-xenon component was less than 0.1%. The krypton mass spectrum contained  $\text{Kr}^{80}$  and  $\text{Kr}^{82}$ , the ratio  $\text{Kr}^{80}/\text{Kr}^{82}$  being 3.8; this practically agreed with computed data. The contribution from atmospheric krypton was less than 0.05%.

The authors wish to thank D. M. Kaminker for kindly permitting the use of the reactor in the A. F. Ioffe Physicotechnical Institute, and I. K. Kirin and Yu. A. Shukolyukov for assistance in the work. Student-Diplomat N. S. Okunev also took active part in the work.

#### LITERATURE CITED

1. D. Barnard, Modern Mass Spectrometry [Russian translation], Moscow, IL (1956). Also D. Beinson, Mass Spectrometry and Its Use in Organic Chemistry [in Russian], Moscow, "Mir," (1964).
2. R. Webster, Collection "Advances in Mass Spectrometry" [Russian translation], Moscow, IL (1963).
3. Yu. A. Shukolyukov and L. K. Levskii, "Zh. analit. khim.," XIX, 1099 (1964).

---

All abbreviations of periodicals in the above bibliography are letter-by-letter transliterations of the abbreviations as given in the original Russian journal. *Some or all of this periodical literature may well be available in English translation.* A complete list of the cover-to-cover English translations appears at the back of this issue.

---

MEASUREMENT OF  $Gd^{156}$  ABSORPTION CROSS SECTION

(UDC 539.172.4)

E. I. Grishanin, G. M. Kukavadze, V. I. Lependin,  
L. Ya. Mamelova, I. G. Morozov, V. V. Orlov, and D. T. Pilipets

Translated from *Atomnaya Énergiya*, Vol. 19, No. 5,  
pp. 459-460, November, 1965

Original article submitted April 2, 1965

To use gadolinium as a heavily shielded burnable poison [1], it is necessary to know the absorption cross section of its unburnable isotopes in order to determine the residual poisoning of a reactor. In the literature dealing with the unburnable gadolinium isotopes, there is only data on activation cross sections with not even that sort of information available for  $Gd^{154}$  and  $Gd^{156}$  because those isotopes do not form radioactive nuclei by the absorption of slow neutrons.

Because of the anomalously large values of the absorption cross sections of the isotopes  $Gd^{155}$  and  $Gd^{157}$ , it is practically impossible to use the existing method of transmission measurements with samples enriched in the pertinent isotope since, in that situation, a very high degree of freedom from the isotopes mentioned above is necessary.

The following method was used in this paper for the determination of the  $Gd^{156}$  absorption cross section. Samples containing gadolinium oxide in the amount of several milligrams were irradiated in the VVR-M reactor at the Institute of Physics, Ukrainian SSR Academy of Science, with varying total thermal neutron fluxes. Following this, the content of  $Gd^{157}$  and  $Gd^{156}$  isotopes was measured on a mass spectrometer. Starting with some value of the total thermal neutron flux, the  $Gd^{157}$  content reached an equilibrium value deriving only from the formation of these nuclei because of neutron absorption by the isotope  $Gd^{156}$ . In the equilibrium state, the following relations hold

$$\sigma_6 \rho_6 = \sigma_7 \rho_7 \quad \text{or} \quad \frac{\sigma_6}{\sigma_7} = \frac{\rho_7}{\rho_6},$$

where  $\sigma_6$ ,  $\sigma_7$  are the effective absorption cross sections of  $Gd^{156}$  and  $Gd^{157}$  corresponding to the neutron spectrum of the reactor in which the irradiation is performed;  $\rho_6$  and  $\rho_7$  are the equilibrium concentrations of these isotopes.

The value of  $\sigma_7$ , obtained by averaging the  $Gd^{157}$  absorption cross sections over the neutron spectrum of the VVR-M reactor with a neutron temperature of  $400 \pm 30^\circ K$ , was  $150,000 \pm 12,000$  barns. In computing the  $Gd^{157}$  cross sections, the resonance parameters given in [2] were used.

Having determined the isotopic composition of the irradiated samples, it was easy to obtain the  $Gd^{156}$  cross section from relation (1). Because the cross section at equilibrium concentration is independent of the value of the total flux, in making measurements of the latter, data on the distribution of the thermal neutron flux and on the amount of power generated by the reactor were employed.

To increase the equilibrium concentration of  $Gd^{157}$ , gadolinium samples enriched to 94.86% in the  $Gd^{156}$  isotope were used. The content of other isotopes in the samples was:  $Gd^{152}$ , 0.01%;  $Gd^{154}$ , 0.14%;  $Gd^{155}$ , 0.83%;  $Gd^{157}$ , 2.93%;  $Gd^{158}$ , 0.89%;  $Gd^{160}$ , 0.34%.

The mass-spectrometric, isotopic analysis of the gadolinium samples was performed with an MI-1311 mass spectrometer. An ion source with surface ionization was used. A strip of tungsten foil 30  $\mu$  thick acted as emitter. The gadolinium samples under investigation were deposited on the emitter in the form of an aqueous solution of the nitrate.

For current values of  $10^{-14}$  to  $10^{-18}$  A, the ion currents were recorded with an electron multiplier, and for  $Gd^{156}$  concentration measurements where the current values were more than  $10^{-14}$  A, a direct-current amplifier was used. Each time, before recording the ion currents, the amplification factor of the multiplier, which equalled  $(5-10) \cdot 10^3$ , was determined.

In carrying out this work, the resolution of the mass spectrometer at the level of 5% of the mass spectrum line intensity was 550 for a chamber vacuum of  $2 \cdot 10^{-7}$  mm Hg. Before each analysis, the emitters underwent conditioning, outgassing, and "burnup" of impurities, and the absence of residual lines in the mass range of interest was checked. As the result of surface ionization, the ions  $GdO^+$  and  $Gd^+$  appeared on the emitter. In the gadolinium samples used, impurities consisting of isotopes of other rare-earth elements were observed. Some of them, praeodymium in the form of the ion  $PrO^+$ , with mass 157 for example, which had very high ionization efficiencies were superimposed on the  $Gd^+$  ions with mass 157 and significantly distorted the results even for the presence of isotopic impurities so small they could not be observed by spectral methods. Changing the emitter temperature failed to get rid of traces of these isotopes, and therefore the work was carried on with  $GdO$  ions because that region proved to be "cleaner." However, in this case, it was necessary to take account of the contributions from  $O^{17}$  and  $O^{18}$  leading to an increase in error because the correction for  $O^{17}$  turned out to be comparable in magnitude with  $Gd^{157}$  concentration. For a total thermal neutron flux of  $10^{20}$  n/cm<sup>2</sup>, the unburned initial concentration of  $Gd^{157}$  was only 2% of the equilibrium concentration; the equilibrium concentration,  $\rho_7$ , was  $(0.0062 \pm 0.0011)\%$ . According to relation (1), such a  $Gd^{157}$  content corresponds to a  $Gd^{156}$  cross section, for the VVR-M reactor spectrum,  $\sigma_6 = (0.0062 \pm 0.0011)\% \cdot \frac{150,000 + 12,000}{(95.65 \pm 0.09)\%} = 9.8 \pm 2.5$  barns. If it is assumed that the  $Gd^{156}$  cross section obeys the  $1/v$  law in the thermal region, its cross section will be  $13 \pm 3$  barns for a neutron energy of 0.025 eV. This result differs considerably from the result in [3].

In conclusion, the authors are grateful to A. A. Belonozhenko and L. A. Stepanov for assistance in measuring the isotopic composition of the samples, and also to G. I. Toshinskii for valuable advice.

#### LITERATURE CITED

1. V. V. Orlov, et al., Paper 354 presented by the USSR at the Third International Conference on the Peaceful Use of Atomic Energy (Geneva, 1964).
2. D. Hughes and J. Harvey, Neutron Cross Sections, BNL-325 (1958).
3. R. I. Holl, ACNP-63, 003, March (1963).



CHANGES IN FAST-NEUTRON SPECTRA  
AFTER PENETRATING ALUMINUM, PARAFFIN, AND WATER

(UDC 539.125.25)

G. G. Doroshenko, V. A. Fedorov, and E. S. Leonov

Translated from *Atomnaya Énergiya*, Vol. 19, No. 5,

pp. 460-462, November, 1965

Original article submitted February 6, 1965

The development of high-efficiency, fast-neutron spectrometers [1] with time-amplitude selection of  $\gamma$ -ray background [2], of automatic stabilization of amplification factor, as well as the development of a reliable matrix method for computing efficiencies [4, 5] taking into account all the factors which determine the line shape of a spectrometer [6, 7], including the actual energy resolution of the detector [8], make it possible to carry out extended precision measurements of fast-neutron spectra at levels that are a fraction of the maximum permissible flux; in addition, it appears possible to investigate the fine structure of the spectra.

In the present work, an attempt was made to follow the changes in fast-neutron spectra with penetration through thick layers of aluminum, paraffin, and water. This is necessary if one is to explain the influence of the energy dependence of the cross sections of the basic materials under investigation on the shape of the fast-neutron spectra. A Po-Be fast-neutron source was used which was placed in a paraffin collimator with a  $48^\circ$  aperture angle in order to reduce the contribution from scattered neutrons. The material under study (aluminum, paraffin), in the form of sheets  $70 \times 70$  cm in size, was located 25 cm from the source. The spectrometer detector was placed on the surface of the material directly above the source. Experimental results for aluminum (44 cm thick) and paraffin (45 cm thick) are shown in Figs. 1 and 2.

Data collection time was 3 h, 40 min and 9 h, respectively. For purposes of comparison, these same figures show results of measurements of the neutron spectrum from a Po-Be source and of the energy dependence of the total interaction cross sections for aluminum and carbon. In addition, the statistical errors of the measurements are indicated. The dashed curve in Fig. 2a represents the theoretically calculated hard portion of the neutron spectrum from a Po-Be source [9]. From Figs. 1 and 2, it is clear that the fine structure of the spectrum in the case of aluminum agrees with the fine structure of the original fast-neutron spectrum from the Po-Be source; in the case of paraffin, the nature of the spectrum is determined by the energy dependence of the total neutron interaction cross section for carbon.

The fast-neutron spectrum after penetration of a 40-cm water layer is shown in Fig. 3 along with the energy dependence of the total neutron interaction cross section for oxygen. The instrumental spectrum was taken from reference [10], in which the experimental geometry is shown. It is clear from Fig. 3 that consideration of energy resolution in analyzing the instrumental spectrum improves the agreement of the neutron spectrum fine structure with the features of the total neutron interaction cross section for oxygen.

The results of this work point to the broad possibilities for the application of the new techniques in fast-neutron spectrometry.

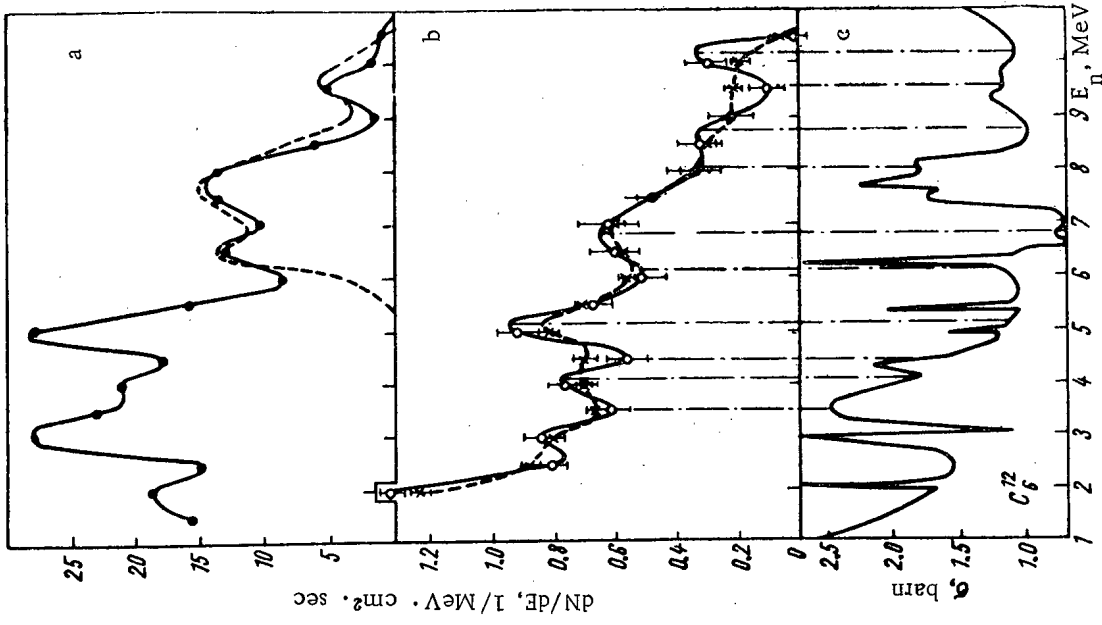


Fig. 2. Spectrum of fast neutrons from Po-Be source before entering shielding (a), after penetrating paraffin sheet (b), and the total neutron interaction cross section for paraffin (c): - - - -) spectrum without allowance for detector resolution; ———) spectrum including detector resolution,  $\sigma_0 = 0.13$  [8].

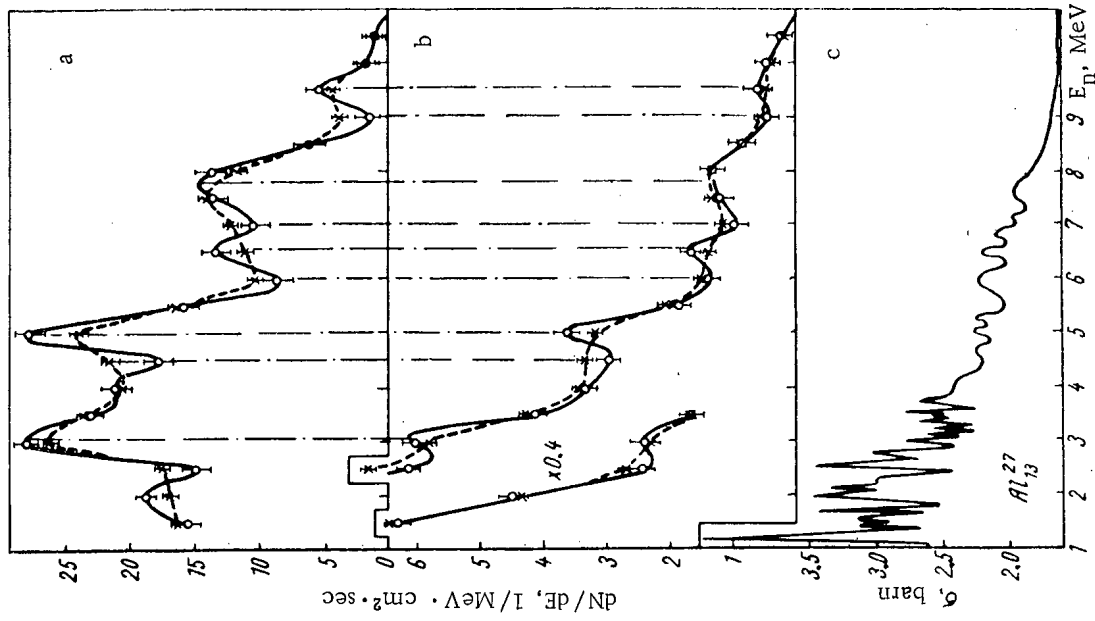


Fig. 1. Spectrum of fast neutrons from Po-Be source before entering shielding (a), after penetrating aluminum sheet (b), and the total neutron interaction cross section for aluminum (c): - - - -) spectrum without allowance for detector resolution; ———) spectrum including detector resolution,  $\sigma_0 = 0.13$  [8].

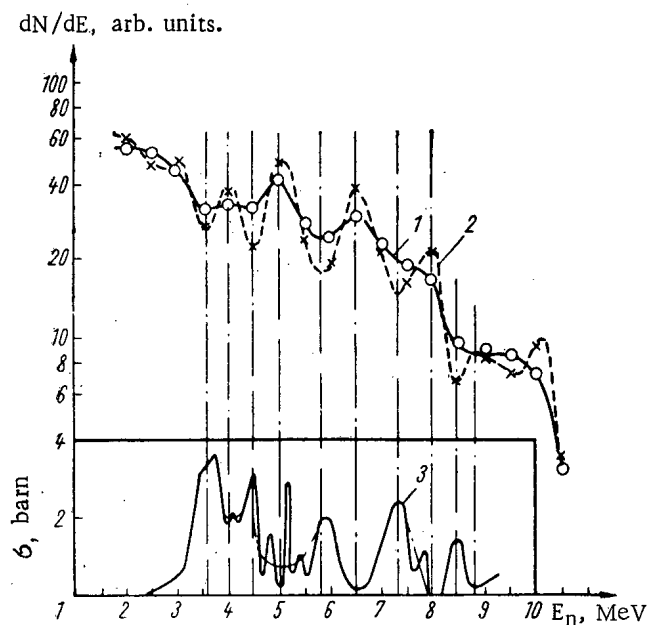


Fig. 3. Fast-neutron spectrum from a Po-Be source after penetrating 40 cm of water: 1) without including resolution; 2) including resolution,  $\sigma_0 = 0.13$  [8]; 3) total neutron interaction cross section for oxygen.

#### LITERATURE CITED

1. G. G. Doroshenko, I. V. Filyushkin, and V. A. Fedorov, "Problems in Dosimetry and Radiation Shielding," No. 3, Moscow, Atomizdat (1964), p. 32.
2. G. G. Doroshenko, I. V. Filyushkin, and V. A. Fedorov, *Izv. AN SSSR, ser. fiz.*, 27, 949 (1963).
3. G. G. Doroshenko, V. A. Fedorov, and E. S. Leonov, *Problems in Dosimetry and Radiation Shielding*, No. 4, Moscow, Atomizdat (1965), p. 143.
4. G. G. Doroshenko et al., *Neutron Dosimetry*, V. 1, Vienna, IAEA (1963), p. 337.
5. G. G. Doroshenko et al., *Izv. AN SSSR, ser. fiz.*, 27, 1308 (1963).
6. V. G. Zolotukhin, G. G. Doroshenko, and B. A. Efimenko, *Atomnaya Énergiya*, 194 (1963).
7. V. G. Zolotukhin and G. G. Doroshenko, *Atomnaya Énergiya*, 18, 287 (1965).
8. G. G. Doroshenko, V. G. Zolotukhin, and B. A. Efimenko, *Atomnaya Énergiya*, 19, 51 (1965).
9. H. Broek and C. Anderson, *Rev. Scient. Instrum.*, 31, 1063 (1960).
10. G. G. Doroshenko and I. V. Filyushkin, *Atomnaya Énergiya*, 16, 152 (1964).

## AN ESTIMATE OF THE ACCURACY OF THE VARIATIONAL METHOD

(UDC 621.039.51)

E. N. Erykalov

Translated from Atomnaya Énergiya, Vol. 19, No. 5,

pp. 462-463, November, 1965

Original article submitted February 13, 1965

For many reactor problems, the determination of critical dimensions is of interest, and a detailed knowledge of neutron distribution is not important. In this situation, the critical dimensions are usually calculated approximately, but one does not always manage to estimate the accuracy with which they are obtained. In this paper, attention is directed to one of the methods by which it is possible to estimate both the upper and lower limit of the eigenvalue of a Hermitian operator. The great accuracy of the eigenvalues obtainable by simple approximations is demonstrated in two examples.

We assume that the neutron flux  $\Phi$  in a reactor is described by a one-group diffusion equation with time constant  $\lambda$ :

$$L\Phi = \lambda\Phi. \quad (1)$$

As is well known, if  $\Phi$  and  $D_{\text{grad}}\Phi$  are continuous, and  $\Phi(R) = 0$  at the reactor boundary ( $r = R$ ), the system of eigenfunctions is orthogonal, the diffusion operator  $L$  is Hermitian and has a discrete spectrum of eigenvalues. Only the maximum eigenvalue of Eq. (1)  $\lambda = \lambda_0$  is of interest as is the eigenfunction  $\Phi_0$  associated with it. In a case where it is difficult to solve Eq. (1), it is possible to approximate  $\Phi_0(r)$  by a simpler function  $\psi_0(r)$ . In such case, it is of interest to know how large the error in the computation of  $\lambda_0$  will be, and also how to choose  $\psi_0(r)$  so that the error is minimized. Following a method similar to one used previously,\* we estimate this error.

We expand the trial function  $\psi_0(r)$  in the complete system of eigenfunctions of Eq. (1):

$$\psi_0(r) = \sum_i c_i \Phi_i(r), \quad i=0, 1, \dots, \quad (2)$$

where the  $c_i$  are real numbers. The function  $\psi$  must satisfy the same boundary conditions that  $\Phi$  does, and also must be continuous along with  $D_{\text{grad}}\psi$ .

Using (2), it is possible to show, on the one hand, that the functional

$$\rho \equiv \frac{(\psi_0, L\psi_0)}{(\psi_0, \psi_0)} \leq \lambda_0, \quad (3)$$

and, on the other

$$\lambda_0 \leq \rho + \Delta\rho,$$

where

$$\Delta\rho = \frac{1}{\rho - \alpha} \cdot \frac{(L\psi_0 - \rho\psi_0, L\psi_0 - \rho\psi_0)}{(\psi_0, \psi_0)}. \quad (4)$$

The quantity  $\alpha$  lies between  $\rho$  and the eigenvalue  $\lambda_1$  which follows  $\lambda_0$ . It follows from (3) that the maximum value of the functional  $\rho$  for various trial functions will be closest to  $\lambda_0$  and that only for  $\psi_0 = \Phi_0$  will the value of  $\rho$  reach the value  $\lambda_0$  and the "error"  $\Delta\rho$  go to zero.

\*G. Temple, Proc. Roy. Soc., 211A, 204 (1952).

We shall show that even simple approximations ensure high accuracy in  $\rho$ . We assume that the cross sections in Eq. (1) are constant so that the first eigenfunction of a plane reactor without reflector and of dimension  $2R$  is

$$\Phi_0(r) \sim \cos\left(\frac{\pi}{2R} r\right). \quad (5)$$

It is approximated by the trial function

$$\psi_0(r) \sim 1 - \left(\frac{r}{R}\right)^2, \quad (6)$$

then, as follows from expression (4), the error  $\Delta\rho$  will be such that the relative error in reactor dimension  $\Delta R/R$  corresponding to it will be  $\sim 1\%$ . If a more complicated function is selected, for example

$$\psi_0(r) \sim \left[1 - \left(\frac{r}{R}\right)^2\right] \left[1 - a \left(\frac{r}{R}\right)^2\right], \quad (7)$$

where the factor  $a$ , selected on the basis of maximum  $\rho$ , turns out to be 0.21, the value of the error  $\Delta R/R$  is  $3 \cdot 10^{-5}$ .

Now, in contrast to the previous problem, let the absorption and fission cross sections have a cosine distribution over the reactor, and let the diffusion coefficient be constant as before. Such a situation can exist in a heavy-water reactor with cosine fuel distribution where it is possible to neglect neutron capture by the moderator and leakage during slowing down. If a trial function is chosen in the form:

$$\psi_n \sim \cos\left[(2n+1)\frac{\pi}{2R} r\right], \quad n=0, 1, \dots, \quad (8)$$

it is possible to compute  $\rho$  from (3) and to estimate the error  $\Delta\rho$  from (4). It turns out that the relative error in reactor dimension does not exceed 0.3% in the critical state ( $\rho = 0$ ). In this same problem, if an equal amount of fuel and absorber are distributed uniformly over the reactor, it is easy to obtain the eigenvalues. In that case, however, the maximum eigenvalue will be less than  $\rho$  by an amount almost 50 times greater than the error  $\Delta\rho$ .

The author is deeply grateful to Yu. V. Petrov, G. S. Danilov, and E. A. Garusov, for valuable comments and a discussion of the results.

COMPARISON OF CALCULATED AND EXPERIMENTAL PARAMETERS  
OF HOMOGENEOUS URANIUM-WATER CRITICAL ASSEMBLIES

(UDC 621.039.520.22)

A. S. Dochenov and N. Ya. Lyashchenko

Translated from Atomnaya Énergiya, Vol. 19, No. 5,

pp. 463-464, November, 1965

Original article submitted January 15, 1965; in revised form April 19, 1965

Method of calculation. The  $P_1$ -approximation equations for neutron transport and the one-velocity equation for the diffusion of thermal neutrons were used as the reactor equations. The slowing-down equations were reduced to a system of multigroup equations of the diffusion type as described in [1]. For this purpose, the entire energy range was broken down into 12 groups, including the thermal group. The method was developed for homogeneous reactor calculations.

Experimental critical assemblies.\* The core of the critical assemblies was a fuel assembly  $70 \times 35 \times 250$  mm in size and with a volume of 0.62 liter. The fuel elements were plates  $250 \times 70 \times 2.7$  mm in size pressed from a mixture of polyethylene and uranium oxide ( $U_3O_8$ ). The uranium enrichment was 90%. The plates were covered on both sides by aluminum foil 0.05 mm thick. In addition to the fuel elements, plates of aluminum, copper, and 1Kh18N9T stainless steel were also used.

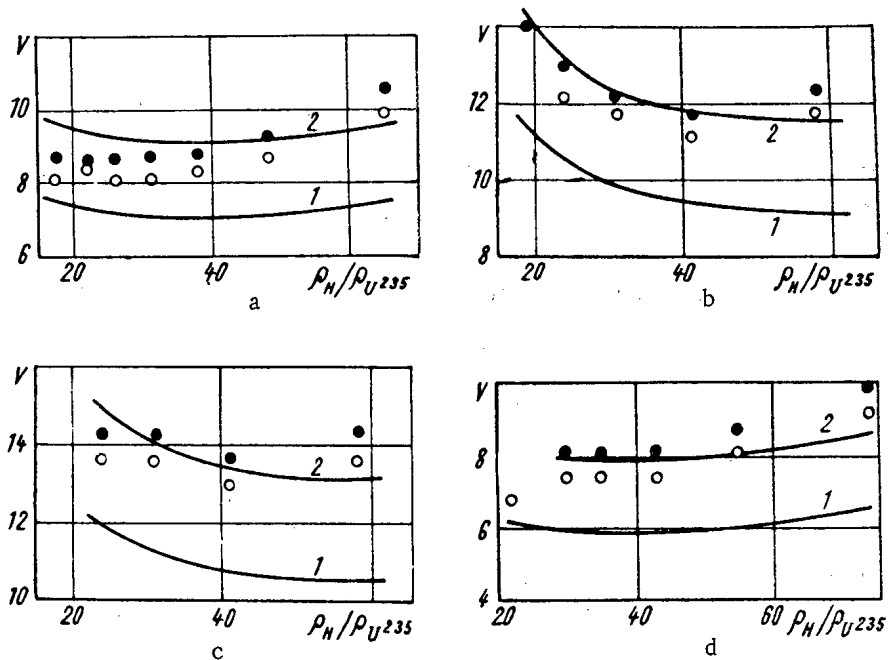
Experiments that were performed showed that a multiplying assembly was quasihomogenous [1] for a hydrogen- $U^{235}$  concentration ratio  $\frac{\rho_H}{\rho_{U^{235}}} \ll 50$ . When  $\frac{\rho_H}{\rho_{U^{235}}} \approx 50$ , the size of the water gap between the plates reached  $\sim 5$  mm and became comparable to the range of thermal neutrons in water. Therefore, it was necessary to consider the effect of heterogeneity in the calculation of critical assemblies with  $\frac{\rho_H}{\rho_{U^{235}}} \gtrsim 50$ . Since the method of calculation being used was suitable only for homogeneous systems, it was possible to compare the computational results with experiment only in the region  $\frac{\rho_H}{\rho_{U^{235}}} \ll 50$ .

Calculation and comparison with experiment. In the calculations, the actual shape of the critical assemblies was replaced by a spherical one, and the thickness of the water reflector was assumed to be 50 cm. To compare the results of calculation with experimental data, it is necessary to convert from a spherical geometry to the geometry of the critical assemblies.

It is well known [2] that the various methods for conversion from a spherical geometry to a cylindrical one, with the height of the cylinder nearly equal its diameter (on the basis of equal volumes or equal geometric parameters, with or without allowance for a reflector), lead to good agreement with experiment. However, conversion on the basis of equal volumes slightly under-estimates cylinder dimensions and, on the other hand, conversion on the basis of equal geometric parameters slightly over-estimates them.

Since the actual critical assemblies had the shape of a rectangular prism, or nearly so, it is possible to take as the upper limit of the critical volume the prism volume which is obtained by equating the geometric parameters of the sphere and prism. Computational results and experimental data are shown in Figs. a, b, c, d. A series

\*The experimental work was performed by E. D. Vorob'ev, V. B. Klimentov, and V. M. Gryazev, and others.



Critical assemblies with aluminum fuel element assembly (a); with aluminum fuel element assembly and aluminum plates with relative concentration of aluminum  $\frac{\rho_{Al}}{\rho_{U^{235}}} = 5.8$  (b); with aluminum fuel element assembly and copper plates with relative concentration of copper  $\frac{\rho_{Cu}}{\rho_{U^{235}}} = 8.3$  (c); and with fuel element assembly

of 1Kh18N9T stainless steel (d): ( $V$ ) core volume, liter; 1) calculated critical volume of sphere; 2) calculated critical volume of prism; ●) supercritical experimental volume; ○) subcritical experimental volume.

of experiments is shown in each of them. The critical assemblies with the ratio  $\frac{\rho_H}{\rho_{U^{235}}} \leq 50$  are intermediate because the thermal neutron contribution to the  $U^{235}$  fission density is less than 50%.

A comparison of the results shows that, on the whole, the calculated and experimental critical volumes are in satisfactory agreement in the region  $\frac{\rho_H}{\rho_{U^{235}}} \leq 50$ .

The experimental values of the critical volumes for the region specified are between the upper and lower computed limits, and the limits themselves differ from one another by 20-25%. The complexity of the critical assembly geometries does not allow any narrowing down of the limits shown.

The critical assembly calculations that were performed and the comparison of the computed and experimental data permits one to conclude that the computing method employed gives satisfactory agreement between calculated and experimental data, and that it can be recommended at least for calculations of the critical dimensions of an intermediate-neutron, homogeneous reactor with hydrogen-containing moderator.

#### LITERATURE CITED

1. S. M. Feinberg et al., Proceedings of the Second International Conference on the Peaceful Use of Atomic Energy, Geneva (1958) [in Russian], Dokl. sovetskikh uchenykh, Vol. 2, Moscow, Atomizdat (1959), p. 334.
2. Callihan, Morfitt, and Thomas, Proceedings of the International Conference on the Peaceful Use of Atomic Energy, Geneva (1955) [in Russian], Vol. 5, Moscow, Izd-vo AN SSSR (1958), p. 179.

TANGENTIAL CHANNELS AND THERMAL COLUMN RECONSTRUCTION  
AT THE VVR-M REACTOR

(UDC 621.039.519)

G. Ya. Vasil'ev, E. A. Kononov, V. G. Pankov,  
and D. A. Yashin

Translated from *Atomnaya Énergiya*, Vol. 19, No. 5,  
pp. 465-467, November, 1965  
Original article submitted April 21, 1965

In planning the VVR-M reactor at the A. F. Ioffe Physical-Technical Institute of the USSR Academy of Sciences, provision was made for nine horizontal channels in the concrete shielding and a tenth channel in the thermal column. All the channels were directed along the normal to the core and had a shutter structure consisting of five shielding disks which overlapped one another in the closed position of the channel aperture. The centers of all the channels were located at 1 m from the floor of the reactor room (reference height, +1.0 mm).

The performance of experiments in channels directed along the normal to the core is hindered considerably by the fact that radiation from the core is incident to a considerable degree on the detection equipment in addition to the radiation under investigation. Thus, in performing studies with a crystal diffraction spectrometer [3], the necessary lead shielding against  $\gamma$ -radiation from the core leads to a decrease in neutron flux at the sample to  $2 \cdot 10^{12}$  n/cm<sup>2</sup> · sec. For that reason, it is essentially impossible to use the high neutron flux of the reactor for such experiments. However, it is possible to reduce the  $\gamma$ -ray background at the sample significantly if the channels are directed tangentially to the surface of the core toward the beryllium reflector or toward the water outside the reflector. In this situation, there will be at the channel exit only secondary  $\gamma$ -radiation scattered in the reflector and  $\gamma$ -radiation from activity induced in the structural materials of the end of the channel.

In November 1961, straight-through channel 10 (Fig. 1), which passed through the recess for the thermal column at 1390 mm from the center of the core, was drilled in the concrete shielding of the VVR-M reactor. The center of the channel was located at the reference height +1.25 m. The orientation of the channel was chosen so that the cast iron shielding ring was not interfered with during the drilling nor were process channels damaged.

Similarly, in September 1963, the two tangential channels 11 and 16, which opened into the thermal column recess, were drilled. Channel 11 was located at a reference height +0.75 m, and was directed toward the beryllium reflector along a tangent to the core. With such a choice of direction, it was expected that a higher ratio of thermal to fast-neutron flux would be achieved at the channel exit. Channel 16 was directed toward the water along a tangent to the beryllium reflector and was located at a reference height +1.25 m. The choice of direction for this channel resulted from the necessity for obtaining a minimal  $\gamma$ -ray background at the channel exit for maximum possible proximity of the channel to the core in order to assure a high neutron flux at the point where the sample under study would be located.

The direction of the channel axes (Fig. 2) was determined, on the one hand, by the distances from the center of the core to the channel axes (412 and 580 mm), and, on the other hand, by the distance from the channel axes to the edge of the cast iron shield. After determining the direction of the channel axes, their centers were marked on the outer surface of the biological shield of the reactor.

Together with the drilling of the tangential channels, there was reconstruction of the thermal column in order to increase the number of horizontal channels available for research in solid state physics. The thermal column (total length 3040 mm) was made up of six graphite disks enclosed in aluminum and installed next to one another in a retractable structure in the recess on the north side of the reactor.



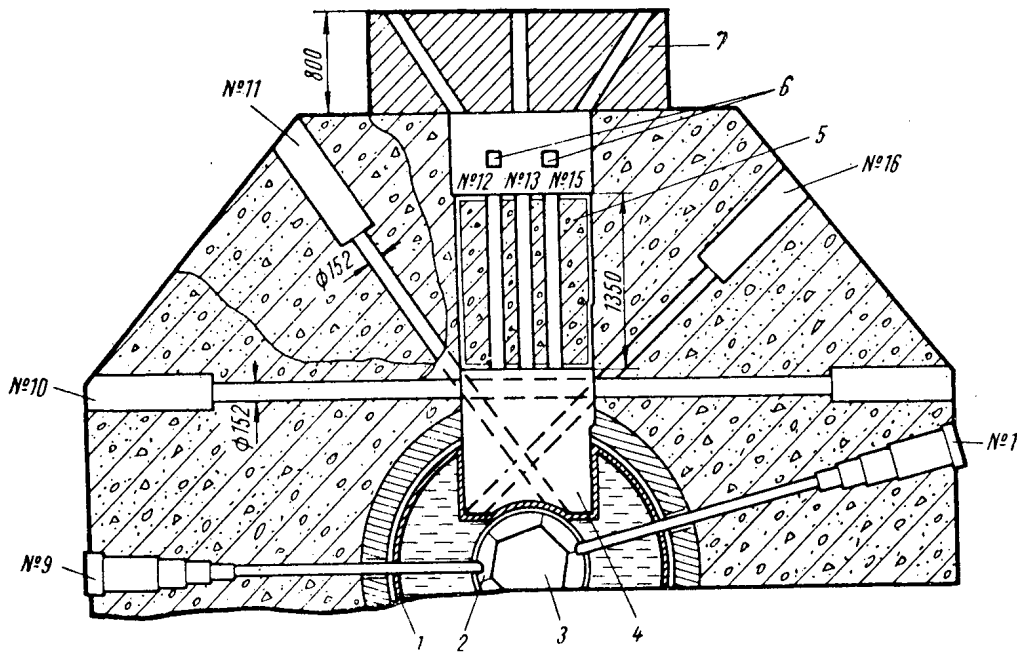


Fig. 1. Locations of new channels in the reactor: 1) reactor vessel; 2) beryllium reflector; 3) core; 4) recess for retractable carriage; 5) concrete shielding disk; 6) physical sensors; 7) retractable cast iron shielding.

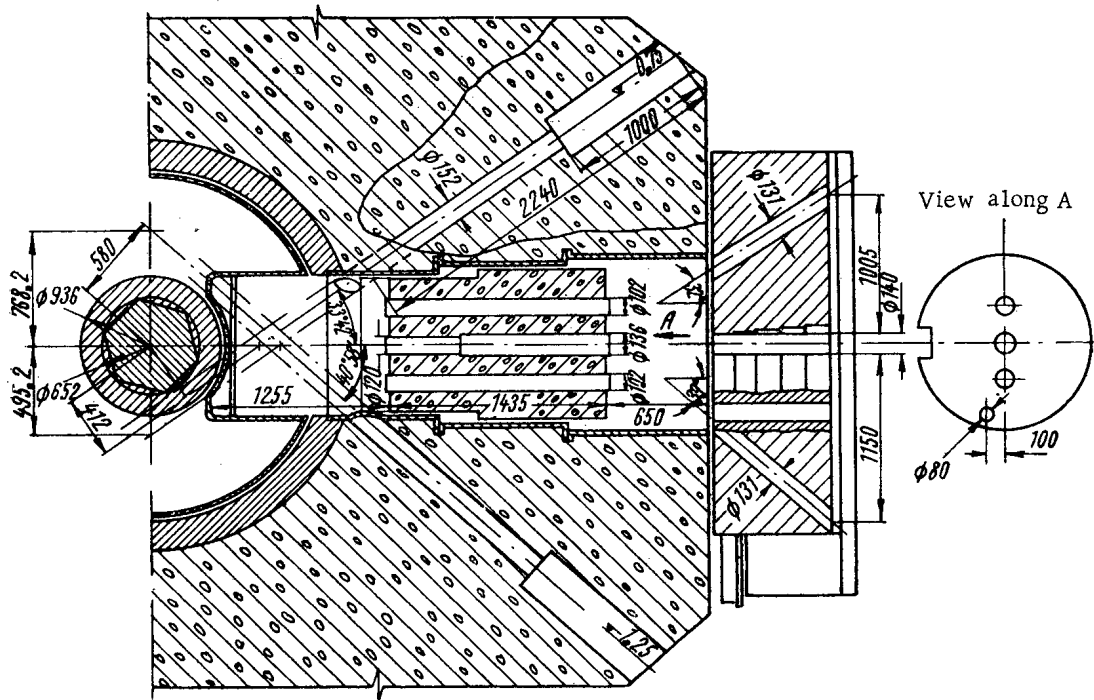


Fig. 2. Orientation of tangential channels and channels in the retractable structure on the north side of the reactor.

In the reconstruction, the five outer graphite disks were replaced by a single concrete one of equivalent shielding. In this disk, four horizontal channels were drilled: at reference height +1.0 m, central channel 13, 120 mm in diameter with a transition to 136 mm at its outer portion, and channels 12 and 15, 102 mm in diameter, as well as channel 14, 80 mm in diameter, at the reference height +0.9 m (see Fig. 2). The concrete disk was installed in the retractable structure so that between it and the retractable cast iron shielding an open space

Physical Parameters of Channels

Channel	Thermal neutrons		Fast neutron flux, n/cm <sup>2</sup> · sec	γ-Ray dose rate at channel exits, × 10 <sup>-3</sup> μR/sec.
	flux, n/cm <sup>2</sup> · sec	cadmium ratio		
1	2.6 · 10 <sup>9</sup>	6.0	3.0 · 10 <sup>8</sup>	6 · 10 <sup>4</sup>
10	2.6 · 10 <sup>6</sup>	—	~ 10 <sup>4</sup>	3
11	6.6 · 10 <sup>7</sup>	21	4.5 · 10 <sup>5</sup>	66
16	6.6 · 10 <sup>7</sup>	25	4.0 · 10 <sup>5</sup>	44

remained where there was located a monocrystal monochromator of Co + Fe (in the magnetic field of permanent magnets or of electromagnets) at angles of 32° and 39° to the axes of channels 12 and 15, respectively, in order to obtain monochromatic, polarized beams of neutrons with  $\lambda_1 = 1.13$  Å and  $\lambda_2 = 1.37$  Å. In this same space, equipment was installed which permitted remote adjustment of the crystals in the neutron beam.

The first graphite disk was intended to shield against scattered radiation which penetrated mainly beneath the retractable structure. During reactor operation at a power of 5 MW without the first graphite disk, the γ-ray dose rate beneath the retractable cast iron shield on the north side of the reactor was 100 times greater than the maximum permissible level. Holes were drilled for channels 12, 14, and 15 in the retractable cast iron shield. For channel 14, the opening penetrated parallel to the axis of channel 13, and for channels 12 and 15, at angles of 32° and 39°, respectively.

Drilling of the channels in the concrete shield of the reactor and in the retractable cast iron shield was done by the Leningrad composite geological expedition of the Northwest Geological Board under the control, and with the participation, of the staff of the Division of reactor operation. In drilling the channels in concrete, several auxiliary metallic structural elements were cut through. When the drilling equipment encountered a metallic structural element, the pressure on the drill bit was reduced and the spindle rotation was decreased. Drilling concrete in which small cast iron shot was incorporated presented no additional difficulties.

It took a little more than three days to cut through the 6000 mm, continuous channel 10, including assembly of the equipment and preliminary operations; to drill two channels in concrete (11 and 16) and three channels in the cast iron shield (12, 14, and 15) took 24 working days, including preparatory, survey, and drilling operations. The drilling of all channels was carried out with satisfactory precision. For example, the error in the distances from the axes of channels 11 and 16 to the center of the core as compared with the specified dimensions was not more than 10 mm.

Steel pipe was installed in all channels cut through the concrete. To shield against radiation, an extensive portion of the channel was closed by water-filled plugs and three cast iron plugs with a total length of 450 mm were installed behind them. A permanent shutter arrangement for these channels is planned for each individual case depending on the nature of the physical apparatus.

Physical parameters were measured for all the newly created channels: thermal-neutron flux, cadmium ratio (using gold), fast-neutron flux, and γ-ray dose rate. These parameters were also measured for channel 1, which is directed along the normal to the core.

The results of the measurements are given in the table, normalized to a power of 10 MW. The data in the table was obtained from measurements with a graphite disk having no openings for the newly created channels installed in the retractable structure. In the absence of the graphite disk, the neutron fluxes at the exits of these channels will be greater [2]. The thermal neutron fluxes were measured with an accuracy of 20%, the cadmium ratio with an accuracy of 15%, and the fast-neutron fluxes with an accuracy of 40%. The γ-ray dose rate was measured with an accuracy of 20%.

Yu. V. Petrov, a member of the staff of the A. F. Physical-Technical Institute, advanced the suggestion for the creation of tangential channel 10 in 1961. In 1963, I. A. Kondurov proposed drilling channels 11 and 16. V. S. Gvozdev assumed a large part of the work on the creation of tangential channels.

The authors take this opportunity to thank the personnel of the Division of Reactor Operation for the rapid and skilfull completion of the job of creating new channels, and also wish to thank D. M. Kaminker for his concern and assistance.

LITERATURE CITED

1. V. V. Goncharov et al., in Proceedings of the Second International Conference on the Peaceful Uses of Atomic Energy, Geneva (1958) [in Russian], Dokl. sovetskikh uchenykh, Vol. 2, Moscow, Atomizdat (1959), p. 243.
2. D. M. Kaminker and K. A. Konoplev, Paper No. 325, presented by the USSR at the Third International Conference on the Peaceful Uses of Atomic Energy, Geneva (1964) [in Russian].
3. O. I. Sumbaev and A. I. Smirnov, Nucl. Instrum. and Methods, 22, 125 (1963).

THE EFFECT OF CORE CONFIGURATION ON NEUTRON SPECTRUM  
FROM A HORIZONTAL CHANNEL OF THE VVR-M REACTOR

(UDC 621.039.519)

V. P. Vertebnyi, M. F. Vlasov, and A. L. Kirilyuk

Translated from *Atomnaya Énergiya*, Vol. 19, No. 5,

pp. 467-468, November, 1965

Original article submitted November 30, 1964

The shape of the slow-neutron spectrum in a beam extracted from a reactor core depends to a great extent on the core configuration close to the region from which the neutron beam is extracted. Finding the optimum core configuration is of interest in time-of-flight studies using mechanical choppers or neutron monochromators. This is necessary in order to obtain the maximum yield of neutrons in a definite region of the spectrum with minimum flux of fast neutrons, i.e., the best signal-to-noise ratio for the largest possible signal. It is well known that the thermal neutron flux can be increased several times in comparison with the average flux in the core by creating a cavity in the moderator surrounding the fuel elements [1]. Although it is impossible to obtain a closed cavity in experiments with beams, one can hope that the thermal neutron flux would be increased if the neutron beam is extracted from the surface of the moderator. Since the flux of resonance neutrons is determined by the well known expression [2]:

$$\Phi(E) = \frac{S}{\xi E \Sigma} \quad (1)$$

The replacement of a light moderator by a heavier one may lead to some increase in the yield of resonance neutrons and also to a shift in the ratio between the intensities of resonance and thermal neutrons. These considerations also led to the setting up of the experiments described below.

With the help of a mechanical neutron chopper installed in one of the horizontal channels of the VVR-M reactor at the Institute of Physics, Ukrainian SSR, and used to investigate the neutron cross sections of separated isotopes [3] a study was made of the neutron spectra for various configurations of the core near this channel (Fig. 1). In the first case (see Fig. 1a), the neutron source was only fuel elements; in the second (see Fig. 1b), it was fuel

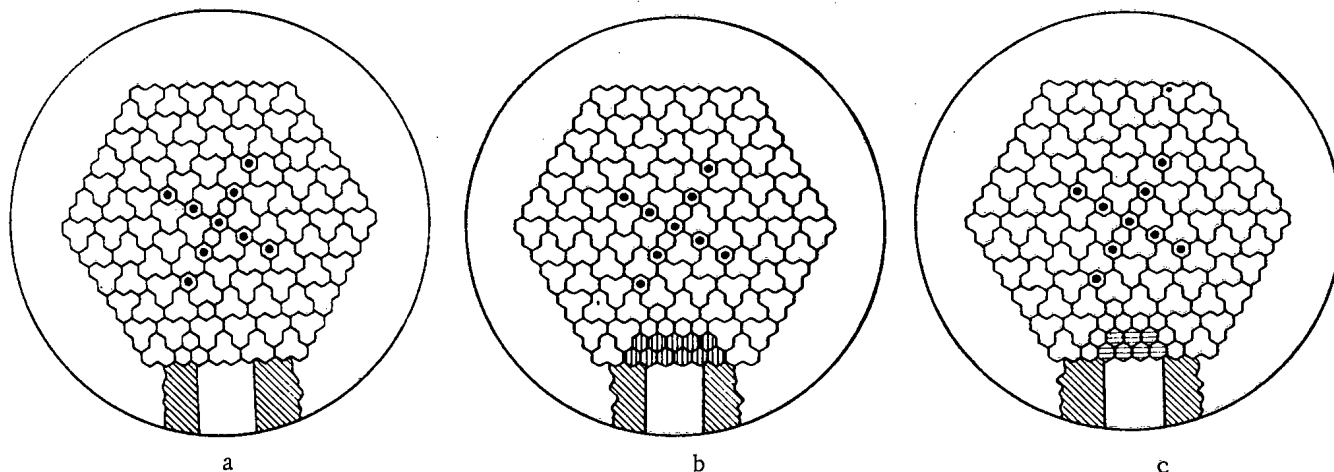


Fig. 1. Core configuration near a horizontal channel of the VVR-M reactor.

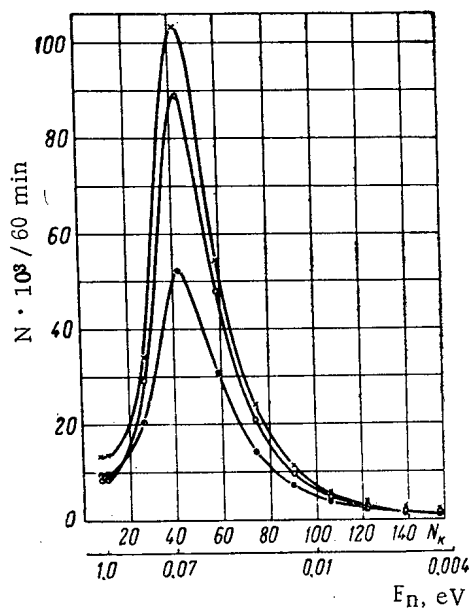


Fig. 2. Effect of core configuration on neutron spectrum from a horizontal channel: ●) fuel elements; ○) fuel elements + water; x) fuel elements + beryllium.

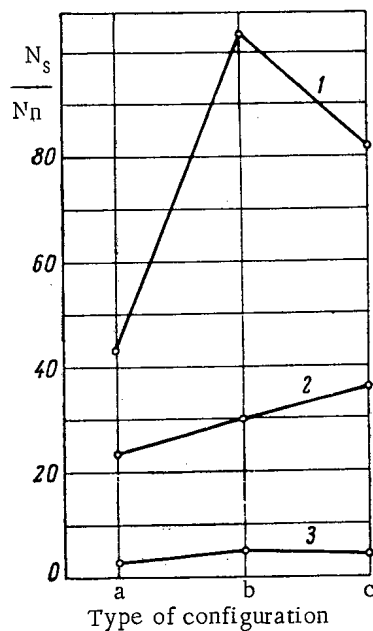


Fig. 3. Effect of core configuration on signal-to-noise ratio: a) fuel elements; b) fuel elements + water; c) fuel elements + beryllium; 1) 0.0253 eV; 2) 1.0 eV; 3) 0.007 eV.

elements and a water layer 5.5 cm thick; in the third (see Fig. 1c), it was fuel elements and a beryllium layer of the same thickness.

The neutron spectra from the horizontal channel are shown in Fig. 2 for all the core configurations mentioned. It is clear from Figs. 2 and 3 that the absolute gain in intensity is close to 2 in the thermal and cold region for water and beryllium. The signal-to-noise ratio in these cases is approximately twice as large as that for extraction of the neutron beam from the surface of the fuel elements. In the resonance region, the counting rate is approximately 1.4 times greater for beryllium than for the other configurations. This behavior is qualitatively explained by expression (1). Therefore, one can consider the arrangement with beryllium moderator as best from the practical point of view.

The authors are grateful to D. T. Pilipets, chief engineer of the VVR-M reactor at the Institute of Physics, Ukrainian SSR Academy of Sciences, and to other members of the staff for assistance in setting up the experiments.

#### LITERATURE CITED

1. M. Osredkar and R. Stephenson, *J. Nucl. Energy*, **5**, 210 (1957).
2. A. Weinberg and E. Wigner, *Physical Theory of Reactors* [Russian translation], Moscow, Izd-vo inostr. lit. (1961).
3. M. F. Vlasov and A. L. Kirilyuk, *Ukr. fiz. zh.*, **8**, 947 (1963).

NEW DATA ON ATMOSPHERIC RADIOACTIVITY  
AND FALLOUT INTENSITY IN THE BLACK SEA BASIN

(UDC 551.577.7:541.182.2/3)

V. P. Kotel'nikov, V. N. Markelov, and B. A. Nelepo

Translated from *Atomnaya Énergiya*, Vol. 19, No. 5,  
pp. 469-470, November, 1965

Original article submitted March 19, 1965

During the 16th voyage of the Mikhail Lomonosov in August-September, 1964, studies were made of the artificial radioactivity of the atmosphere in the Black Sea basin. As a result of these studies, determinations were made of the concentration and isotopic composition of the radioactive aerosols in the surface layer of the atmosphere, of the shortlived radioactive isotopes in the surface layer of the atmosphere, and of the intensity of radioactive fallout and its isotopic composition. In addition, studies were made of the correlation between concentration of radioactive aerosols and the intensity of radioactive fallout at the surface of the sea under various meteorological conditions.

The route of the voyage made it possible to collect samples from a considerable area of the Black Sea during a relatively short time.

The aerosol particles were collected by a filtration apparatus using an FPP-15 filter. The capacity of the equipment was 225 m<sup>3</sup>/h. The filter was exposed for 48 h. Analysis and measurement of sample activity was accomplished by standard techniques. To determine the content of short-lived decay products of radon and thoron, measurement of filter activity was started within 1-1.2 h after removal of the filter, and was carried on continuously for several days. The decrease in sample activity was investigated, and then the decay curve was analyzed.

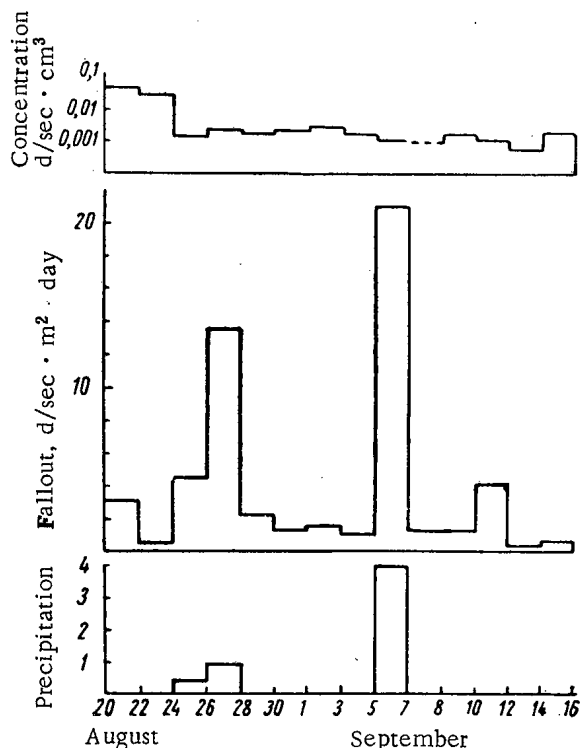


Fig. 1. Concentration and average daily intensity of fallout for radioactive aerosols.

Counts were taken with a type PP-8 (Volna) radiometer employing an end-window MST-17 counter. Determination of the value of the factor for converting from counts to sample activity had been done previously under laboratory conditions. The error in measurement was 5-10%.

Radioactive fallout was collected in stainless steel pots with an area of 0.64 m<sup>2</sup>. An oil-saturated filter paper was placed in the bottom of the pot. The collection efficiency was practically unity. The pots were set up on the upper bridge of the ship at a height of 14 m above the surface of the water. The length of exposure for the pots was two days. After completion of collection, the paper was removed, ashed, and calcined under the same conditions as those for the FPP-15 filters. On rainy days, the moisture which accumulated in the pot was evaporated, and the dry residue was mixed with the ash from the oiled paper. Samples were prepared from the ash residue for measurement of total  $\beta$  activity, just as was done for the FPP-15 filters.

To study the isotopic composition of the samples collected, a scintillation spectrometer with a 40 x 40 mm NaI(Tl) crystal and a 100-channel AI-100 (Radura) pulse

## Concentration and Rate of Radioactive Fallout in 1960 and 1964

Year	Concentration d/sec · m <sup>3</sup>	Fallout-rate, d/sec · m <sup>2</sup> · day
1960	$30 \cdot 10^{-4}$	$492 \cdot 10^{-2}$
1964	$34.4 \cdot 10^{-4}$	$462 \cdot 10^{-2}$

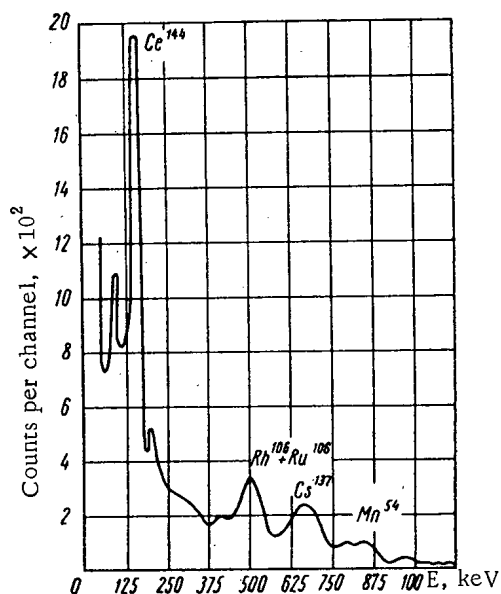


Fig. 2.  $\gamma$ -Ray spectrum of atmospheric fallout sample.

day, the fallout intensity was  $211 \cdot 10^{-1}$  d/sec · m<sup>2</sup> · day, the concentration  $19.9 \cdot 10^{-4}$  d/sec · m<sup>3</sup>, the effective height of the "cleared layer" 10,500 m/day, while on a day without precipitation, the average values of these same quantities was  $18.1 \cdot 10^{-1}$  d/sec · m<sup>2</sup> · day,  $45.5 \cdot 10^{-4}$  d/sec · m<sup>3</sup>, and 390 m/day, respectively. Fallout activity on September 6, 1964, was 11 times greater than the magnitude of the average daily fallout on days without precipitation.

Thus there is a correlation between the concentration of long-lived radioactive products present in the atmosphere, the average daily fallout intensity, and atmospheric precipitation. The average values for the concentrations of the natural radioactive decay products of radon and thoron in the atmosphere above the Black Sea during August-September, 1964, was  $9.2 \cdot 10^{-1}$  and  $17.7 \cdot 10^{-3}$  d/sec · m<sup>3</sup>, respectively. From the data obtained, it follows that the concentration of radon decay products in the atmosphere is three orders of magnitude greater than the concentration of long-lived radioactive aerosols from fission products.

In the spectrum from air samples (Fig. 2), the following radioactive elements were identified: Ce<sup>144</sup> (134 keV), Ru<sup>106</sup> + Rh<sup>106</sup> (513 keV), Cs<sup>137</sup> (661 keV); a  $\gamma$ -ray line at  $\sim 800$  keV indicates the presence of Mn<sup>54</sup>.

The isotopic composition of the radioactive products found in the atmosphere as determined by us differs from published data.\*

An analysis of the information obtained during the 16th voyage of the Mikhail Lomonosov shows an insignificant increase in concentration and a reduction in the intensity of the average daily fallout of radioactive products on the surface of the sea in comparison with the 9th voyage (October, 1960).

\*V. P. Shvedov, et al., Radioactive Contamination of the Seas and Oceans, Moscow, Nauka (1964), p. 49.

The isotopic composition of the radioactive products found in the atmosphere, and the rapid variations in their fallout intensity as a function of atmospheric precipitation indicate that there still remains in the stratosphere a considerable amount of radioactive products, produced as the result of nuclear testing, which enter the lower layers of the atmosphere.



## THE RELATIVE LEVELS OF STRATOSPHERIC FISSION FRAGMENT FALLOUT

(UDC 551.577.7)

P. I. Chalov and M. A. Tsevelev

Translated from *Atomnaya Énergiya*, Vol. 19, No. 5,

pp. 470-472, November, 1965

Original article submitted February 13, 1965

It is possible to obtain information about the arrival of nuclear test products from the stratosphere by studying the time changes in the concentration of radioactive aerosols in the surface layer of the atmosphere, particularly during the time when such tests are prohibited. As the result of several investigations (see, for example, [1]), it was

established that the aerosol concentration in the surface layer of the atmosphere exhibited a seasonal variation, increasing in the spring-summer period and then falling in the fall and winter. The existence of the maxima mentioned is usually explained by seasonal variation in the rate of transfer of air masses from the stratosphere to the troposphere. A similar seasonal change in concentration in the surface layer of the atmosphere is observed for ozone and  $\text{Be}^7$  [2], which are produced in large amounts in the stratosphere. During the ban on atmospheric nuclear testing, the spring-summer maximum in the concentration of radioactive aerosols in the surface layer of the atmosphere can be uniquely associated with the arrival of fission fragments from the stratosphere.

In this paper, a possible relative level of stratospheric fission fragment fallout is determined by comparison of the fallout intensity (total fission fragments and several long-lived isotopes) in 1962, when tropospheric fallout was still possible, and in 1963, when it is possible to consider the fallout as purely stratospheric as a result of the prohibition of atmospheric nuclear testing in 1962.

Fallout intensity was determined from mean monthly samples whose activity was assigned as the activity of the mean date of sampling. Fallout was collected on a water surface by samplers with a collecting area of  $0.3 \text{ m}^2$  [3]. Samples were prepared for measurement by methods described in the literature [4]. The total  $\beta$ -activity of the samples was measured with a B-2 radiometer having a SI-2B counter which was calibrated with a  $\text{Sr}^{90}$  source. Long-lived  $\gamma$ -emitters were analyzed with a scintillation spectrometer using an AI-100-1 analyzer (resolution for the  $\text{Cs}^{137}$  photopeak, about 10%). Results of observations from October 1961 to December 1963 are shown in Fig. 1 in the form of a histogram. It is clear that the fallout intensity for total fission fragments,  $\text{Cs}^{137}$ ,  $\text{Ce}^{144}$ , and  $\text{Ru}^{106}$  exhibits the seasonal variation ordinarily observed for the concentration of radioactive aerosols in the surface layer

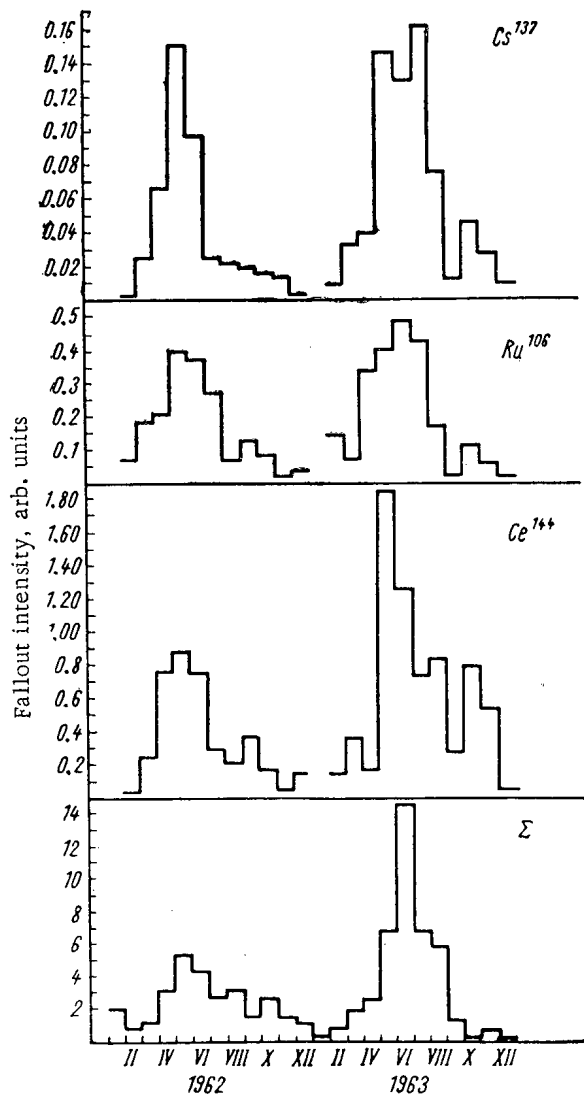


Fig. 1. Time variation in fallout intensity for total fission fragments and for several long-lived  $\gamma$ -emitters.



ATMOSPHERIC RADIOACTIVITY ABOVE THE ATLANTIC OCEAN  
DURING MAY-JULY, 1964

(UDC 551.594.1 : 541.182.2)

L. I. Gedeonov, V. N. Dmitriev, B. A. Nelepo, A. V. Stepanov,  
and G. V. Yakovleva.

Translated from *Atomnaya Énergiya*, Vol. 19, No. 5,  
pp. 472-474, November, 1965  
Original article submitted March 1, 1965

During the 15th voyage of the Mikhail Lomonosov, atmospheric radioactivity and fallout was studied (track of the ship is shown in Fig. 1). Samples of radioactive aerosols were collected by filtering air through an FPP-15 filter. Radioactive fallout was collected in a flanged pot with sticky bottom. A scintillation  $\gamma$ -spectrometer with an AI-100 analyzer was used for sample analysis. The atmospheric content of aerosols of artificially radioactive materials and their rate of fallout (in terms of total activity) are shown in Fig. 2, and the results of  $\gamma$ -analysis are shown in Fig. 3. The  $Sr^{90}$  concentration in the atmosphere was determined by radiochemical methods. For this purpose, samples collected in the southern hemisphere (south of  $80^\circ S$ ) were combined and analyzed together. The same treatment was given to samples collected in the northern hemisphere (north of  $8^\circ N$ ) and in the equatorial region ( $8^\circ N$  to  $8^\circ S$ ). The results of the atmospheric sample studies are given in the table.

A comparison of the results in this paper (see table) with data obtained on the 12th voyage of the Mikhail Lomonosov (at the end of 1962) [1] showed the specific activity of aerosols in the surface layer of the atmosphere and the fallout rate were, in the spring of 1964, more than an order of magnitude lower than at the end of 1962 because of the ban on atmospheric nuclear testing.

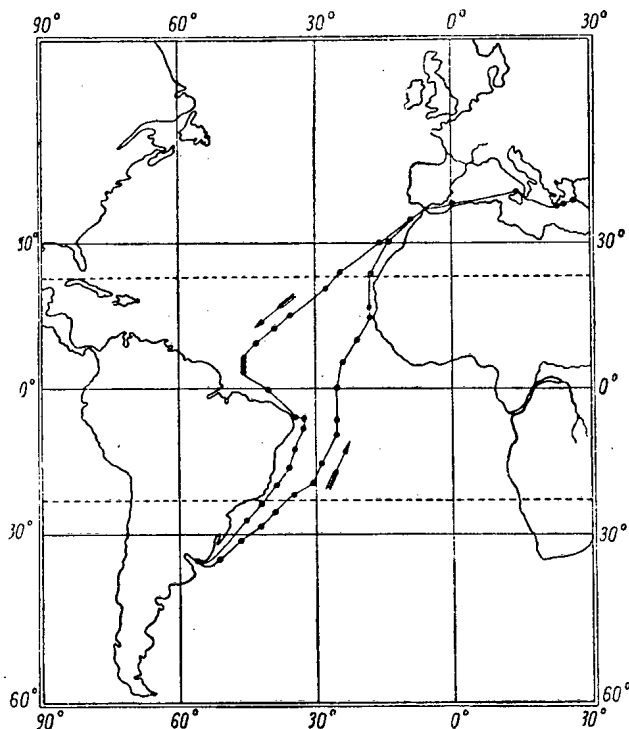


Fig. 1. Track of the 15th Voyage of Mikhail Lomonosov.

It is clear from Figs. 2 and 3 that the radioactive aerosol concentration was practically independent of latitude in the range  $5^\circ N$  to  $38^\circ N$ . This is explained by the fact that the data obtained were typical of the northeast trades zone where the lower layers of the atmosphere are intensely mixed in the meridional direction. In addition, it is clear from Fig. 2 that there is no direct correlation between radioactive aerosol concentration and fallout rate, on the one hand, and between radioactive aerosol concentration and the mean daily values of atmospheric temperature

Average Atmospheric Concentration of Radioactive Isotopes ( $\times 10^{-15} Ci/m^3$ )

Collection area	Isotope				
	Mn <sup>54</sup>	Sr <sup>90</sup>	Ru <sup>106</sup>	Cs <sup>137</sup>	Ce <sup>144</sup>
Southern hemisphere	0,13	0,13	0,84	0,16	1,2
Equatorial region	0,14	0,13	1,1	0,22	1,8
Northern hemisphere	—	4,9	—	—	—

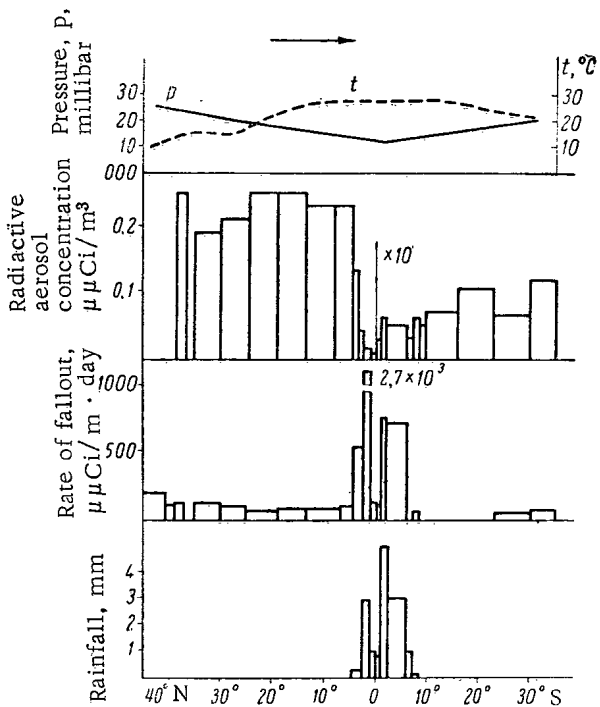


Fig. 2. Radioactive aerosol concentration and fallout rate for ship travel from north to south.

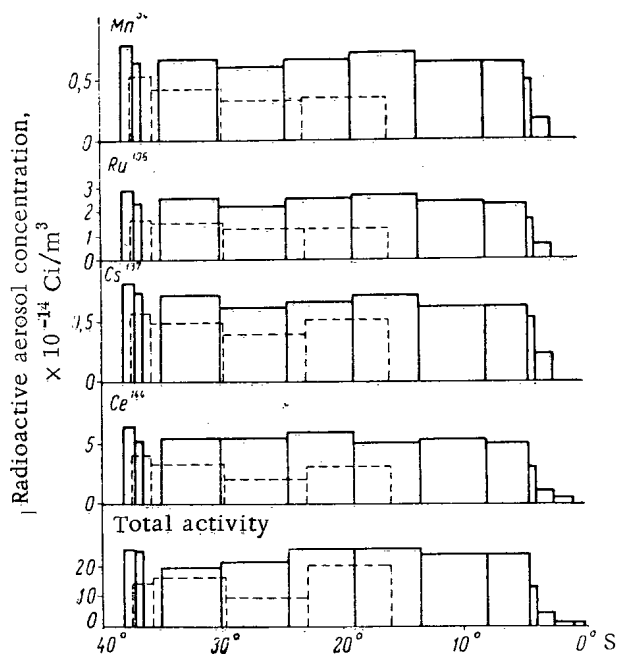


Fig. 3. Radioactive aerosol concentration in the northern hemisphere: ———) outbound (22 April-15 May, 1964); - - -) return (16-24 July, 1964).

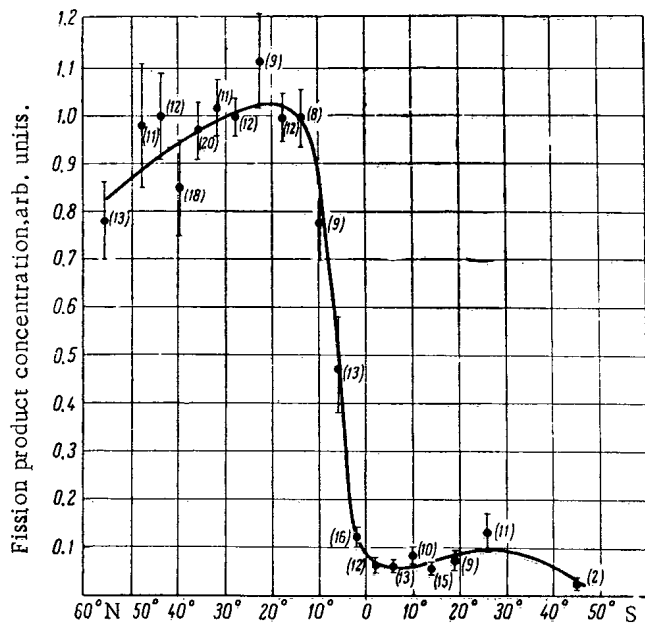


Fig. 4. Mean latitudinal distribution of fission product concentration in the lower layer of the atmosphere.

10% of the value typical of the northern hemisphere. Some reduction in the concentration of atmospheric fission products was observed in the range 50-60° N.

In conclusion, the authors consider it their pleasure to express their deep appreciation to V. M. Vdovenko and A. G. Kolesnikov for making it possible to carry out this work. The authors thank I. N. Maksimov and L. N. Sysoeva for assistance in analyzing the results.

and pressure, on the other. The high radioactive fallout rate in the equatorial region is explained by intense precipitation in the form of rain which washed out the radioactive aerosols in the lower layers of the atmosphere.

Concentration values in the equatorial region and in the southern hemisphere were much lower than in the northern hemisphere.

Statistical analysis of the published results of observations made during previous voyages of the *Mikhail Lomonosov* [1-3] made it possible to establish an average picture of the latitudinal distribution of fission products in the lower layers of the atmosphere above the Atlantic Ocean. Results of the averaging are shown in Fig. 4 where the vertical lines indicate the mean square deviation in the concentration of atmospheric fission products, and the number of averaged quantities is given in parentheses. It is clear that the maximum distribution in latitude of fission products in the northern hemisphere is located between 14 and 40° N. South of 10° N, a sharp decrease is observed in the concentration of atmospheric fission products. The specific activity of aerosols in the southern hemisphere is not more than

LITERATURE CITED

1. V. A. Blinov, et al., Proceedings of the Maritime Hydrophysical Institute, AN UkrSSR [in Russian], Vol. XXXI, Kiev, Izd-vo AN USSR (1965).
2. V. N. Lavrenchik, Atomnaya Énergiya, 13, 72 (1962).
3. V. N. Lavrenchik et al., Atomnaya Énergiya, 14, 569 (1963).

FEATURES OF THE EQUILIBRIUM SHIFT IN THE URANIUM-RADIUM SERIES  
IN URANIUM DEPOSITS WITH HARD BITUMENS

(UDC 553.495)

G. N. Kotel'nikov

Translated from *Atomnaya Énergiya*, Vol. 19, No. 5,  
pp. 474-475, November, 1965  
Original article submitted February 25, 1965

The variation in the radioactive equilibrium coefficient at deposits of uraniferous hard bitumens has been studied in three regions separated hundreds and thousands of kilometers apart. The first region, where the basic observations were performed, features mountainous and taiga terrain, with absolute heights of 900 to 1600 m, a 15-25° (and in points as much as 40°) curvature of slope, a yearly precipitation average of 700-800 mm. The second region is in a moderate climate zone at heights of 400 to 450 m, slope angles 10-15°, and precipitation in the 400-450 mm range. The third region is semi-arid and desert-like, bare of forest stands or grass cover; the slopes are gentle (5-10°); the yearly precipitation average is 200-300 mm. All three regions are severely denuded. The thickness of coeval overlying deposits ranges 1 to 5 m.

The deposits of uraniferous hard bitumens (anthraxolites) are located between paleozoic crystalline shales and sandstones, and are represented in two of the regions by zones of rock fracture and almost-vertically dipping beds, in the third region by gently sloped (8-10°) sheet deposits.

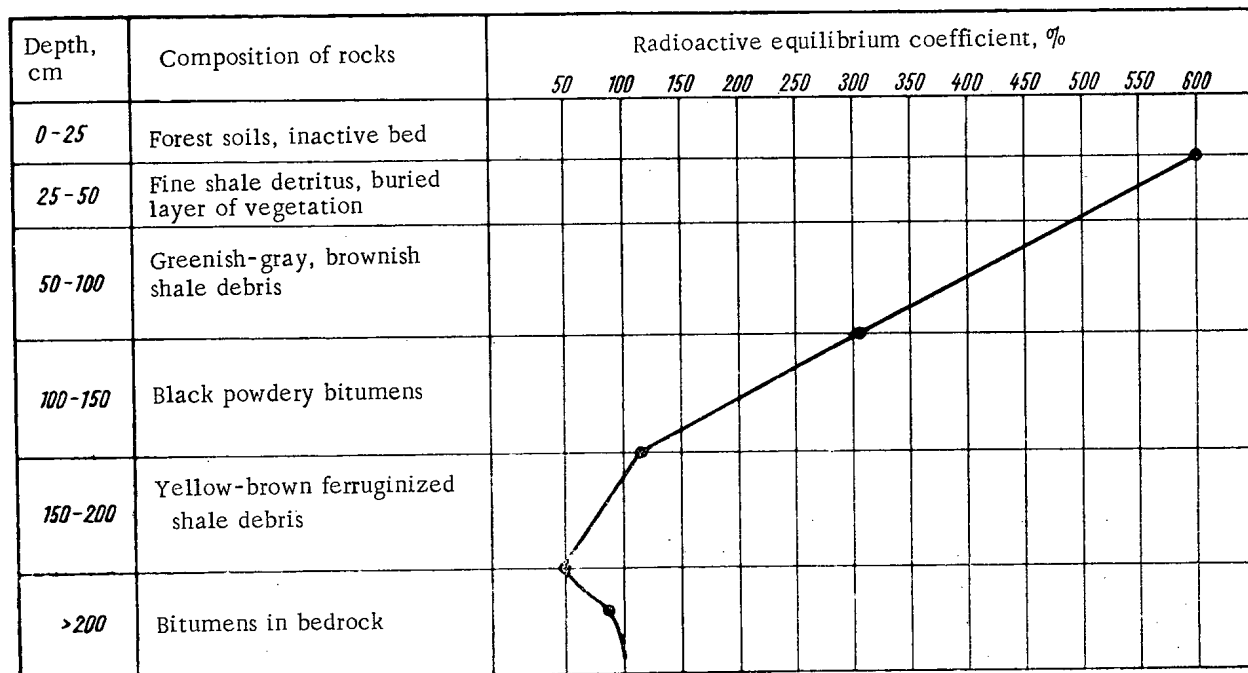
When radioactive anomalies due to mechanical and salt dispersion halos in a deluvial layer are uncovered by trenching and sampling, regular variations in the radioactive equilibrium coefficient are established in both vertical and horizontal planes depending on the distance to ore bodies bedded in bedrock formations.

The top layer, 0-0.25 m thick, is made up of wood soils, loams, is usually free of radioactive elements, and is characterized by  $\gamma$ -radiation in the normal background range (see diagram). The next depth interval (0.25-0.5 m) is a level showing a maximum equilibrium shift of up to 600% or more in the direction of radium. Further on the radioactive equilibrium coefficient decreases gradually with increased depth: to 200-300% in the 1.0-1.5 m range, to 120-150% in the 1.5-2.0 m range. Equilibrium ores prevail from there on down. The lowest talus bed directly overlying an ore body shows an abrupt depletion in radium. The equilibrium ratio is usually 40-60% in that level.

The radioactive equilibrium coefficient stays at a 80-90% level to greater depths in uraniferous hard bitumens found among unaltered host rocks.

Vertical changes in the radioactive equilibrium coefficient both along the strike and athwart the strike of ore bodies is also observed in underground mines worked in host rock around massive lenses of uraniferous anthraxolites. The equilibrium coefficient is 70-90% in the central portions of the ore lenses, gradually increases to 120-200% at a distance of 0.2-2.0 m as the uranium content simultaneously drops to tenths or fractions of tenths. The dispersion halos of ore bodies lying alongside run together in the plane of the ore bodies and the equilibrium coefficient does not exceed 200%.

Radioactive equilibrium shifts gradually toward radium in ore-bearing deposits as the distance from the ore bodies in bedrock increases in the horizontal plane. The radioactive equilibrium is 120 to 200% in the first few meters distance from the ore bodies; it rises to 300-400% as the distance stretches to the first few decameters, and to 600-1000% in the range of tens and hundreds of meters. But this extent of change in the equilibrium coefficient can be traced only along a minimum-shift horizon which, as mentioned, is situated in the bottom of a talus bed bounded by bedrock. As the distance from the ore bodies increases, the horizons featuring equilibrium shift toward uranium or featuring an equilibrium state disappear, and the minimum-shift horizon moves closer to the surface. The most remote anomalies appear to be purely radium anomalies (shift to 1000% or more) and are localized in



Vertical variation of radioactive equilibrium coefficient.

buried beds of vegetation 0.2-0.5 m down from the surface. The size of these salt anomalies varies from 1 to 20 m<sup>2</sup>, and the intensity can attain 600  $\mu$ r/h (after screening drifts have been stripped off).

In the lower-precipitation regions all three dispersion halos are situated in a belt 10-15 m wide, and the zone located near ore bodies and characterized by a 120-200% equilibrium shift is a little different in size from the corresponding zone in the first region. A sharp reduction in size to a strip 2-4 m wide is observed for the zone of 300-400% equilibrium coefficient, while the third zone, the zone of salt dispersion halos, either disappears completely or narrows to 5-6 m.

These regularities can be used most readily in prospecting bedrock ore bodies of uraniferous hard bitumens over an ore field with extensively developed radioactive talus deposits. They must be taken into account in determining conversion factors for appraisal of ore reserves from logging data.

## CHRONICLES, COMMUNICATIONS

## A GLOVE BOX TRAIN

G. I. Lukishov, K. D. Rodionov, and N. I. Noskov

Translated from Atomnaya Énergiya, Vol. 19, No. 5,  
pp. 486-488, November, 1965

The State All-Union Planning Institute GKIAÉ has developed a modularized glove box train (TsBP-1) designed for handling  $\alpha$ -active and  $\beta$ -active materials in standard modularized junior laboratories following the three-zone planning principle [1].

The glove boxes forming the train are equipped with process instrumentation for packing solid and liquid radio-active materials, but the train can also be used for other work handling a variety of toxic materials when the proper equipment is provided.

The train of glove boxes (see photographs) consisted of three airtight boxes and a vehicle carrier, fabricated as a single unit at the point of manufacture, so that the facility can be brought into operation with little delay and with assembly operations minimized.

The modular design of the glove boxes provides a simple solution of zoned baffling to separate the operator zone and overhaul-inspection zone, by directly joining the boxes in line. The joints between modules are made pressure-tight by adhesive PVC lining or by heat-sealing backing strips.

The casings of the glove boxes and the vehicle are made of stainless steel, supports for the glove boxes and modules are made of carbon steel. Each glove box unit is equipped with a ventilation system which rarefies the air in the interior of the boxes to not less than 20 mm Hg; the volume turnover of the ventilating system is 30 volumes per hour.

Intake and exhaust filters [2], each presenting a filtering surface area of 0.4 square meter, are mounted above the glove boxes. The exhaust filter is a two-stage unit: dacron fiber and FPP-15 fabric (V-04 filter). This design lengthens the service life of the second stage. The (aerosol) clean-up factor of the filters is 99.9%. When it is time to change replace filters, the connecting ducts to the ventilating system are valved shut.

Each work place is illuminated by luminescent panels giving off 80 W (4 tubes of 20 W power each). This provides 350 lux illumination for the table-top surface.

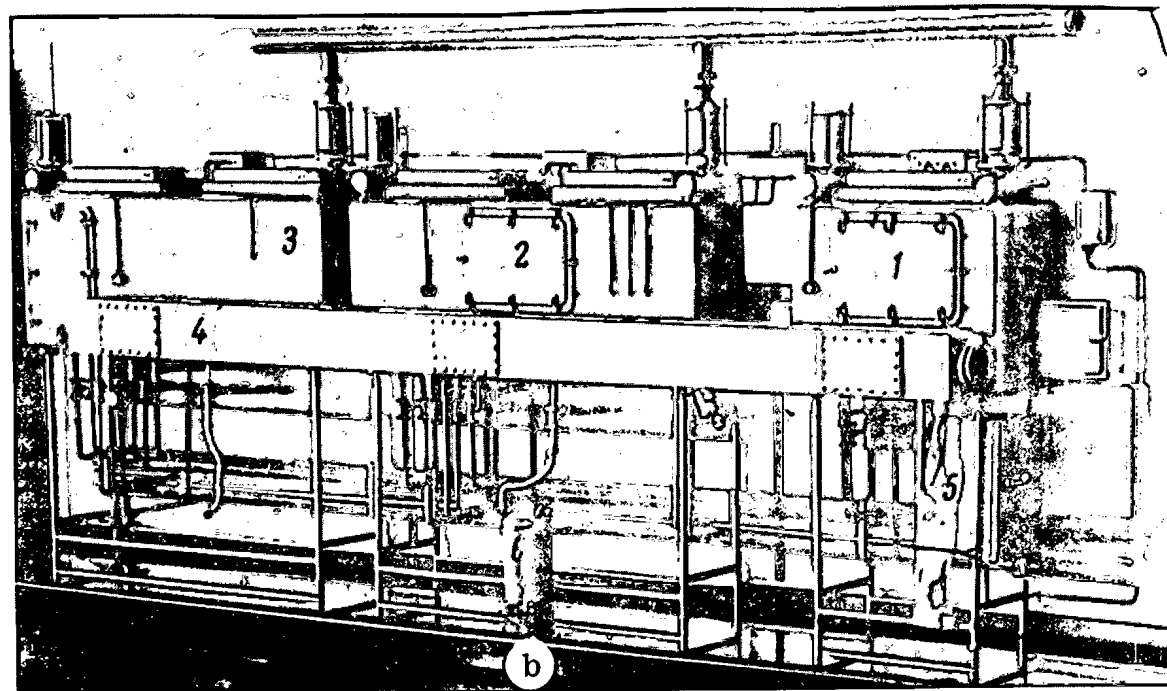
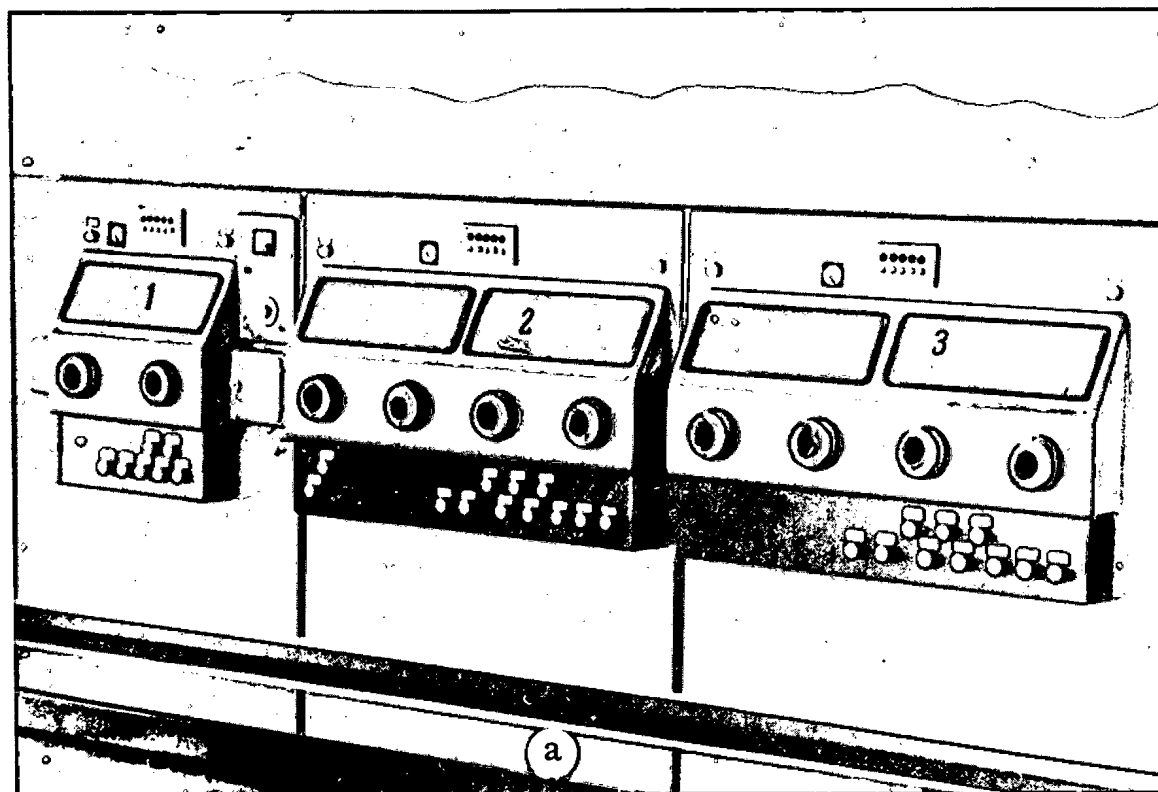
Control desks and electric switchgear panels are built into the unit. Each glove box has an access door in back with a pressure-locked sliding mechanism for hooking up the vehicle, a pressure-tight door for inspection and maintenance, a wash faucet and an overflow drain. Seven process piping manifolds communicate to the glove boxes underneath the work-table (hot and cold running water, vacuum pipe, compressed air, gas duct, overflow drainage, stand-by line).

The intake box in the train has two transfer compartments at a single work station. The left compartment is for introducing and removing radioactive materials, with the outer hatch door opening into the inspection and maintenance zone. The right-hand transfer compartment is for delivering clean materials and wares, the outer door opening into the operator zone. Preliminary unpacking of radioactive materials takes place in this box.

The packing box has two work stations equipped with proper tools [3] for opening isotope casks, penicillin vials, ampules and cans, an ampule sealer, and an electrically driven mixer. This box has a set of syringes and remote controls (gripping tongs), as well as clamping stands and dripping trays. Liquid, solid, and powdered materials are packed in this box.

The box for weighing packed materials is equipped with OVM-100 balances on which the set of weights can be positioned by remote control. The balance can handle 100 g to within 0.1 mg precision. There are also wire cutters to cut radio active wire to calibrated lengths.





The TsBP-1 glove box train: a) forward view; b) view from the rear. 1) Intake box; 2) packaging box; 3) weighing box; 4) vehicle; 5) solid wastes receptacle assembly; 6) KZhO-10 carboy for liquid wastes.

The carrier vehicle is placed behind the glove boxes and is a pressure-tight box structure 250 mm by 250 mm in cross section. The vehicle box frame is pinned to the glove boxes in a pressure-tight joint. A moving-platform carriage is located inside the box frame. The carriage has a load-carrying capacity of 10 kg. The platform lift drive is manual or by cable. The carriage control hand wheel is located in the center zone of the glove box train.

A solids receptacle assembly is found at the left extreme of the vehicle (at the intake box) [4] — it is a long PVC sack connected by a pressute-tight joint to the bottom of the vehicle. When wastes are discharged a part of the PVC bag (in the wastes zone) is heat-sealed by a special sealing device and is then cut off at the seam. Solid wastes are removed with danger of spills or contact by this procedure. The solid wastes discharge assembly may also be used in the opposite direction for delivering materials in an air-tight connection.

The vehicle has one glove port on the side of the solid wastes discharge assembly and a window on the top of the box frame, as well as inspection handholes. Liquid wastes are removed via traps in the glove boxes and collect inside the vehicle. High-level wastes are drained into a KZhO-10 carboy, while low-level wastes to into a special drainage system.

#### L I T E R A T U R E C I T E D

1. Standard GSPI "GKIAE" project. Junior laboratory for handling radioactive materials. Type 1 [in Russian].
2. V. M. Krupchatnikov, Ventilation in work with radioactive materials. Moscow, Atomizdat (1964) [in Russian].
3. Shielding techniques. V/O Izotop catalog. Moscow, Atomizdat (1964) [in Russian].
4. E. Ya. Spitsyn, Treatment and disposal of laboratory radioactive wastes. Moscow, Atomizdat (1965) [in Russian].

## NEW GERMAN WHOLE BODY COUNTER

Yu. V. Sivintsev

Translated from *Atomnaya Énergiya*, Vol. 19, No. 5,  
pp. 488-489, November, 1965

A novel shielding technique was employed in the design of the German Democratic Republic's first whole-body counter [1]. The designers chose  $\gamma$ -ray NaI(Tl) crystal spectrometer as best suited to their purpose of devising an equipment to analyze accident cases and for experimental research (they also plan to build a new spectrometer using several crystals of the same type).

The absence of steel melted down prior to testing a nuclear weapon led to the use of plaster for shielding against external background radiation. Plaster has a density ranging from 1.3 to 1.8 g/cm<sup>3</sup> and is better suited for shielding structures than other nonmetallic materials (concrete, chalk, asbestos, etc.) tested by the authors of references [2-4]. The specific activity of plaster of the brand tested is 10<sup>-14</sup> to 10<sup>-15</sup> Ci/g and is due to  $\gamma$ -emitters whose energies lie below 400 keV; no signs of K<sup>40</sup> or Ra<sup>226</sup> have been detected. Only water of very low specific activity is used in mixing the plaster. The shielding is no less than 75 cm thick at any point, with a density of 1.6 g/cm<sup>3</sup>, equivalent to about 15 cm thickness of iron (120 g/cm<sup>2</sup>).

The measuring chamber is made of a section of iron pipe (140 cm inner diameter, 200 cm in length) made in 1925. This pipe is placed between the plaster blocks (Fig. 1) whose specific activity was first verified, and the pipe is then covered with unhardened plaster. The bent section of pipe serves as inlet duct to the measuring chamber.

The spectrometer detector consists of a NaI(Tl) crystal 100 mm in diameter and 70 mm high, series Z, fabricated at the Karl Zeiss plant in Jena, and a S-12 FS-100 photomultiplier tube. The sodium iodide and the materials used in packaging it are not chosen for their specific activity, so that the crystal contains a potassium impurity on the order of 10<sup>-4</sup>%. The detector is packaged in aluminum, while other parts in the interior of the spectrometer chamber are made of electrolytically refined copper and brass. The inner surface of the pipe is polished and left unpainted.

The detector is mounted on two guides so that it can be moved along the chamber length (Fig. 2). The mounting design also makes it possible to vary the distance from the detector to the patient vertically or on an inclined path.

Holes are left as air passages in the vertical panel delimiting the counting chamber (the air is not cleaned) and also serve as outlets for electrical wiring.

This shielding turned out to be quite effective (Fig. 3). In the energy range around 1 MeV the shielding depresses the background count rate tenfold; it becomes even more effective at lower  $\gamma$ -energies. In the region of soft  $\gamma$ -rays (100 keV), the background count rate is lowered by a factor of 23. The shielding depresses the background 14-fold on the average, the 1083 counts per minute, in the operating range (0.1 to 2 MeV). The 1083 count is 7.8 · 10<sup>3</sup> counts per hour per kg as converted to unit scintillator weight, for comparison. This is roughly twice the background [5] for a crystal of the same geometry placed under a lead shield. The higher background is due in large measure to K<sup>40</sup> impurities in the NaI(Tl) crystal and in the glass of the phototubes. The fraction due to this source is 280 counts per minute, i.e., about 26% of the integrated background count rate. Several measures have been proposed to reduce this background: choice of crystal, introducing additional lead lining as shielding, filtering the intake air, installing a labyrinthine entrance to the measuring chamber.

Note that the shielding built here is relatively cheap. The cost of similar shielding made of chalk and steel blocks would be three times or six times, respectively, the cost of the new shielding.

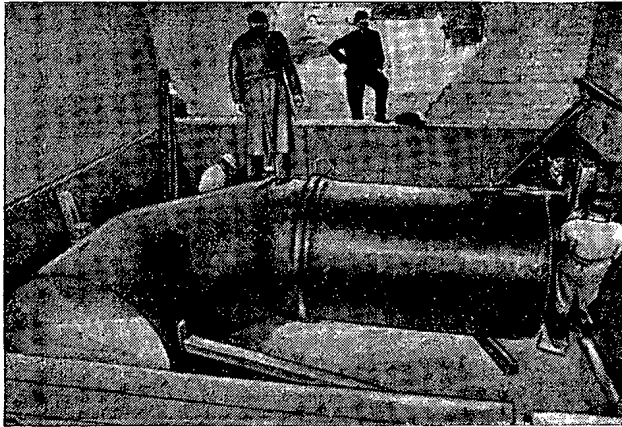


Fig. 1. Laying plaster blocks in place.

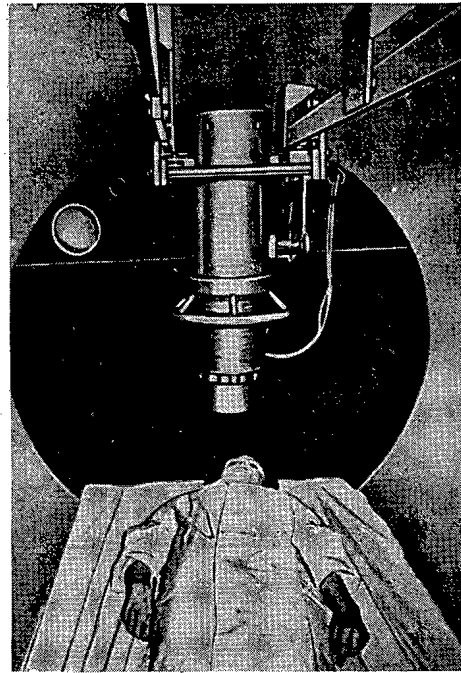


Fig. 2. Interior view of whole-body counter.

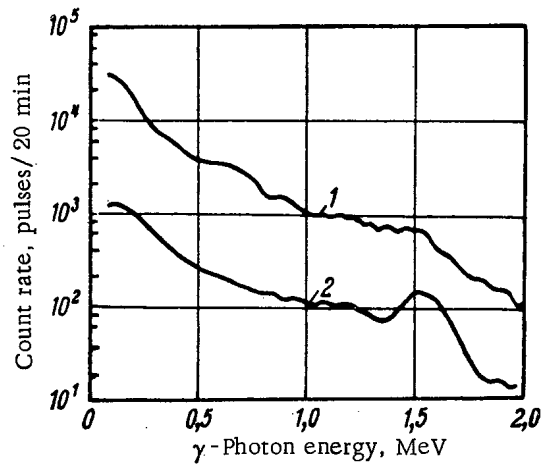


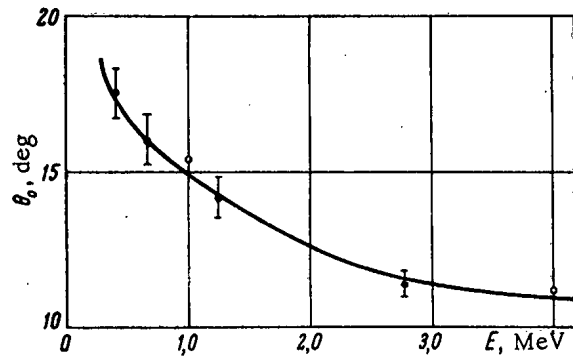
Fig. 3. Effect of plaster shielding on background count rate of NaI(Tl) crystal 100 mm in diameter and 70 mm high (channel width 20 keV): 1) unshielded; 2) shielded.

#### LITERATURE CITED

1. K. Poulcheim and H. Hoesselbarth, *Health Physics*, 11, (1), 52 (1965).
2. *Low-Level Counting Installations*; Nuclear Enterprises, September (1963).
3. R. McCall, *Health Physics*, 2, (3), 304 (1960).
4. T. Sargent, *Whole Body Counting*, Proc. of Symp., IAEA, Vienna (1962), p. 449.
5. H. Mehl and J. Rundo, *Health Physics*, 9, (6), 607 (1963).

ERRATUM

In "Angular Distribution of the Intensity of Gamma-Radiation Scattered by Lead and Water,"  
by L. M. Shirkin (Vol. 19, No. 4, p. 1388), Fig. 2 should appear as follows:



## SOVIET JOURNALS AVAILABLE IN COVER-TO-COVER TRANSLATION

This list includes all Russian journals which—to the publisher's knowledge—were available in cover-to-cover translation on June 30, 1965, or for which definite and immediate plans for cover-to-cover translation had been announced by that date. The list reflects only *current* publication arrangements, but the date and issue listed for first publication refer to translations available from any source. Thus, earlier volumes of a translation journal may have been published by an organization other than that listed as the current publisher, and possibly under a different title (and, for *Doklady Akademii Nauk SSSR*, in a different arrangement of sections).

Five bits of information are furnished, separated by bullets:

1. The abbreviation(s) by which the journals are most frequently referred to in Russian bibliographies (if the name of the journal is customarily spelled out, no abbreviation is given).
2. The transliterated full name of the journal.
3. The full name of the translation journal (in bold type).
4. The year, volume (in parentheses), and issue of first publication of the translation (parentheses are empty if the Russian journal does not use volume numbers).
5. The current publisher of the translation [AGI—American Geological Institute, AGU—American Geophysical Union, AIP—American Institute of Physics, CB—Consultants Bureau, CH—Clearing House for Federal Scientific and Technical Information, CS—The Chemical Society (London), FP—Faraday Press, IEEE—Institute of Electrical and Electronic Engineers, ISA—Instrument Society of America, PP—Pergamon Press].

For convenience in locating bibliographic references the journals are listed in alphabetical order of the *abbreviated* titles.

- AE • Atomnaya énergiya • **Soviet Journal of Atomic Energy** • 1956(1)1 • CB
- Akust. zh. • Akusticheskii zhurnal • **Soviet Physics—Acoustics** • 1955(1)1 • AIP
- Astrofiz. • Astrofizika • **Astrophysics** • 1965(1)1 • FP
- Astr(om). zh(urn). • Astronomicheskii zhurnal • **Soviet Astronomy—AJ** • 1957(34)1 • AIP
- Avtomat. i telemekh. • Avtomatika i telemekhanika • **Automation and Remote Control** • 1956(27)1 • ISA
- Avto(mat). svarka • Avtomaticheskaya svarka • **Automatic Welding** • 1959(12)1 • British Welding Research Association
- Avtometriya • **Autometry** • 1965(1)1 • CB
- Biokhim. • Biokhimiya • **Biochemistry** • 1956(21)1 • CB
- Byul. éksp(erim). biol. (i med.) • Byulleten' éksperimental'noi biologii i meditsiny • **Bulletin of Experimental Biology and Medicine** • 1959(41)1 • CB
- DAN (SSSR) • see *Doklady AN SSSR*
- Defektoskopiya • **Soviet Defectoscopy** • 1965(1)1 • CB
- Diff. urav. • Differentsial'nye uravneniya • **Differential Equations** • 1965(1)1 • FP
- Dokl(ady) AN SSSR; DAN (SSSR) • **Doklady Akademii Nauk SSSR** • The translation of *Doklady* is published in various journals, according to subject matter. The sections of *Doklady* contained in each of the translation journals are listed in parentheses.
- Doklady Biochemistry** (biochemistry) • 1957(112)1 • CB
- Doklady Biological Sciences Sections** (anatomy, cytology, ecology, embryology, endocrinology, evolutionary morphology, parasitology, physiology, zoology) • 1957(112)1 • CB
- Doklady Biophysics** (biophysics) • 1957(112)1 • CB
- Doklady Botany** (botany, phytopathology, plant anatomy, plant ecology, plant embryology, plant physiology, plant morphology) • 1957(112)1 • CB
- Doklady Chemical Technology** (chemical technology) • 1956(106)1 • CB
- Doklady Chemistry** (chemistry) • 1956(106)1 • CB
- Doklady Earth Sciences Sections** (geochemistry, geology, geophysics, hydrogeology, lithology, mineralogy, paleontology, permafrost, petrography) • 1959(124)1 • AGI
- Doklady Physical Chemistry** (physical chemistry) • 1957(112)1 • CB
- Doklady Soil Science** (soil science) • 1964(154)1 • Soil Science Society of America
- Soviet Mathematics—Doklady** (mathematics) • 1960(130)1 • American Mathematical Society
- Soviet Oceanography** (oceanology) • 1959(124)1 • AGU
- Soviet Physics—Doklady** (aerodynamics, astronomy, crystallography, cybernetics and control theory, electrical engineering, energetics, fluid mechanics, heat engineering, hydraulics, mathematical physics, mechanics, physics, technical physics, theory of elasticity) • 1956(106)1 • AIP
- Élektrokhiimiya • **Soviet Electrochemistry** • 1965(1)1 • CB
- Élektrosvyaz' • combined with *Radiotekhnika in Telecommunications and Radio Engineering* • 1957(16)1 • IEEE
- Élektrotekh. • Élektrotekhnika • **Soviet Electrical Engineering** • 1965(36)1 • FP
- Éntom(ol). oboz(r). • Éntomologicheskoe obozrenie • **Entomological Review** • 1958(37)1 • Entomological Society of America
- Fiz. goreniya i vzryva • Fizika goreniya i vzryva • **Combustion, Explosion, and Shock Waves** • 1965(1) • FP
- Fiziol(ogiya) rast. • Fiziologiya rastenii • **Soviet Plant Physiology** • 1957(4)1 • CB
- Fiz.-khim. mekh(anika) mater(ialov); FkHMM • Fizikokhimicheskaya mekhanika materialov • **Soviet Materials Science** • 1965(1)1 • FP
- Fiz. met. i metallov.; FMM • Fizika metallov i metallovedenie • **Physics of Metals and Metallurgy** • 1957(5)1 • Acta Metallurgica
- Fiz.-tekhn. probl. razr. polezn. iskopaem. • Fizikotekhnicheskie problemy razrabotki poleznykh iskopaemykh • **Soviet Mining Science** • 1965(1)1 • CB
- Fiz. tv(erd). tela; FTT • Fizika tverdogo tela • **Soviet Physics—Solid State** • 1959(1)1 • AIP
- FKhMM • see *Fiz.-khim. mekhanika materialov*
- FMM • see *Fiz. met. i metallov.*
- FTT • see *Fiz. tverd. tela*
- Geliotekh. • Geliotekhnika • **Applied Solar Energy** • 1965(1)1 • FP
- Geol. nefi i gaza • Geologiya nefi i gaza • **Petroleum Geology** • 1958(2)1 • Petroleum Geology, Box 171, McLean, Va.
- Geomagnet. i aéronom. • Geomagnetizm i aéronomiya • **Geomagnetism and Aeronomy** • 1961(1)1 • AGU
- Inzh.-fiz. zh. • Inzhenerno-fizicheskii zhurnal • **Journal of Engineering Physics** • 1965(8)1 • FP
- Inzh. zh. • Inzhenernyi zhurnal • **Soviet Engineering Journal** • 1965(5)1 • FP
- Iskusstv. sputniki Zemli • Iskusstvennye sputniki Zemli • **Artificial Earth Satellites** • 1958(1)1 • CB [superseded by *Kosmich. issled.*]
- Izmerit. tekhn(ika) • Izmeritel'naya tekhnika • **Measurement Techniques** • 1958(7)1 • ISA
- Izv. AN SSSR, o(td.) kh(im.) n(auk) (or ser. khim.) • **Izvestiya Akademii Nauk SSSR: Otdelenie khimicheskikh nauk (or Seriya khimicheskaya)** • **Bulletin of the Academy of Sciences of the USSR: Division of Chemical Science** • 1952(16)1 • CB
- Izv. AN SSSR, ser. fiz(ich). • **Izvestiya Akademii Nauk SSSR: Seriya fizicheskaya** • **Bulletin of the Academy of Sciences of the USSR: Physical Series** • 1954(18)3 • Columbia Technical Translations
- Izv. AN SSSR, ser. fiz. atm. i okeana • **Izvestiya Akademii Nauk SSSR: Seriya fiziki atmosfery i okeana** • **Izvestiya, Atmospheric and Oceanic Physics** • 1965( )1 • AGU
- Izv. AN SSSR, ser. fiz. zemli • **Izvestiya Akademii Nauk SSSR: Seriya fiziki zemli** • **Izvestiya, Physics of the Solid Earth** • 1965( )1 • AGU
- Izv. AN SSSR, ser. geofiz. • **Izvestiya Akademii Nauk SSSR: Seriya geofizicheskaya** • **Bulletin of the Academy of Sciences of the USSR: Geophysics Series** • 1957(7)1 • AGU [superseded by *Izv. AN SSSR, ser. fiz. atm. i okeana and Izv. AN SSSR, ser. fiz. zemli*]
- Izv. AN SSSR, ser. geol. • **Izvestiya Akademii Nauk SSSR: Seriya geologicheskaya** • **Bulletin of the Academy of Sciences of the USSR: Geologic Series** • 1958(23)1 • AGI
- Izv. AN SSSR, ser. neorgan. mat(er). • **Izvestiya Akademii Nauk SSSR: Seriya neorganicheskie materialy** • **Inorganic Materials** • 1965(1)1 • CB

- Izv. AN SSSR, tekhn. kiber(netika) • Izvestiya Akademii Nauk SSSR: Tekhnicheskaya kibernetika • **Engineering Cybernetics** • 1963(1)1 • IEEE
- Izv. v(yssh.) u(ch.) z(av.) aviats. tekhn. • Izvestiya vysshikh uchebnykh zavedenii. Aviatsionnaya tekhnika • **Aviation Engineering** • 1963(6)1 • CH
- Izv. v(yssh.) u(ch.) z(av.) fiz. • Izvestiya vysshikh uchebnykh zavedenii. Fizika • **Soviet Physics Journal** • 1965(8)1 • FP
- Izv. v(yssh.) u(ch.) z(av.) geodez. i aérofot. • Izvestiya vysshikh uchebnykh zavedenii. Geodeziya i aérofotos'emka • **Geodesy and Aerophotography** • 1959(4)1 • AGU
- Izv. v(yssh.) u(ch.) z(av.) priborostr. • Izvestiya vysshikh uchebnykh zavedenii. Priborostroenie • **Izvestiya VUZOV. Instrument Building** • 1962(5)1 • CH
- Izv. v(yssh.) u(ch.) z(av.) radiofiz. • Izvestiya vysshikh uchebnykh zavedenii. Radiofizika • **Izvestiya VUZOV. Radiophysics** • 1958(1)1 • CH
- Izv. v(yssh.) u(ch.) z(av.) radiotekhn(ika) • Izvestiya vysshikh uchebnykh zavedenii. Radiotekhnika • **Izvestiya VUZOV. Radio Engineering** • 1959(2)1 • CH
- Izv. v(yssh.) u(ch.) z(av.) tekhn. teks. prom. • Izvestiya vysshikh uchebnykh zavedenii. Tekhnologiya tekstilnoi promyshlennosti • **Technology of the Textile Industry, USSR** • 1960(4)1 • The Textile Institute (Manchester)
- Kauch. i rez. • Kauchuk i rezina • **Soviet Rubber Technology** • 1959(18)3 • Maclaren and Sons Ltd.
- Khim. getero(tsik). soed. • Khimiya geterotsiklicheskih soedinenii • **Chemistry of Heterocyclic Compounds** • 1965(1)1 • FP
- Khim. i nef. mash(inostr). • Khimicheskoe i neftyanoe mashinostroenie • **Chemical and Petroleum Engineering** • 1965( )1 • CB
- Khim. i tekhnol. topliv i masel. • Khimiya i tekhnologiya topliv i masel • **Chemistry and Technology of Fuels and Oils** • 1965( )1 • CB
- Khim. prirod. soed. • Khimiya prirodnykh soedinenii • **Chemistry of Natural Compounds** • 1965(1)1 • FP
- Kib. • Kibernetika • **Cybernetics** • 1965(1)1 • FP
- Kinet. i katal. • Kinetika i kataliz • **Kinetics and Catalysis** • 1960(1)1 • CB
- Koks i khim. • Koks i khimiya • **Coke and Chemistry, USSR** • 1959( )8 • Coal Tar Research Assn. (Leeds, England)
- Kolloidn. zh(urn). • Kolloidnyi zhurnal • **Colloid Journal** • 1952(14)1 • CB
- Kosmich. issled. • Kosmicheskie issledovaniya • **Cosmic Research** • 1963(1)1 • CB
- Kristallog. • Kristallografiya • **Soviet Physics—Crystallography** • 1957(2)1 • AIP
- Liteinoe proiz(vo). • Liteinoe proizvodstvo • **Russian Castings Production** • 1961(12)1 • British Cast Iron Research Association
- Mag. gidrodin. • Magnitnaya gidrodinamika • **Magneto-hydrodynamics** • 1965(1)1 • FP
- Mekh. polim. • Mekhnika polimerov • **Polymer Mechanics** • 1965(1)1 • FP
- Metalloved. i term. obrabotka metal.; MiTOM • Metallovedenie i termicheskaya obrabotka metallov • **Metal Science and Heat Treatment** • 1958(6)1 • CB
- Metallurg • Metallurgist • 1957( )1 • CB
- Mikrobiol. • Mikrobiologiya • **Microbiology** • 1957(26)1 • CB
- MiTOM • see Metalloved. i term. obrabotka metal.
- Ogneupory • **Refractories** • 1960(25)1 • CB
- Opt. i spektr.; OS • Optika i spektroskopiya • **Optics and Spectroscopy** • 1959(6)1 • AIP
- Osnovan. fund. i mekh. gruntov • Osnovaniya fundamenty i mekhanika gruntov • **Soil Mechanics and Foundation Engineering** • 1964( )1 • CB
- Paleon. zh(urn). • Paleontologicheskii zhurnal • **Journal of Paleontology** • 1962( )1 • AGI
- Plast. massy • Plasticheskie massy • **Soviet Plastics** • 1960(8)7 • Rubber and Technical Press, Ltd.
- PMM • see Prikl. matem. i mekhàn.
- PMTF • see Zhur. prikl. mekhan. i tekhn. fiz.
- Pochvovedenie • **Soviet Soil Science** • 1958(53)1 • Soil Science Society of America
- Poroshk. met. • Poroshkovaya metallurgiya • **Soviet Powder Metallurgy and Metal Ceramics** • 1962(2)1 • CB
- Priborostroenie • **Instrument Construction** • 1959(4)1 • Taylor and Francis, Ltd.
- Pribory i tekhn. éksp(erimenta); PTÉ • Pribory i tekhnika éksperimenta • **Instruments and Experimental Techniques** • 1958(3)1 • ISA
- Prikl. biokhim. i mikrobiol. • Prikladnaya biokhimiya i mikrobiologiya • **Applied Biochemistry and Microbiology** • 1965(1)1 • FP
- Prikl. matem. i mekh(an.); PMM • Prikladnaya matematika i mekhanika • **Applied Mathematics and Mechanics** • 1958(22)1 • PP
- Probl. pered. inform. • Problemy peredachi informatsii • **Problems of Information Transmission** • 1965(1)1 • FP
- Probl. severa • Problemy severa • **Problems of the North** • 1958( )1 • National Research Council of Canada
- PTÉ • see Pribory i tekhn. éksperimenta
- Radiokhim. • Radiokhimiya • **Soviet Radiochemistry** • 1962(4)1 • CB
- Radiotekh. • Radiotekhnika • combined with Élektrosvyaz' in **Telecommunications and Radio Engineering** • 1961(16)1 • IEEE
- Radiotekhn. i élektron(ika) • Radiotekhnika i élektronika • **Radio Engineering and Electronic Physics** • 1961(6)1 • IEEE
- Stal' • **Stal' in English** • 1959(19)1 • The Iron and Steel Institute
- Stanki i instr. • Stanki i instrument • **Machines and Tooling** • 1959(30)1 • Production Engineering Research Association
- Stek. i keram. • Steklo i keramika • **Glass and Ceramics** • 1956(13)1 • CB
- Svaroch. proiz(vo). • Svarochnoe proizvodstvo • **Welding Production** • 1959(5)4 • British Welding Research Association (London)
- Teor. i éksp(erim). khim. • Teoreticheskaya i éksperimental'naya khimiya • **Theoretical and Experimental Chemistry** • 1965(1)1 • FP
- Teor. veroyat. i prim. • Teoriya veroyatnostei i ee primenenie • **Theory of Probability and Its Application** • 1956(1)1 • Society for Industrial and Applied Mathematics
- Teploténergetika • **Thermal Engineering** • 1964(11)1 • PP
- Teplifiz. vys(ok). temp. • Teplifizika vysokikh temperatur • **High Temperature** • 1963(1)1 • CB
- Tsvet. metally • Tsvetnye metally • **The Soviet Journal of Nonferrous Metals** • 1960(33)1 • Primary Sources
- Usp. fiz. nauk; UFN • Uspekhi fizicheskikh nauk • **Soviet Physics—Uspekhi** • 1958(66)1 • AIP
- Usp. khim.; UKh • Uspekhi khimii • **Russian Chemical Reviews** • 1960(29)1 • CS
- Usp. mat. nauk; UMN • Uspekhi matematicheskaya nauk • **Russian Mathematical Surveys** • 1960(15)1 • Cleaver-Hume Press, Ltd.
- Vest. Akad. med. nauk SSSR • Vestnik Akademii meditsinskikh nauk SSSR • **Vestnik of USSR Academy of Medical Sciences** • 1962(17)1 • CH
- Vest. mashinostroeniya • Vestnik mashinostroeniya • **Russian Engineering Journal** • 1959(39)4 • Production Engineering Research Association
- Vest. svyazi • Vestnik svyazi • **Herald of Communications** • 1954(14)1 • CH
- Vysoko(molek). soed(ineniya) • Vysokomolekulyarnye soedineniya (SSSR) • **Polymer Science (USSR)** • 1959(1)1 • PP
- Yadernaya fizika • **Soviet Journal of Nuclear Physics** • 1965(1)1 • AIP
- Zashch(ita) met(allo) • Zashchita metallov • **Protection of Metals** • 1965(1)1 • CB
- Zav(odsk). lab(oratoriya); ZL • Zavodskaya laboratoriya • **Industrial Laboratory** • 1958(24)1 • ISA
- ZhÉTF pis'ma redaktsiyu • **JETP Letters** • 1965(1)1 • AIP
- Zh(ur). anal(it). khim(ii); ZhAKh • Zhurnal analiticheskoi khimii • **Journal of Analytical Chemistry** • 1952(7)1 • CB
- Zh(ur). éks(perim). i teor. fiz.; ZhÉTF • Zhurnal éksperimental'noi i teoreticheskoi fiziki • **Soviet Physics—JETP** • 1955(28)1 • AIP
- Zh(ur). fiz. khim(ii); ZhFKh • Zhurnal fizicheskoi khimii • **Russian Journal of Physical Chemistry** • 1959(33)7 • CS
- Zh(ur). neorg(an). khim.; ZhNKh • Zhurnal neorganicheskoi khimii • **Russian Journal of Inorganic Chemistry** • 1959(4)1 • CS
- Zh(ur). obshch. khim.; ZhOKh • Zhurnal obshchei khimii • **Journal of General Chemistry of the USSR** • 1949(19)1 • CB
- Zh(ur). org. khim.; ZhOrKh(im) • Zhurnal organicheskoi khimii • **Journal of Organic Chemistry of the USSR** • 1965(1)1 • CB
- Zh(ur). prikl. khim.; ZhPKh • Zhurnal prikladnoi khimii • **Journal of Applied Chemistry of the USSR** • 1950(23)1 • CB
- Zh(ur). prikl. mekhan. i tekhn. fiz. • Zhurnal prikladnoi mekhaniki i tekhnicheskoi fiziki • **Journal of Applied Mechanics and Technical Physics** • 1965( )1 • FP
- Zh(ur). prikl. spektr. • Zhurnal prikladnoi spektroskopii • **Journal of Applied Spectroscopy** • 1965(2)1 • FP
- Zh(ur). strukt(urnoi) khim.; ZhSKh • Zhurnal strukturnoi khimii • **Journal of Structural Chemistry** • 1960(1)1 • CB
- Zh(ur). tekhn. fiz.; ZhTF • Zhurnal tekhnicheskoi fiziki • **Soviet Physics—Technical Physics** • 1956(26)1 • AIP
- Zh(ur). vses. khim. ob-va im. Mendeleeva • Zhurnal vsesoyuznogo khimicheskogo obshchestva im. Mendeleeva • **Mendeleev Chemistry Journal** • 1965(10)1 • FP
- Zh(ur). vychis. mat. i mat. fiz. • Zhurnal vychislitel'noi matematika i matematicheskoi fiziki • **USSR Computational Mathematics and Mathematical Physics** • 1962(1)1 • PP
- ZL • see Zavodsk. laboratoriya

**RUSSIAN TO ENGLISH**

# scientist-translators wanted

You can keep abreast of the latest Soviet research in your field while supplementing your **income** by translating **in your own home** on a part-time basis! In the expanding Consultants Bureau publishing program, we **guarantee a continuous flow of translation** in your specialty. If you have a native command of English, a good knowledge of Russian, and experience and academic training in a scientific discipline, you may be qualified for our program. Immediate openings are available in the following fields: physics, chemistry, engineering, biology, geology, and instrumentation. Call or write now for additional information: TRANSLATIONS EDITOR



**CONSULTANTS BUREAU**

227 West 17 Street, New York, N. Y. 10011 • (Area Code: 212) AL-5-0713



# MATSCIENCE SYMPOSIA ON THEORETICAL PHYSICS

Alladi Ramakrishnan, Editor

*A Plenum Press continuing series of proceedings of Matscience symposia held at the Institute of Mathematical Sciences, Madras, India.*

## Volume 1: *Proceedings of the First Anniversary Symposium*

This symposium was arranged in tribute to Prof. R. E. Marshak, who accepted the first Niels Bohr visiting professorship at the new Institute of Mathematical Sciences. Prof. Marshak contributed the paper "Group Symmetries with R-Invariance" included in this proceedings. The other 12 papers also deal mainly with complex problems of particle symmetries and resonances.

**CONTENTS:** Introductory material, Alladi Ramakrishnan • Symmetries and resonances, T. K. Radha • Group symmetries with R-invariance, R. E. Marshak • Pion resonances, T. S. Santhanam • Pion-nucleon resonances, K. Venkatesan • The influence of pion-nucleon resonance on elastic scattering of charged pions by deuterons, V. Devanathan • Pion-hyperon resonances, R. K. Umerjee • Determination of spin-parity of resonances, G. Ramachandran • Regge poles and resonances, T. K. Radha • On Regge poles in perturbation theory and in weak interactions, K. Raman • Some remarks on recent experimental data and techniques, E. Segre • On the new resonances, Bogdan Maglic • The higher resonances in the pion-nucleon system, G. Takeda.

165 pages

1965

\$9.50

## Volume 2: *Proceedings of the Second Anniversary Symposium*

**CONTENTS:** Origin of internal symmetries, E. C. G. Sudarshan • Construction of the invariants of the simple Lie groups, L. O'Raifeartaigh • Temperature cutoff in quantum field theory and mass renormalization, S. P. Misra • Some current trends in mathematical research, M. H. Stone • Recent mathematical developments in cascade theory, S. K. Srinivasan • Semigroup methods in mathematical physics, A. T. Bharucha-Reid • On peratization methods, N. R. Ranganathan • Muon capture by complex nuclei, V. Devanathan • The theory of a general quantum system interacting with a linear dissipation system, R. Vasudevan • Recent developments in the statistical mechanics of plasmas, Hugh DeWitt • Electrodynamics of superconductors, B. Zumino • Crossing relations and spin states, M. Jacob • Large-angle elastic scattering at high energies, R. Hagedorn • The multiperipheral model for high-energy processes, K. Venkatesan • Effective-range approximation based on Regge poles, B. M. Udgaonkar • Regge poles in weak interactions and form factors, K. Raman • Some applications of separable potentials in elementary particle physics, A. N. Mitra • Introduction to quantum statistics of degenerate Bose systems, F. Mohling • Form factors of the three-nucleon systems  $H^3$  and  $He^3$ , T. K. Radha.

Approx. 260 pages

1966

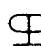
\$12.50

## Volume 3: *Proceedings of the First Matscience Summer School*

In preparation

## Volume 4: *Proceedings of the Third Anniversary Symposium*

In preparation

 **PLENUM PRESS** 227 West 17th Street, New York, New York 10011